NUREG-1824
Supplement 1

EPRI 3002002182

Verification and Validation of Selected Fire Models for Nuclear Power Plant Applications

Supplement 1

Draft Report for Comment

U.S. Nuclear Regulatory Commission
Office of Nuclear Regulatory Research
Washington, D.C. 20555-0001

Electric Power Research Institute
3412 Hillview Avenue
Palo Alto, CA 94303

U.S.NRC
United States Nuclear Regulatory Commission
Protecting People and the Environment

EPRI ELECTRIC POWER RESEARCH INSTITUTE

AVAILABILITY OF REFERENCE MATERIALS IN NRC PUBLICATIONS

NRC Reference Material

As of November 1999, you may electronically access NUREG-series publications and other NRC records at the NRC's Public Electronic Reading Room at http://www.nrc.gov/reading-rm.html. Public records include NUREG-series publications; *Federal Register* notices; applicant, licensee, and vendor documents and correspondence; NRC correspondence and internal memoranda; bulletins and information notices; inspection and investigative reports; licensee event reports; and Commission papers and their attachments.

NRC publications in the NUREG series, NRC regulations, and Title 10, "Energy," in the *Code of Federal Regulations* (10 CFR) may also be purchased from one of these two sources:

1. The Superintendent of Documents
   U.S. Government Printing Office
   Mail Stop SSOP
   Washington, DC 20402-0001
   Internet: bookstore.gpo.gov
   Phone: 202-512-1800
   Fax: 202-512-2250

2. The National Technical Information Service
   Springfield, VA 22161-0002
   Internet: www.ntis.gov
   Phone: 1-800-553-6847 or, locally, 703-605-6000

A single copy of each NRC draft report for comment is available free, to the extent of supply, on written request to the following:

Address: Office of the Chief Information Officer,
Reproduction and Distribution
Services Section
U.S. Nuclear Regulatory Commission
Washington, DC 20555-0001
E-mail: DISTRIBUTION@nrc.gov
Fax: 301-415-2289

Some of the NUREG-series publications posted under http://www.nrc.gov/reading-rm/doc-collections/nuregs are updated periodically and might differ from the last printed version. Although references to material found on a Web site bear the date the material was accessed, the material available on the date cited might subsequently be removed from the site.

Non-NRC Reference Material

Documents available from public and special technical libraries include all open literature items, such as books, journal articles, and transactions, *Federal Register* notices, Federal and State legislation, and congressional reports. Such documents as theses, dissertations, foreign reports and translations, and non-NRC conference proceedings may be purchased from their sponsoring organization.

Copies of industry codes and standards used in a substantive manner in the NRC regulatory process are maintained at:

The NRC Technical Library
Two White Flint North
11545 Rockville Pike
Rockville, MD 20852-2738

These standards are available for reference by the public. Codes and standards are usually copyrighted and may be purchased from their originating organization, or, if they are American National Standards, from:

American National Standards Institute
11 West 42nd Street
New York, NY 10036-8002
Internet: www.ansi.org
Phone: 212-642-4900

Legally binding regulatory requirements are stated only in laws; NRC regulations; licenses, including technical specifications; or orders, not in NUREG-series publications. The views expressed in contractor-prepared publications in this series are not necessarily those of the NRC.

The NUREG series comprises (1) technical and administrative reports and books prepared by the staff (NUREG-XXXX) or agency contractors (NUREG/CR-XXXX), (2) proceedings of conferences (NUREG/CP-XXXX), (3) reports resulting from international agreements (NUREG/IA-XXXX), (4) brochures (NUREG/BR-XXXX), (5) knowledge-management reports (NUREG/KM-XXXX), and (6) compilations of legal decisions and orders of the Commission and Atomic and Safety Licensing Boards and of Directors' decisions under 10 CFR 2.206, "Requests for Action under This Subpart" (NUREG-0750).

Verification and Validation of Selected Fire Models for Nuclear Power Plant Applications

NUREG-1824
Supplement 1

EPRI 3002002182

Draft for Comment
November 2014

U.S. Nuclear Regulatory Commission
Office of Nuclear Regulatory Research (RES)
Washington, D.C. 20555-0001

U.S. NRC-RES Project Manager
M.H. Salley

Electric Power Research Institute (EPRI)
3420 Hillview Avenue
Palo Alto, CA 94304-1338

EPRI Project Manager
A. Lindeman

DISCLAIMER OF WARRANTIES AND LIMITATION OF LIABILITIES

This document was prepared by the organization(s) named below as an account of work sponsored or cosponsored by the Electric Power Research Institute, Inc. (EPRI). neither EPRI, any member of EPRI, any cosponsor, the organization(s) below, nor any person acting on behalf of any of them:

(a) makes any warranty or representation whatsoever, express or implied, (i) with respect to the use of any information, apparatus, method, process, or similar item disclosed in this document, including merchantability and fitness for a particular purpose, or (ii) that such use does not infringe on or interfere with privately owned rights, including any party's intellectual property, or (iii) that this document is suitable to any particular user's circumstance

(b) assumes responsibility for any damages or other liability whatsoever (including any consequential damages, even if EPRI or any EPRI representative has been advised of the possibility of such damages) resulting from your selection or use of this document or any information, apparatus, method, process, or similar item disclosed in this document.

Reference herein to any specific commercial product, process, or service by its trade name, trademark, manufacturer, or otherwise, does not necessarily constitute or imply its endorsement, recommendation, or favoring by EPRI

The following organization(s) prepared this report:

U.S. Nuclear Regulatory Commission, Office of Nuclear Regulatory Research

Electric Power Research Institute

Hughes Associates, Inc.

National Institute of Standards and Technology

The technical contents of this document were **not** prepared in accordance with the EPRI nuclear quality-assurance program manual that fulfills the requirements of the following:

- Appendix B, "Quality Assurance Criteria for Nuclear Power Plants and Fuel Reprocessing Plants," to Title 10 of the *Code of Federal Regulations* (10 CFR) Part 50, "Domestic Licensing of Production and Utilization Facilities"
- Regulations in 10 CFR Part 21, "Reporting of Defects and Noncompliance"
- American National Standards Institute (ANSI) n45.2-1977 or the intent of ISO-9001 (1994).

Use of the contents of this document in nuclear-safety or nuclear-quality applications requires additional actions by the user in accordance with their internal procedures.

NOTE

For further information about EPRI, call the EPRI Customer Assistance Center at 800.313.3774 or send e-mail to askepri@epri.com.

COMMENTS ON DRAFT REPORT

Any interested party may submit comments on this report for consideration by the U.S. Nuclear Regulatory Commission (NRC) staff. Comments may be accompanied by additional relevant information or supporting data. Please specify the report designation "Supplement 1 to NUREG-1824" in your comments, and send them by the end of the comment period specified in the *Federal Register* notice announcing the availability of this report.

Addresses: You may submit comments by any one of the following methods. Please include Docket ID **NRC-2014-0206** in the subject line of your comments. Comments submitted in writing or in electronic form will be posted on the NRC website and on the Federal rulemaking website http://www.regulations.gov.

Federal Rulemaking Web site: Go to http://www.regulations.gov and search for documents filed under Docket ID **NRC-2014-0206**. Address questions about NRC dockets to Carol Gallagher at 301-287-3422 or by e-mail to Carol.Gallagher@nrc.gov.

Mail comments to: Cindy Bladey, Chief, Rules, Announcements, and Directives Branch (RADB), Division of Administrative Services, Office of Administration, Mail Stop: 3WFN-06-A44MP, U.S. Nuclear Regulatory Commission, Washington, DC 20555-0001.

For any questions about the material in this report, please contact: David Stroup, Senior Fire Protection Engineer, U.S. Nuclear Regulatory Commission, Office of Nuclear Regulatory Research, Phone: 301-251-7609 or Email: David.Stroup@nrc.gov.

Please be aware that any comments that you submit to the NRC will be considered a public record and entered into the Agencywide Documents Access and Management System (ADAMS). Do not provide information you would not want to be publicly available.

ABSTRACT

There is a movement to introduce risk-informed and performance-based (RI/PB) analyses into fire-protection engineering practice, both domestically and worldwide. This movement exists in both the general fire-protection and the nuclear power-plant (NPP) fire-protection communities. The U.S. Nuclear Regulatory Commission (NRC) has used risk-informed insights as part of its regulatory decisionmaking since the 1990s.

In 2001, the National Fire Protection Association (NFPA) issued the 2001 Edition of NFPA 805, "Performance-Based Standard for Fire Protection for Light-Water Reactor Electric Generating Plants." In July 2004, the NRC amended its fire-protection requirements in Section 50.48, "Fire Protection," of Title 10, "Energy," of the *Code of Federal Regulations* (10 CFR 50.48) to permit existing reactor licensees to voluntarily adopt fire-protection requirements contained in NFPA 805 as an alternative to the existing deterministic fire-protection requirements. In addition, the NPP fire-protection community has been using RI/PB approaches and insights to support fire-protection decisionmaking in general.

One key tool needed to further the use of RI/PB fire protection is the availability of verified and validated (V&V) fire models that can reliably predict the consequences of fires. Section 2.4.1.2 of NFPA 805 requires that only fire models acceptable to the authority having jurisdiction (AHJ) shall be used in fire-modeling calculations. Furthermore, Sections 2.4.1.2.2 and 2.4.1.2.3 of NFPA 805 state that fire models shall only be applied within the limitations of the given model and shall be verified and validated.

In 2007, the NRC, together with the Electric Power Research Institute (EPRI) and the National Institute of Standards and Technology (NIST), conducted a research project to verify and validate five fire models that have been used for NPP applications. The results of this effort were documented in a seven-volume report, NUREG-1824 (EPRI 1011999), "Verification and Validation of Selected Fire Models for Nuclear Power Plant Applications."

This supplement expands on the previous V&V effort and evaluates the latest versions of the five fire models including additional test data for validation of the models. As with the previous effort, the results are reported in the form of ranges of accuracies for the fire model predictions and, the project was performed in accordance with the guidelines that ASTM International (formerly the American Society for Testing and Materials) set forth in ASTM E1355-12, "Standard Guide for Evaluating the Predictive Capability of Deterministic Fire Models" (2012).

CONTENTS

Note: During the public comment period, the CD containing the appendices can be obtained by sending an e-mail request to david.stroup@nrc.gov.

FIGURES

TABLES

EXECUTIVE SUMMARY

In 2007, the U.S. Nuclear Regulatory Commission (NRC) and the Electric Power Research Institute (EPRI) jointly published, under a Memorandum of Understanding (MOU), NUREG-1824 (EPRI 1011999) "Verification and Validation of Selected Fire Models for Nuclear Power Plant Applications." This supplement builds on and furthers the original verification and validation (V&V) of the five selected fire models commonly used in support of risk-informed and performance-based (RI/PB) fire protection at U.S. nuclear power plants (NPPs).

Background

Since the 1990s, when it became the policy of the NRC to use risk-informed methods to make regulatory decisions where possible, the nuclear power industry has been moving from prescriptive rules and practices toward the use of risk information to supplement decisionmaking. Several initiatives have furthered this transition in the area of fire protection. In 2001, the National Fire Protection Association (NFPA) completed the development of the 2001 Edition of NFPA Standard 805, "Performance-Based Standard for Fire Protection for Light-Water Reactor Electric Generating Plants." Effective July 16, 2004, the NRC amended its fire-protection requirements in Section 50.48(c) of Title 10, "Energy," of the *Code of Federal Regulations* (10 CFR 50.48(c)) to permit existing reactor licensees to voluntarily adopt fire-protection requirements contained in NFPA 805 as an alternative to the existing deterministic fire-protection requirements. RI/PB fire protection often relies on fire modeling for determining the consequences of fires. NFPA 805 requires that the "fire models shall be verified and validated," and "only fire models that are acceptable to the Authority Having Jurisdiction (AHJ) shall be used in fire modeling calculations."

Objectives

The objective of this study is to quantify the predictive capabilities of five different fire models by comparison with selected and available experimental data that is representative of NPP fire scenarios.

Approach

This project team previously performed V&V studies on five selected models: (1) the NRC's NUREG-1805 "Fire Dynamics Tools" (FDT^s), (2) EPRI's "Fire-Induced Vulnerability Evaluation" (FIVE), (3) National Institute of Standards and Technology's (NIST's) "Consolidated Model of Fire Growth and Smoke Transport" (CFAST), (4) Electricité de France's (EdF's) MAGIC, and (5) NIST's "Fire Dynamics Simulator" (FDS). The team based these studies on the guidelines of ASTM E1355, "Standard Guide for Evaluating the Predictive Capability of Deterministic Fire Models." The scope of these V&V studies was limited to the capabilities of the selected fire models and did not cover certain potential fire scenarios that fall outside the capabilities of these fire models. This is documented in Volume 1 of the original NUREG-1824 (EPRI 1011999) report published in 2007. This supplement uses the latest versions of each model and expands on the original work.

Results

This study focuses mainly on model *validation* (that is, the quantification of model uncertainty). Validation is a process to determine the appropriateness of the governing equations as a mathematical model of the physical phenomena of interest. Typically, validation involves comparing model results with experimental measurement. Differences that cannot be explained in terms of numerical errors in the model or uncertainty in the measurements are attributed to

the assumptions and simplifications of the physical model. Model *verification* (that is, testing of mathematical robustness and accuracy) is not addressed directly in this report. Rather, references are provided to the models' documentation and published reports.

For each predicted quantity, such as plume temperature, and each model, a bias factor and relative standard deviation are calculated based on comparison of the model predictions and full-scale measurements. These two metrics indicate the extent to which the model under- or overpredicts the quantity of interest, on average, and the extent to which its predictions are scattered about the mean. The calculation of these metrics takes into consideration the uncertainty in the experimental measurements.

EPRI Perspective

The use of fire models to support fire-protection decisionmaking requires a good understanding of their limitations and predictive capabilities. This supplement to NUREG-1824 expands on the previous report to provide validation of the latest versions of the fire models (FDT^s, FIVE, CFAST, MAGIC, and FDS), considers additional test data to expand the validity of fire models, and provides a quantifiable assessment of model accuracy. An improvement from the original version replaces the qualitative color chart with a table providing quantitative estimates of fire-model uncertainty. This allows the analyst to characterize fire-model uncertainty in combination with user-selected input parameters. The V&V establishes acceptable use and limitations of specific fire models. It is the responsibility of the analyst to justify the appropriateness of each fire model for the specific applications.

Keywords

fire hazard analysis (FHA)
fire modeling
fire probabilistic risk assessment (PRA)
fire probabilistic safety assessment (PSA)
fire protection
fire safety
nuclear power plant
risk-informed performance-based (RI/PB) regulation
verification and validation (V&V)

PREFACE

This is the first formal expansion of a verification and validation study of five different mathematical models that are commonly used in fire-hazard analyses of nuclear power plants (NPPs). The original report was published as seven individual volumes in 2007. For this expansion, it was decided to combine the original seven volumes into a single published volume along with supplemental material that is to be released only in electronic form. This single volume contains the analyses, summary information, and conclusions necessary to evaluate each model for use in NPP applications. The electronic appendices contain the data summaries that support the conclusions in the main report. In the original NUREG-1824 (EPRI 1011999), the reader would have to refer to each volume to evaluate a specific model. The information contained in the original NUREG-1824 (EPRI 1011999) remains valid for the versions of the models for which the V&V documented in that report was conducted. Here are some other notable differences between this supplement and the original study:

- Supplement 1 includes measurements from 16 different series of experiments, compared to the 5 that were included in the original study. The number of individual experiments has expanded to 340 compared to the 26 in the original study.
- Supplement 1 uses the latest versions of the modeling software available at the time of the report. As newer versions of these models are released in the future, the information in this report can be used as guidance in conducting V&V of these new versions. In addition, some of the model authors might choose to publish revised V&V information on their own as they develop new versions of their modeling software.
- Supplement 1 combines the assessment of the NRC and EPRI collections of empirical correlations referred to as the Fire Dynamics Tools (FDT^s) and the Fire Induced Vulnerability Evaluation (FIVE). In the original V&V study, these tools were evaluated separately, and there were several inconsistencies in the application of the various calculation methods.
- Supplement 1 adds additional model output quantities to the evaluation, including sprinkler and smoke-detector activation time and electrical-cable failure time.
- Supplement 1 provides a more quantifiable assessment of model accuracy. The original study used a simple qualitative scheme to assess the models that proved to be difficult to implement in practice. The new method allows modelers to assign meaningful uncertainty bounds to model outputs.
- Supplement 1 was designed to complement the NUREG-1934 (EPRI 1023259) “Nuclear Power Plant Fire Modeling Analysis Guidelines (NPP FIRE MAG).” The original V&V study was published in 2007 and did not include clear guidance on the use of the results of the study. The NPP FIRE MAG provides eight practical examples showing how to use the results of the validation study in typical NPP fire-modeling analyses.

CITATIONS

This report was prepared by:

U.S. Nuclear Regulatory Commission,
Office of Nuclear Regulatory Research (RES)
Washington, DC 20555-0001

Principal Investigator:
D. Stroup

Electric Power Research Institute (EPRI)
3420 Hillview Avenue
Palo Alto, CA 94304

Principal Investigator:
A. Lindeman

National Institute of Standards and Technology
100 Bureau Drive, Stop 8600
Gaithersburg, MD 20899-8600

Principal Investigators:
K. McGrattan
R. Peacock
K. Overholt

Hughes Associates, Inc.
3610 Commerce Drive, Suite 817
Baltimore, MD 21227

Principal Investigators:
F. Joglar
S. LeStrange
S. Montanez

This report describes research sponsored jointly by the U.S. Nuclear Regulatory Commission's (NRC's) Office of Nuclear Regulatory Research (RES) and the Electric Power Research Institute (EPRI) and performed under a formal Memorandum of Understanding (MOU).

The report is a corporate document that should be cited in the external literature in the following manner:

Verification and Validation of Selected Fire Models for Nuclear Power Plant Applications, U.S. Nuclear Regulatory Commission, Office of Nuclear Regulatory Research (RES), Washington, D.C., and Electric Power Research Institute (EPRI), Palo Alto, CA, 2014, NUREG-1824, Supplement 1, and EPRI 3002002182.

The report should be cited internally in other NRC documents in this way:

U.S. Nuclear Regulatory Commission, Supplement 1 to "Verification and Validation of Selected Fire Models for Nuclear Power Plant Applications," NUREG-1824 (Electric Power Research Institute (EPRI) 3002002182), November 2014.

ACKNOWLEDGMENTS

The work documented in this report benefited from contributions and considerable technical support from several organizations.

The verification and validation (V&V) studies for the Fire Dynamics Tools (FDT^s), Consolidated Model of Fire Growth and Smoke Transport (CFAST), and Fire Dynamics Simulator (FDS) models were conducted in collaboration with the Fire Research Division of the U.S. Department of Commerce's National Institute of Standards and Technology (NIST). Since the inception of this project in 1999, the U.S. Nuclear Regulatory Commission (NRC) has collaborated with NIST through an interagency memorandum of understanding (MOU) and conducted research to provide the necessary technical data and tools to support the use of fire models in nuclear power-plant fire-hazard analysis (FHA).

The following individuals or organizations contributed experimental data for use in the model validation study:

- Felix Gonzalez of the Office of Nuclear Regulatory Research and Steve Nowlen of Sandia National Laboratories (SNL) added more experimental data from the SNL/Factory Mutual (FM) experiments. Steve Nowlen also contributed data from the Cable Response to Live Fire (CAROLFIRE) program.
- David Sheppard of the Bureau of Alcohol, Tobacco, and Firearms (ATF) contributed data from the ATF Corridor Experiments.
- Simo Hostikka of VTT Technical Research Centre of Finland contributed data from the VTT Large Hall Experiments.
- Rob Fleury of the University of Christchurch, New Zealand, contributed radiation heat-flux measurement data.
- Ulf Wickström of the SP Technical Research Institute of Sweden contributed data from the SP Adiabatic Surface Temperature experiments.
- The Fire Protection Research Foundation of the National Fire Protection Association contributed data from the Underwriters Laboratories (UL)/National Fire Protection Research Foundation (NFPRF) experiments.
- The U.S. Navy contributed data from its high bay hangar experiments in Hawaii and Iceland.
- NIST contributed data from experiments performed by Anthony Hamins, Kenneth Steckler, Richard Peacock, Robert Vettori, and Alexander Maranghides.

ACRONYMS AND ABBREVIATIONS

ACH	air changes per hour
AHJ	authority having jurisdiction
ANSI	American National Standards Institute
ASET	available safe egress time
AST	adiabatic surface temperature
ASTM	(no longer an abbreviation; formerly the American Society for Testing and Materials)
ATF	Bureau of Alcohol, Tobacco, Firearms and Explosives
BE	Benchmark Exercise
CAROLFIRE	Cable Response to Live Fire
CFAST	Consolidated Fire Growth and Smoke Transport Model
CFD	computational fluid dynamics
CFR	*Code of Federal Regulations*
DB	Deal and Beyler correlation
EdF	Electricité de France
EPRI	Electric Power Research Institute
FDS	Fire Dynamics Simulator
FDT^s	Fire Dynamics Tools (NUREG-1805)
FHA	fire hazard analysis
FIVE	Fire Induced Vulnerability Evaluation Model
FM/SNL	Factory Mutual & Sandia National Laboratories
FPA	Foote, Pagni, and Alvares
HGL	hot gas layer
HRR	heat release rate
HVAC	heating, ventilation, and air conditioning
iBMB	Institut für Baustoffe, Massivbau und Brandschutz
ISO	International Organization for Standardization
LES	Large Eddy Simulation
LLNL	Lawrence Livermore National Laboratory
MCR	Main Control Room
MQH	McCaffrey, Quintiere, and Harkleroad
MOU	memorandum of understanding
NBS	National Bureau of Standards (now NIST)
NEI	Nuclear Energy Institute
NFPA	National Fire Protection Association
NFPRF	National Fire Protection Research Foundation
NIST	National Institute of Standards and Technology
NPP	nuclear power plant
NRC	U.S. Nuclear Regulatory Commission
NRR	Office of Nuclear Reactor Regulation (of the NRC)
PRA	Probabilistic Risk Assessment
PS	point source radiation model
PWR	pressurized water reactor
RES	Office of Nuclear Regulatory Research (of the NRC)
RI/PB	Risk-Informed and Performance-Based
RTI	Response Time Index

SF	solid flame radiation model
SFPE	Society of Fire Protection Engineers
SNL	Sandia National Laboratories
SP	SP Technical Research Institute of Sweden
TC	thermocouple
THIEF	Thermally Induced Electrical Failure Model
TP	thermoplastic
TS	thermoset
UL	Underwriters Laboratories
USN	United States Navy
V&V	verification and validation
VTT	VTT Technical Research Centre of Finland
WTC	World Trade Center
YT	Yamana and Tanaka smoke-filling correlation

NOMENCLATURE

Roman symbols:

A	area (m^2)
A_o	opening area (m^2)
c_p	specific heat, gas at constant pressure (kJ/kg/K)
D	fire diameter (m)
E	experimental measurement
g	acceleration of gravity (m/s^2)
H	ceiling height (m)
H_f	height of base of fire above floor (m)
H_o	opening height (m)
k	thermal conductivity (kW/m/K)
L	compartment length (m)
L_f	flame height (m)
$\dot{m}$	mass loss or flow rate (kg/s)
$\dot{m}''$	mass-loss rate per unit area ($kg/s/m^2$)
M	model prediction
P	probability
p	pressure (Pa)
$\dot{q}''$	heat flux (kW/m^2)
$\dot{Q}$	heat-release rate (kW)
$\dot{Q}^*$	fire Froude number
r	radial distance (m)
r_cj	ceiling jet distance (m)
t	time (s)
T	temperature (°C)
V	volume (m^3)
$\dot{V}$	volume flow rate (m^3/s)
W	compartment width (m)
y	product yield (kg/kg)
Y	mass fraction (kg/kg)

Greek symbols:

δ	model bias factor
ΔH	heat of combustion (kJ/kg)
Δp	pressure difference (Pa)
φ	equivalence ratio
μ	mean
ρ	density (kg/m^3)
σ	standard deviation
$\tilde{\sigma}_E$	relative standard deviation of the experiment
$\tilde{\sigma}_M$	relative standard deviation of the model

1 INTRODUCTION

1.1 Background

In 2001, the National Fire Protection Association (NFPA) issued the first edition (the 2001 Edition) of NFPA 805, "Performance-Based Standard for Fire Protection for Light-Water Reactor Electric Generating Plants." Effective July 16, 2004, the U.S. Nuclear Regulatory Commission (NRC) amended its fire-protection requirements in subsection 50.48(c) of Title 10, "Energy," of the *Code of Federal Regulations* (10 CFR 50.48(c)) to permit existing reactor licensees to voluntarily adopt fire-protection requirements contained in NFPA 805 following a performance-based approach as an alternative to the existing deterministic fire-protection requirements. One important element in a performance-based approach is the estimation of fire hazard using mathematical fire models. Fire modeling is often used in constructing Fire PRAs to determine the effects of fire hazard so that the associated risk can be quantified.

As part of its fire-modeling requirements, NFPA 805 states that "fire models shall be verified and validated" (Section 2.4.1.2.3) and that "only fire models that are acceptable to the authority having jurisdiction (AHJ) shall be used in fire modeling calculations" (Section 2.4.1.2.1). This is an important requirement because the verification and validation (V&V) of fire models is intended to ensure the correctness, suitability, and overall quality of the method. Specifically, verification is the process used to determine whether a model correctly represents the developer's conceptual description (i.e., whether it was "built" correctly), while validation is used to determine whether a model is a suitable representation of the real world and is capable of reproducing phenomena of interest (i.e., whether the correct model was "built").

In 2007, the NRC's Office of Nuclear Regulatory Research (RES) and the Electric Power Research Institute (EPRI) completed a collaborative project for the V&V of five select fire-modeling tools. The results of this study, which was performed under an NRC/RES-EPRI Memorandum of Understanding (MOU), were documented in NUREG-1824 (EPRI 1011999), "Verification and Validation of Selected Fire Models for Nuclear Power Plant Applications." The National Institute of Standards and Technology (NIST) was also an important partner in developing this publication, providing extensive fire-modeling and experimentation expertise.

Subsequently, the NRC conducted a phenomena identification and ranking table (PIRT) exercise for nuclear power-plant (NPP) fire-modeling applications. A PIRT is a formal structured expert elicitation process that focuses on identifying phenomena relevant to a given analysis application (figure of merit) and then ranking the identified phenomena for both importance and current state of knowledge. The process involves the consideration of a series of specific scenarios by a panel of knowledgeable experts (the PIRT panel). For the fire-modeling PIRT, the panel considered four typical NPP fire scenarios. The scenarios included a main control room (MCR) electrical cabinet fire, a switchgear fire, a turbine building lubricating oil fire, and a cable fire in the annulus region inside containment. The potential needs associated with improving fire models for use in NPP fire-modeling applications were assessed using the PIRT results. The results of the PIRT are documented in NUREG/CR-6978, "A Phenomena Identification and Ranking Table (PIRT) Exercise for Nuclear Power Plant Fire Modeling Applications," published in 2008.

In 2012, RES and EPRI completed a collaborative project to develop a set of guidelines to assist users of fire models in applying the technology to the NPP environment. NUREG-1934 (EPRI 1023259), "Nuclear Power Plant Fire Modeling Analysis Guidelines (NPP FIRE MAG)," presents a step-by-step process for using fire modeling in NPP applications. The process described in the guide addresses most of the technical elements relevant to fire-modeling analysis, such as the selection and definition of fire scenarios and the determination and implementation of input values, sensitivity analysis, uncertainty quantification, and documentation. In addition, requirements associated with fire-modeling analyses and analytical fire-modeling tools are addressed through generic guidance, recommended best practices, and example applications. The results from the original NUREG-1824 (EPRI 1011999) were used and expanded to demonstrate the implications of fire model V&V on NPP applications.

This report expands on the previous V&V effort and builds on the lessons learned from the PIRT and the NPP FIRE MAG. The latest versions of the five fire models are used in this V&V exercise. Additional fire test data has been incorporated into this supplement to expand the range of validity of the fire models. In the original NUREG-1824, (EPRI 1011999) two suites of algebraic models, FDT^s and FIVE Revision 1, were selected for V&V. This supplement focuses on the validation of the individual models within the two suites. As a result of work on NUREG-1934 (EPRI 1023259), the qualitative color chart used in the original NUREG-1824 (EPRI 1011999) report has been superseded with a quantitative assessment of fire-model uncertainty. The use of these quantitative estimates of the uncertainties associated with each model's predictions represents a significant step forward in the use of fire modeling for NPP applications.

1.2 Objectives

The purpose of this supplement is to expand the evaluation of the predictive capabilities of certain fire models for applications specific to NPPs. The use of fire models in NPP applications has been previously documented in NUREG-1934 (EPRI 1023259). Section 2.4.1.2 of NFPA 805 states that only fire models acceptable to the AHJ shall be used in fire-modeling calculations. Further, Sections 2.4.1.2.2 and 2.4.1.2.3 of NFPA 805 state that fire models shall only be applied within the limitations of the given fire model and shall be verified and validated. Thus, V&V is necessary to establish acceptable uses and limitations of fire models. In addition, analysts need to justify the appropriateness of fire models for specific applications.

Verification and validation of a calculation method are intended to ensure the correctness and suitability of the method. Verification is the process to determine that a model correctly represents the developer's conceptual description. It is used to decide whether the model was "built" correctly. Validation is the process to determine that a model is a suitable representation of the real world and is capable of reproducing phenomena of interest. It is used to decide whether the right model was "built."

1.3 Scope

Numerous fire models have been developed and maintained by various organizations to predict fire-generated conditions. This study selects the following five of these fire models commonly used for NPP Fire Hazard Analysis (FHA), which represent a wide range of capabilities and mathematical and computational sophistication:

1. NRC's Fire Dynamics Tools (FDT^s version 1805.1)
2. EPRI's Fire-Induced Vulnerability Evaluation (FIVE- Rev2)

3. National Institute of Standards and Technology's (NIST's) Consolidated Model of Fire Growth and Smoke Transport (CFAST Version 6.3.1)
4. Electricité de France's (EdF) MAGIC (Version 4.1.3)
5. NIST's Fire Dynamics Simulator (FDS Version 6.0.0)

These particular models were chosen based on the fact that most of them have been used to calculate fire conditions in NPP fire-protection applications, or were developed by stakeholders within the nuclear industry for NPP fire-protection applications. Details of the models are included in Chapter 4.

1.4 Approach

This report follows the guidelines of ASTM E1355, "Evaluating the Predictive Capability of Deterministic Fire Models" (2012). This standard identifies the necessary steps in the evaluation of predictive fire models. Another useful reference is the Society of Fire Protection Engineers' "Guidelines for Substantiating a Fire Model for a Given Application" (2011).

Chapter 2: Define typical NPP fire scenarios and predicted quantities of interest. This list of fire scenarios is intended to be a reflection of the wide range of fire scenarios found in NPPs (i.e., the scope of scenarios for which models would need validation). However, some aspects of these scenarios cannot be predicted with available models or do not have any available experimental data to support a quantitative model evaluation.

Chapter 3: Select experimental data to perform the quantitative validation. The selected experiments contain a variety of elements typical of the fire scenarios in NPPs. In addition, these experiments are well documented, the data is publicly available, the major parameters (such as the heat-release rate of the fire) are well characterized, and the measurement laboratories are recognized for their experience in the area of fire measurements.

Chapter 4: Select and describe the fire models for which an evaluation can be conducted. To be consistent with ASTM E1355, the description of the selected fire models includes a review of their theoretical basis and fundamental assumptions and an assessment of their mathematical and numerical robustness.

Chapter 5: Conduct the quantitative validation study for each fire-modeling tool. The quantitative validation studies are conducted by comparing experimental measurements with model predictions of quantities deemed of importance in NPP fire scenarios. For each selected output quantity, the difference between the models and the experiments is expressed in the form of a bias factor and a relative standard deviation. Examples of using these uncertainty metrics are given in NUREG-1934 (EPRI 1023259).

Chapter 6: Conclusions. This section presents the conclusions from this V&V study.

Chapter 7: References. This section contains the list of references used in this report.

In addition, several electronic files are available as supporting material. These additional files include four reports that present the results of comparisons between the model calculations and individual experiments (empirical correlations, CFAST, MAGIC, and FDS); the input files for the model comparisons; and the versions of the FDT^{s}, CFAST, and FDS used for this study. FIVE and MAGIC are only available through EPRI (www.epri.com).

The electronic files are included on the CD accompanying this report and are also available for download from the following web site:[1]

http://www.nrc.gov/reading-rm/doc-collections/nuregs/staff/

[1] During the public comment period, the electronic files may be obtained by sending an e-mail request to david.stroup@nrc.gov.

2
IDENTIFICATION OF FIRE-MODELING CAPABILITIES

To conduct the verification and validation (V&V) study in accordance with ASTM E1355, it is necessary to identify the fire scenarios of interest against which the model will be evaluated. Specifically, the identification of fire scenarios provides a broad definition for the scope of the V&V study. The term “fire scenario” as used in fire-modeling applications for the commercial nuclear industry is a broad term capturing various elements characterizing a fire event. These elements include ignition, fire growth, fire propagation to secondary combustibles, detection and suppression features and activities, and damage to plant equipment. Fire models for these applications are used to quantify or predict some of these elements. Fire growth, propagation to secondary combustibles, and damage to plant equipment are the elements often evaluated using fire-modeling tools. This chapter expands on such elements with the purpose of identifying specific fire phenomena predicted by the selected fire models that will form the basis for the V&V study.

The fire phenomena forming the basis for the V&V analysis are selected based on significant research conducted over the last ten years by NRC and EPRI identifying and modeling typical nuclear power plant (NPP) fire scenarios. Specifically:

- Volume 1 of NUREG-1824 (EPRI 1011999) presented a list of fire scenarios that are routinely evaluated, and
- NUREG-1934 (EPRI 1023259) provides detailed examples of how the fire scenarios identified in NUREG-1824 (EPRI 1011999) can be analyzed using the fire models within the scope of this V&V study.

The material in this chapter is based on the research published in the two references listed above. It is not the intent of this V&V study to reproduce or expand the library of fire scenarios already developed and in use by the industry. Instead, this chapter focuses on describing and justifying the specific fire-induced phenomena (i.e., fire dynamics) within these fire scenarios that are the subjects of the V&V study.

2.1 Library of Nuclear Power-Plant Fire Scenarios

The concept of “the library of nuclear power-plant fire scenarios” is used for defining the scope of the V&V study. The library of scenarios consists of a list of fire events that are routinely postulated and analyzed for commercial NPP applications using a combination of modeling tools. Within this library of scenarios, specific fire-induced phenomena are predicted by fire models. This section summarizes the fire scenarios included in the library as introduction to the description of the specific fire-induced phenomena that are the subjects of the V&V. A brief summary of the process for selecting such scenarios is presented first.

2.1.1 Fire-Scenario Selection Process

The process for selecting the fire scenarios included in the library was based on the following activities:

- Review the range of possible configurations that contribute to the postulated fire scenarios in the U.S. commercial nuclear industry. The review focused on parameters considered important in the definition of fire scenarios.
- Identification of potentially risk-significant fire scenarios through review of recent experience in developing probabilistic risk assessments for fires, and
- Examination of past industry experience with fire modeling in support of regulatory applications to help define these fire scenarios.

As a result of these activities, the library of fire scenarios analyzed in NUREG-1934 (EPRI 1023259) was developed. These scenarios are summarized next for completeness purposes. Detailed fire-modeling analyses for these scenarios are available in NUREG-1934 (EPRI 1023259).

2.1.2 Summary of Nuclear Power-Plant Fire Scenarios

This section provides a summary of the selected NPP fire scenarios. The scenarios are:

Fire Scenarios in Switchgear Rooms: Switchgear rooms house key power-distribution equipment to support the plant. Consequently, it is one of the plant locations where detailed fire-modeling analysis is conducted in support of the requirements of a fire-protection program. Typical ignition sources in switchgear rooms include electrical cabinets, transformers and transient fires. Fire modeling is often used for determining plume temperatures, flame radiation conditions, and hot gas layer temperatures in the room. Fire-modeling analysis is also used for determining the time at which specific cables will be damaged or ignited and the heat-release rate generated by fire propagating through cable trays.

Fire Scenarios in Cable-Spreading Rooms: Cable-spreading rooms (CSRs) are another critical location in commercial NPPs because they often contain redundant instrumentation and control circuits needed for plant operation. These rooms generally contain high concentrations of electrical cable (in cable trays and/or conduits), where fire propagation in open cable trays can be an important aspect of fire modeling. Some plants also have areas called cable shafts, cable tunnels, or cable lofts, which present similar challenges. These areas might also contain significant amounts of cables in trays or conduits and might contain redundant circuits. Typical ignition sources in these rooms include low-voltage electrical cabinets and transient fires. Fire modeling is often used for determining plume temperatures, flame radiation conditions, and hot gas layer temperatures in the room. Fire-modeling analysis is also used for determining the time at which specific cables will be damaged or ignited and the heat-release rate generated by fire propagating through cable trays.

Fire Scenarios in Main Control Rooms: The main control room (MCR) contains redundant instrumentation and control circuits that are critical to plant control and operation. Analyses of fires in MCRs pose unique challenges, including timing of fire detection, smoke generation, migration, and habitability (including visibility and concentration of species); fire propagation within very large panels; and fire propagation between panels. It should also be noted that some plants have areas (i.e., a relay room, auxiliary equipment room, or remote shutdown panel) that are similar to control rooms in that they contain redundant instrumentation and control circuits

that are critical to plant control and safe shutdown. However, such areas are not constantly manned as MCRs are and might instead be equipped with automatic suppression systems. A fire in this location might lead to a situation in which the reactor cannot be controlled from the MCR because of damage to the instrumentation and control circuits and must be shut down from an alternative or dedicated location. The source of a fire in this scenario might be, for example, a control cabinet. The size of the fire will depend on the type and amount of cables within the cabinet, as well as on cabinet ventilation and detection and suppression activities in the constantly manned control room. MCRs are usually equipped with smoke purge systems that can be accounted for in fire-modeling analyses. Important targets are adjacent control cabinets exposed to radiant heat flux or flame impingement. Another important aspect of MCR fire scenarios is the habitability conditions in the room as the fire progresses. Habitability conditions refer to smoke concentration (which affects visibility and toxicity), heat flux from the hot gas layer, and room temperature. These conditions are important for determining when operators might need to leave the MCR as a result of relatively high temperatures or low visibility.

Fire Scenarios in Pump Rooms: This location represents areas in a plant where a relatively large fire is possible in a small enclosure. However, not all pump rooms are small, because relatively large pumps can be found in large open areas such as turbine building elevations. The source of a fire in this scenario might be ignition of an oil pool spilled from a pump. The size of the fire will depend on the type and amount of oil spilled, as well as the area and depth of the pool itself. The growth of this fire typically will be fast, and depending on the size of the room, the fire could possibly generate flashover conditions that might challenge integrity of the walls and ceiling. Targets of interest in these scenarios might be the walls and ceiling of the enclosure, which are fire barriers, as well as any other safety-related equipment and cables located in the room or area. These targets might be exposed to direct flame impingement, flame radiation or plumes, ceiling jets, or hot gas layer conditions.

Fire Scenarios in Turbine Buildings: A turbine building is usually a very large open multi-level enclosure[2], in which the top level is commonly referred to as the turbine operating deck. A fire scenario just below the turbine deck was selected to examine large (e.g., turbine lube oil) or small (e.g., transient or panel) fires in large enclosures with high ceilings. The scenario can apply to buildings with one or more turbines. The source of a fire in this scenario might be ignition of an oil pool spilled from one of the turbines. The size of the fire will depend on the type and amount of oil spilled, as well as the area and depth of the pool itself. The growth of this fire will be fast. Other sources of fire in the turbine building could be electrical fires (e.g., high-energy arcing faults), transformer or switchgear fires, and hydrogen fires. Turbine buildings are often naturally ventilated, with many open shafts (e.g., open equipment hatches), doors, and windows. There might also be mechanical ventilation using roof-mounted exhaust fans and/or mechanical supply. Targets of interest in these scenarios might be structural steel members and fire barriers, as well as any other safety-related equipment and cables located in the area and exposed to the fire. Fire conditions affecting the targets might include direct flame impingement, fire plume conditions, or flame radiation.

Fire Scenarios in Multi-Compartment Configurations: Most NPPs have areas with multiple compartments that open into a common space or corridor. Fire scenarios in these areas involve

[2] Some NPPs (typically in warmer climates) do not have a turbine building; instead, the main turbine is open to the elements.

both natural and mechanical ventilation and the propagation of smoke over considerable distances. Targets of interest are typically safety-related equipment and cables located in the corridor outside the room where the fire originates or in an adjacent room.

Fire Scenarios in Multi-Level Buildings: Most NPPs have areas with multiple levels connected by open hatches or staircases. A typical example is the turbine building. The source of a fire in a turbine building might be ignition of an oil pool spilled from an oil tank located under one of the turbine generators. The heat and smoke created will flow through the mezzanine opening between levels. Ventilation is typically natural through openings on the upper level. There might also be mechanical ventilation using roof-mounted exhaust fans and/or mechanical supply.

Fire Scenarios in Containment Buildings: The containment building in a PWR plant is unique because of its cylindrical geometry, high domed ceiling, and large volume. It has internal air-recirculation systems with cooling units. No fresh air is added to the containment building during normal operation. The target of interest in this scenario is an elevated cable tray located outside the fire plume. These targets might be exposed to direct flame impingement, flame radiation or plumes, ceiling jets, or hot gas layer conditions.

Fire Scenarios in Battery Rooms: Battery rooms are typically small concrete enclosures containing large banks of batteries. These rooms are kept closed and are typically free of transient combustibles and fixed ignition sources other than the batteries themselves. EPRI's Fire Events Database suggests two types of scenarios: (1) explosion of the battery cells during the charging phase of the battery and (2) fires in battery terminals as a result of defective or unsecured terminals. Rooms are usually mechanically ventilated. The targets of interest in this scenario are nearby cables and batteries. These targets might be exposed to direct flame impingement, flame radiation or plumes, ceiling jets, or hot gas layer conditions.

Diesel Generator Room: Diesel generator rooms house the standby diesel generator (SBDG) and associated electrical cabinets. This scenario consists of a fuel oil fire near the diesel generator. The size of the fire will depend on the type and amount of fuel oil spilled, as well as the area and depth of the pool itself. The growth of this fire will be fast. The ventilation conditions in the room will be mechanical ventilation with leakage around closed doors. Targets of interest in these scenarios might be cables located in the room exposed to HGL temperatures. These targets might be exposed to direct flame impingement, flame radiation or plumes, ceiling jets, or hot gas layer conditions.

Computer or Relay Room: Computer rooms are typically located in close proximity to the MRCs in NPPs. In addition to computers and other office equipment, some computer rooms might house control cabinets or banks of relay panels. The ignition source for this scenario is a transient combustible fire, namely a computer workstation. The size of the fire will depend on the amount and type of materials involved. The ventilation conditions will be mechanical ventilation. The targets of interest might be control cabinets or banks of relay panels or cables above the fire. These targets might be exposed to direct flame impingement, flame radiation or plumes, ceiling jets, or hot gas layer conditions.

Outdoors: Outdoor fire scenarios can involve large oil-filled transformers or hydrogen tanks; such fires can affect or propagate to nearby equipment. Nearby equipment can include other transformers, other electrical equipment, turbine building walls, etc. Considering that fires will be outdoors, fire conditions that could affect targets include flame radiation and exposure to fire plumes. In the case of transformers, fires can be attributable to oil leaks or spills or electrical faults. Consequences will depend on the type of fire analyzed (i.e., a "regular" fire vs. an explosion).

2.2 Fire-Induced Phenomena for Verification and Validation

A comprehensive review of the fire phenomena (i.e., fire dynamics) developing in the scenarios described in the previous section was performed to identify capabilities within the fire models that should be verified and validated. This comprehensive review also considered the available experimental data that could support the validation process. The result of the review is a list of fire-induced phenomena that (1) can be predicted by the modeling tools within the scope of this study, (2) yield fire-modeling results that can be compared with experimental data, and (3) are routinely used in commercial nuclear plant fire-modeling applications. Consequently, the V&V study presented in this report does not cover all the predictive capabilities of each model and focused only on the identified capabilities. The specific fire-modeling capabilities subjected to the verification and validation process include:

Temperature of the hot gas layer (HGL): The HGL temperature is particularly important in NPP fire scenarios because it is an indicator of overhead target damage (e.g., to cable trays) away from the ignition source. The empirical correlations and zone models typically predict an average HGL temperature, while CFD models predict the local gas temperature in each computational grid cell.

Height of the hot gas layer: The height of the HGL is also important in NPP fire scenarios because it indicates whether a given target is immersed in high-temperature gases. HGL height is a direct output of a two-zone model and can be calculated from local gas temperatures predicted by a CFD model. The empirical correlations can predict the HGL height only for very simple compartment geometries.

Temperature of the ceiling jet: The ceiling jet is the shallow layer of hot gases that spreads radially below the ceiling as the fire plume flow impinges on it. This layer of hot gases has a distinct temperature that is higher than the temperature associated with the HGL. The ceiling-jet temperature is important for modeling NPP fire scenarios in which targets are located just below the ceiling and for determining activation of heat-detection devices. A variety of empirical correlations predict the ceiling-jet temperature and are embedded in the zone models. CFD models compute the ceiling-jet temperature directly.

Plume temperature: The fire plume is the buoyant flow of hot gases rising from the base of the fire. The fire plume transports hot gases into the HGL. Its temperature is greater than the ceiling jet and HGL temperature. It is particularly important in NPP fires because of the numerous postulated scenarios that involve targets directly above a potential fire. A variety of empirical correlations predict the plume temperature and are embedded in the zone models. CFD models compute the plume temperature directly.

Flame height: The height of the flame is important in those NPP fire scenarios in which targets are located close to the ignition source. Some of these scenarios subject the target to flame temperatures because the distance between the target and the ignition source is less than the predicted flame height. A typical example would be cable trays above an electrical cabinet. A variety of empirical correlations predict the flame height and are embedded in the zone models. CFD models compute the flame height directly as a consequence of the combustion model.

Heat flux to targets: Thermal radiation and convection are important modes of heat transfer in fire events. The models included in this study address heat flux with various levels of sophistication, from simply estimating flame radiation from a point source to solving the full radiation-transport equation. The empirical models include simple estimates of flame radiation from a point or cylindrical source. Zone models include these same estimates, as well as

radiation exchange between hot and cold layers and surfaces. CFD models solve the radiation-transport equation that predicts the gains and losses of thermal radiation from each individual gas- and solid-phase grid cell.

Heat flux to surfaces (walls, floors, and ceilings): Surface heat flux refers to the incident or net heat fluxes received by room surfaces such as walls, floors, or ceilings. As an example of the use of these predictions, consider the evaluation of heat fluxes from room surfaces and the hot gas layer to the floor in a control-room fire for determining whether operators need to abandon the room. For the purposes of the V&V, these model outputs are considered separately to determine whether the zone and CFD models have any particular strengths or weaknesses depending on the particular surface considered. The empirical correlations do not address heat flux to the various compartment surfaces.

Target temperature: Target temperature refers to the surface temperature of specific items within the computational domain. The calculation of target temperature is perhaps the most common objective of fire-modeling analyses. A typical nuclear power-plant application is the calculation of cable temperatures caused by fire-generated conditions. The zone and CFD models calculate the surface temperature of the target as a function of time and consider the heat conducted into the target material.

Cable failure time: Cable failure time is one of the most important fire-modeling outputs because it is often compared with the time to start detection and suppression activities. It specifically refers to the time it takes a fire to increase the surface or internal temperature of a cable to its damage or ignition temperature. Zone and CFD models predict the temperature and heat-flux levels surrounding a cable. The models use such predictions for estimating surface and internal cable temperatures. For calculating the surface or internal temperature of the cable, hand calculations, such as the model for the Thermally Induced Electrical Failure (THIEF) of cables (Supplement 1 to NUREG-1805), treat the gas temperature surrounding the cables as an input to the model.

Surface (wall, floor, and ceiling) temperature: Surface temperature refers to the increase in the temperature of room surfaces such as walls, floors, or ceilings caused by fire-generated conditions. As an example of the use of these predictions, consider the evaluation of heat fluxes from room surfaces and the hot gas layer to the floor in a control-room fire for determining whether operators need to abandon the room. For the purposes of the V&V, these outputs are considered separately to determine whether the zone or CFD models have any particular strengths or weaknesses depending on the particular surface considered. The empirical correlations do not address the temperatures of the various compartment surfaces.

Smoke concentration: The smoke concentration can be an important attribute in NPP fire scenarios that involve rooms where operators might need to perform actions during a fire. This attribute specifically refers to soot concentration, which affects visibility. It can also be used for determining smoke-detector activation. Zone and CFD models calculate smoke concentration as a function of time. While the empirical correlation spreadsheets can provide visibility estimates, these calculation methods were not evaluated in this V&V study.

Oxygen concentration: Oxygen concentration is an indicator of a fire becoming underventilated, a pre-cursor to flashover. The zone models calculate the oxygen concentration in the upper and lower layers; CFD models calculate the oxygen concentration in each grid cell. Some of the empirical correlations contain oxygen-concentration calculations embedded in individual spreadsheets. These embedded calculations were not considered in this V&V study.

Room pressure: Room pressure is a rarely used quantity in NPP fire modeling. It might be important when it contributes to smoke migration to adjacent compartments or modeling mechanically ventilated spaces. Zone and CFD models calculate room pressure as they solve energy and mass balance equations for individual compartments. Empirical correlations only apply in the simplest of room geometries.

Sprinkler activation time: Sprinkler activation time is an important fire-modeling output because it is often compared with the cable or target damage time. It specifically refers to the time it takes a fire to increase the temperature of the activation element[3] in a sprinkler or heat-detector device. Zone and CFD models predict the temperature and heat flux levels surrounding the sprinkler and calculate its thermal response considering its “response-time index” (RTI). Hand calculations operate in a similar way but consider only ceiling jet conditions heating the sprinkler or heat-detector device.

Smoke-detector activation time: Smoke-detector activation is often the trigger for suppression activities, either by automatic systems or a fire brigade, in the analysis of fire scenarios. Smoke-detector activation time specifically refers to the time it takes a fire to generate the smoke-concentration conditions necessary to activate the smoke-detection device. Zone and CFD models predict the temperature levels surrounding the smoke detector and determine whether they have exceeded an activation temperature serving as a surrogate for smoke concentration. Hand calculations operate in a similar way.

The fire-modeling capabilities listed above are the bases for the validation study. Fire experiments properly designed and instrumented for collecting data associated with the fire phenomena predicted by the models provide the measured values used for comparison with the model predictions. The following chapters describe the selected experiments, the technical approach for comparing experimental results with model predictions, and the validation results.

[3] For sprinklers, the activation element is typically a fusible link or glass bulb. For heat detectors, the activating element is typically a eutectic metal or bimetal strip.

3
EXPERIMENTAL DATA

This chapter describes the experiments selected for the validation study. Section 3.1 presents a brief description of the experiments. Section 3.2 defines the overall range of experimental parameters. Section 3.3 discusses the experimental uncertainty.

3.1 Description of Experiments

High-quality experimental data are essential to performing a sound validation study. Every effort has been taken to ensure that only reputable high-quality data were used in this project. The experiments described below were conducted at a variety of test labs over the past 30 years. The respective test reports contain different amounts of information relevant to modeling. Where appropriate, modeling assumptions have been provided in cases in which the test report is lacking in information. The criteria for selecting a particular set of experimental measurements are as follows:

- The experiments are representative of the NPP fire scenarios described in Chapter 2.1.2.
- The test report and data are of sufficient detail, are well documented, and are publicly available.
- The HRR of the fire is well characterized, meaning that its relative standard uncertainty is less than 10 percent.
- The experiments have well-defined initial and boundary conditions.
- The experimental test series includes multiple experiments, preferably replicates.

All of the 26 experiments included in the 2007 edition of NUREG-1824 (EPRI 1011999) are included below. While data from Benchmark Exercises #4 and #5 of the International Collaborative Fire Model Project (ICFMP) (Röwekamp, 2008) has been retained for consistency, this supplement uses the data only for HGL temperature and depth comparisons. Supplement 1 to NUREG-1824 (EPRI 3002002182) now includes new data sets from multiple and replicate experiments that span and expand the parameter space covered by the original benchmark exercises.

3.1.1 ATF Corridor Experiments

A series of eighteen experiments (six sets of three replicates) were conducted in a two-story structure with long hallways and a connecting stairway at the Bureau of Alcohol, Tobacco, Firearms, and Explosives' (ATF's) Fire Research Laboratory in Ammendale, Maryland, in 2008 (Sheppard and Klein, 2009).

Geometry: A diagram of the test structure is displayed in Figure 3-1. Two 17 m long (55.8 ft long) hallways were connected by a stairway consisting of two staircases and an intermediate landing. The first-floor hallway was closed to the outside. The end of the second-floor hallway was open with a 0.4 m (1.3 ft) soffit near the ceiling. The two staircases were separated by a 0.4 m wide (1.3 ft wide) gap.

Wall Linings: The walls and ceilings of the test structure were constructed of 1.2 cm (0.5 in) gypsum wallboard. The flooring throughout the structure, including the stairwell landing floor, consisted of one layer of 1.3-cm-thick (0.5-in-thick) cement board on one layer of 1.9 cm thick

(0.75 in thick) plywood supported by wood joists. The stairs were constructed of 2.5 cm thick (1 in thick) clear pine lumber.

Heat Release Rate: A natural gas diffusion burner was used for the fire. Six sets of three replicate experiments were performed. The HRRs were 50 kW, 100 kW, 240 kW, 250 kW, 500 kW, and a combination of HRRs ramped up and down. The burner surface was horizontal and square, measured 0.45 m (1.5 ft) on each side, was 0.37 m (1.3 ft) above the floor, and was filled with gravel. The burner was located near the end of the first floor away from the stairs. There is no reported radiative fraction; thus, a value of 0.25 was chosen, which would be typical of a relatively large methane fire.

Measurements: Vertical arrays of bare-bead thermocouples and bidirectional probes were positioned at various locations in the corridors; one also extended the height of the stairwell.

Please see the report “Burn Tests in Two Story Structure with Hallways” (Sheppard and Klein, 2009) for details concerning the ATF Corridor Experiments.

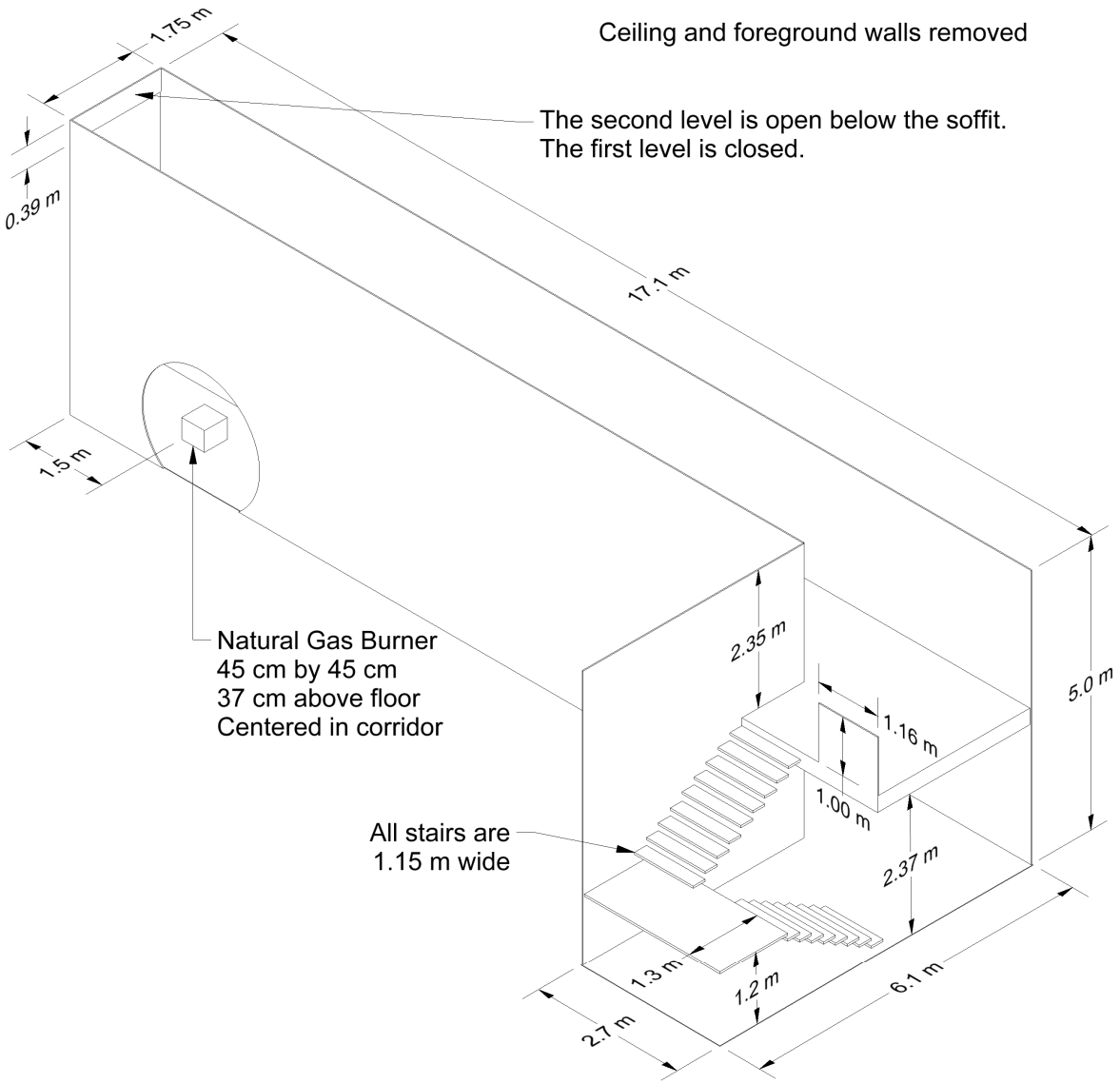

Figure 3-1. Drawing of the ATF Corridor Experiment.

3.1.2 CAROLFIRE – Cable Response to Live Fire

CAROLFIRE was a project sponsored by the U.S. Nuclear Regulatory Commission to study the fire-induced thermal response and functional behavior of electrical cables (NUREG/CR-6931, Vol. 3). The primary objective of CAROLFIRE was to characterize the various modes of electrical failure (e.g., hot shorts and shorts to ground) within bundles of power, control, and instrument cables. A secondary objective of the project was to test a simple model to predict thermally induced electrical failure of cables. The measurements were conducted at Sandia National Laboratories (SNL) and are described in Volume 2 of the CAROLFIRE test report (NUREG/CR-6931, 2007). The experiments were conducted within a heated cylindrical enclosure where single and bundled cables were exposed to various heat fluxes and the electrical failure modes recorded. The experiments used for the validation study do not involve a fire.

The THIEF model is described in Volume 3 of the CAROLFIRE test report. It is basically the solution of the one-dimensional heat-conduction equation within a homogenous non-reacting cylinder with a constant thermal conductivity and specific heat.

Please see the three-volume report “Cable Response to Live Fire (CAROLFIRE)” (NUREG/CR-6931, 2007) for details concerning the CAROLFIRE – Cable Response to Live Fire Experiments.

3.1.3 Fleury Heat-Flux Measurements

Rob Fleury, a student at the University of Canterbury in Christchurch, New Zealand, measured the heat flux from a variety of propane fires (Fleury, 2010). The objective of the work was to evaluate a variety of empirical heat-flux calculation methods.

Heat Release Rate: The fires were fueled by propane burners with dimensions of 0.3 m (1 ft) by 0.3 m (1 ft) (1:1 burner), 0.6 m (2 ft) by 0.3 m (1 ft) (2:1 burner), and 0.9 m (3 ft) by 0.3 m (1 ft) (3:1 burner). The heat-release rates were set to 100 kW, 150 kW, 200 kW, 250 kW, and 300 kW. Fifteen experiments were conducted. The radiative fraction of the fires was assumed to be 0.35.

Measurements: Heat-flux gauges were mounted on moveable dollies that were placed in front of, and to the side of, the burners. The gauges were mounted at heights of 0 m, 0.5 m (1.6 ft), 1.0 m (3.3 ft), and 1.5 m (4.9 ft) relative to the top edge of the burner. The horizontal distance from the center of the burner varied between 0.5 m (1.6 ft) and 2 m (6.6 ft).

Please see the report “Evaluation of Thermal Radiation Models for Fire Spread between Objects” (Fleury, 2010) for details concerning the Fleury Heat Flux Measurements.

3.1.4 FM/SNL Experiments

The Factory Mutual & Sandia National Laboratories (FM/SNL) series consisted of 25 compartment-fire experiments conducted in 1985 for the NRC by Factory Mutual Research Corporation (FMRC), under the direction of SNL (NUREG/CR-4681). The primary purpose of these experiments was to provide data with which to validate computer models for various types of compartments typical of nuclear power plants. Six of the experiments were conducted with a full-scale control-room mockup in place. Parameters varied during the experiments included fire intensity, enclosure ventilation rate, and fire location. The current validation study uses data from nineteen experiments (Tests 1 through 17, 21, and 22) in which propylene gas burners, heptane pools, and methanol pools were used as fire sources.

Geometry: The experiments were conducted in an enclosure measuring approximately 18 m (59 ft) long by 12 m (39 ft) wide by 6 m (19.7 ft) high, constructed at the FMRC fire test facility in Rhode Island. A drawing is included in Figure 3-2.

Heat Release Rate: The peak heat-release rates varied from 500 kW to 2000 kW following a 4-minute *t*-squared growth profile. The test report contains detailed time histories of Tests 4, 5, and 21. The time histories of the other fires are assumed to be similar. The radiative fraction was not measured during the experiment, but in this study it is assumed to equal 0.35, which is typical for hydrocarbon fuels that generate visible smoke.

Ventilation: All of the experiments included forced ventilation to simulate typical power-plant conditions. The rate varied from 1 to 10 air changes per hour.

Measurements: Four types of measurements were conducted during the FM/SNL test series that are used in the current model evaluation study, including the HGL temperature and depth and the ceiling jet and plume temperatures. Aspirated thermocouples (TCs) were used to make all of the temperature measurements. Generally, aspirated TC measurements are preferable to bare-bead TC measurements, because systematic radiative exchange measurement error is reduced. Data from all of the vertical TC trees were used when reducing the HGL height and temperature. For the majority of the tests, the TC data from different locations in the compartment was weighted evenly when computing the HGL temperature and depth.

Please see the reports “An Experimental Investigation of Internally Ignited Fires in Nuclear Power Plant Control Cabinets” (Volume 2 of NUREG/CR-4527, 1988) and “Enclosure Environment Characterization Testing for the Base Line Validation of Computer Fire Simulation Codes” (NUREG/CR-4681, 1987) for details concerning the FM/SNL Experiments.

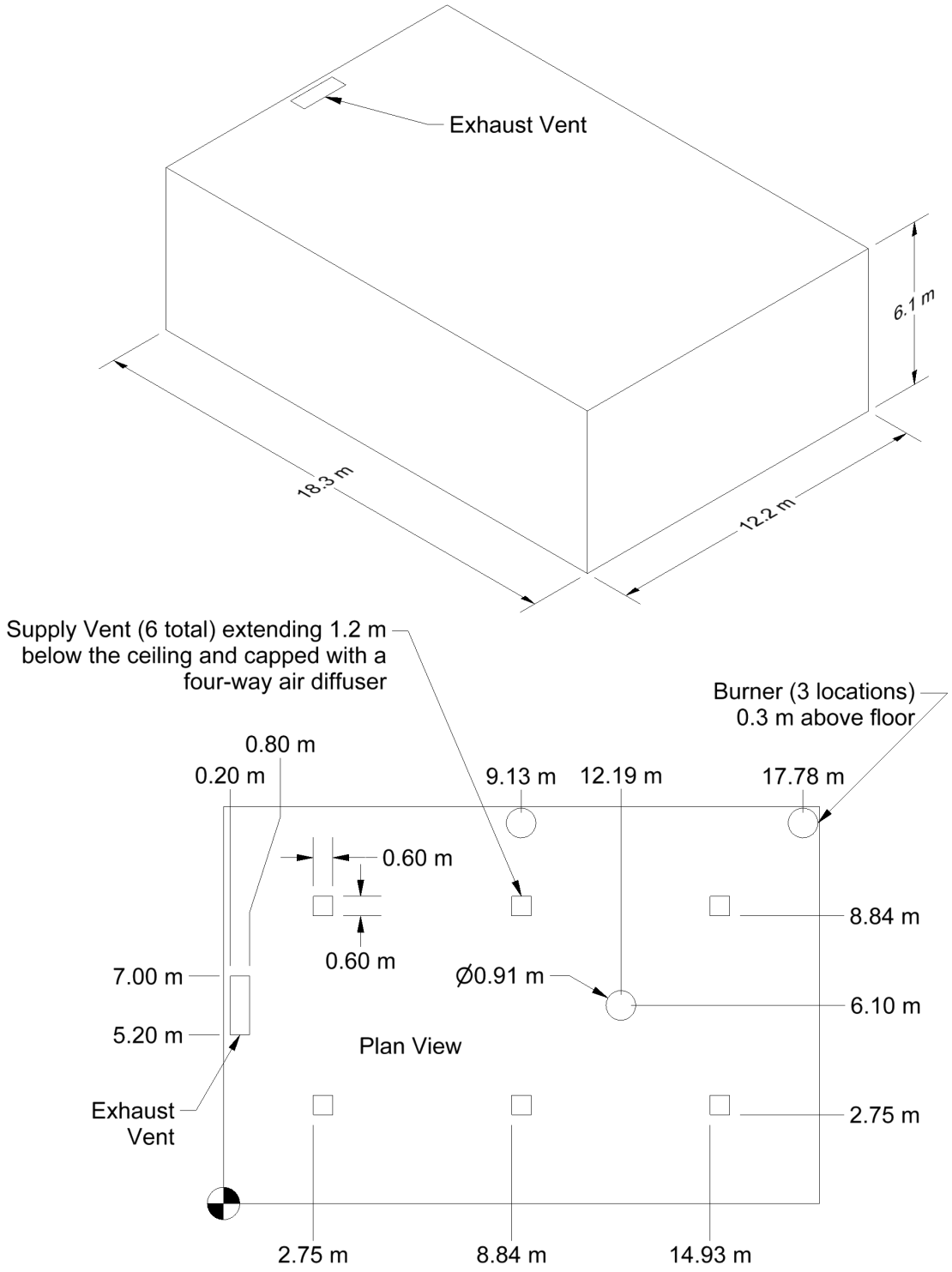

Figure 3-2. Drawing of the FM/SNL compartment.

3.1.5 iBMB Experiments

Experiments were conducted at the Institut für Baustoffe, Massivbau und Brandschutz (iBMB) of Braunschweig University of Technology in Germany. The results from two sets of experiments were contributed to the International Collaborative Fire Model Project (ICFMP) (Röwekamp, 2008) and documented in reports by Klein-Heβling (2006) and Riese (2006). These experiments, referred to as Benchmark Exercises (BEs) #4 and #5, involved relatively large fires in a relatively small concrete enclosure. Despite concerns expressed in the 2007 edition of NUREG-1824 (EPRI 1011999) regarding the use of this data, one experiment from each series was used in the original report because they span an important parameter space for fire-model validation. While new datasets have now been added to Supplement 1 to NUREG-1824 (EPRI 3002002182) that cover the range of test parameters spanned by the iBMB data, these two experiments are being retained in this report for consistency. However, only the HGL temperature and depth measurements are being used in the current study.

Geometry: BE #4 was conducted in a 3.6 m (12 ft) by 3.6 m (12 ft) by 5.7 m (19 ft) concrete enclosure (Figure 3-3). The compartment was configured slightly differently for BE #5 (Figure 3-4). Its height was 5.6 m (18.4 ft) and its doorway was also of a different height.

Heat Release Rate: The fuel source for BE #4 was a 1 m (3.3 ft) by 1 m (3.3 ft) square pan filled with Type A-1 jet fuel. The test report (Klein-Heβling, 2006) indicates the thermophysical properties of the jet fuel were similar to dodecane. The peak HRR for this test was estimated from mass-loss measurements to be approximately 3500 kW. As indicated in the test report, several difficulties were encountered in measuring the mass-loss rate, including data loss attributed to an instrument malfunction and significant fluctuations in the measured mass-loss rate. Because of the measurement issues and because the combustion efficiency was not well characterized, the HRR was assigned a relatively large expanded uncertainty of ±25 percent in the original 2007 edition of NUREG-1824 (EPRI 1011999).

BE #5 consisted of realistically routed cables in a concrete enclosure. In one of the experiments, the compartment was preheated for 20 minutes with a 0.5 m^2 (5.4 ft^2) pan containing ethyl alcohol. After preheating, a propane gas burner was used to ignite the cables. The HRR was measured using oxygen-consumption calorimetry. Only the preheating stage of this single experiment was used in the 2007 edition of NUREG-1824 (EPRI 1011999) because the burning rate of the cables was erratic and its HRR was difficult to measure.

The radiative fraction of the jet fuel in BE #4 was taken as 0.35, similar to that of other smoky hydrocarbons. The radiative fraction for the relatively smoke-free ethanol pool fire in BE #5 was taken as 0.20.

Ventilation: For BE #4, the original test specification called for the ventilation system within the test compartment to be closed. However, measurements made during the experiments suggest that the ventilation system was not closed, and the test report (Klein-Heβling, 2006) indicates that the volume flow rate through the ventilation system was as high as 2.25 m^3/s (5,000 ft^3/min) during the experiment. According to additional information provided by one of the authors of the test report, this measurement was made at a single point within an exhaust duct with dimensions 0.4 m (1.3 ft) wide and 0.8 m (2.6 ft) high. Given the complexity of the air movement within the compartment and the exhaust system, the single volumetric flow measurement is highly uncertain.

Measurements: Vertical arrays of bare-bead thermocouples were positioned within the enclosure for determining HGL temperature and depth.

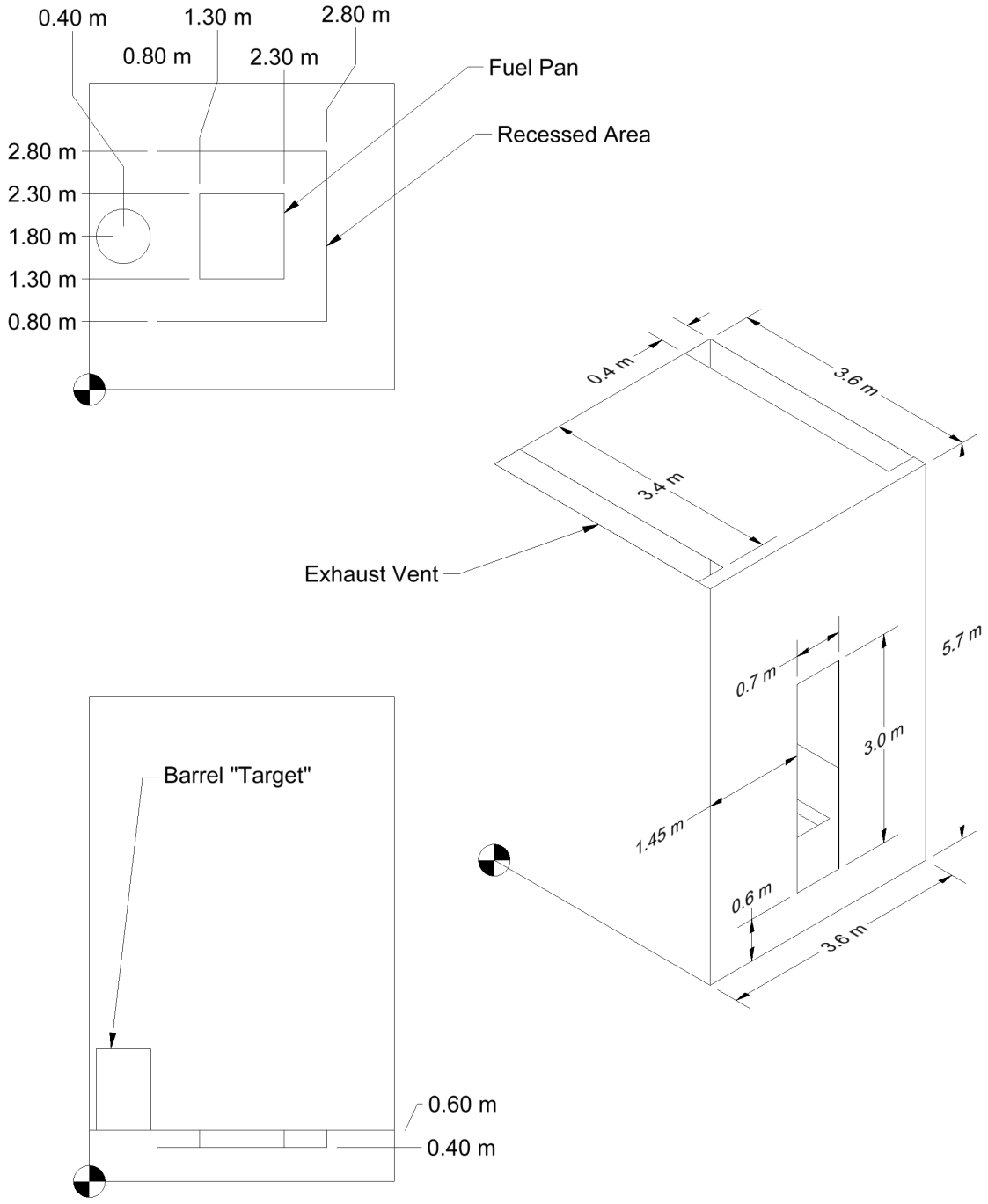

Figure 3-3. Drawing of the iBMB compartment used in Benchmark Exercise #4.

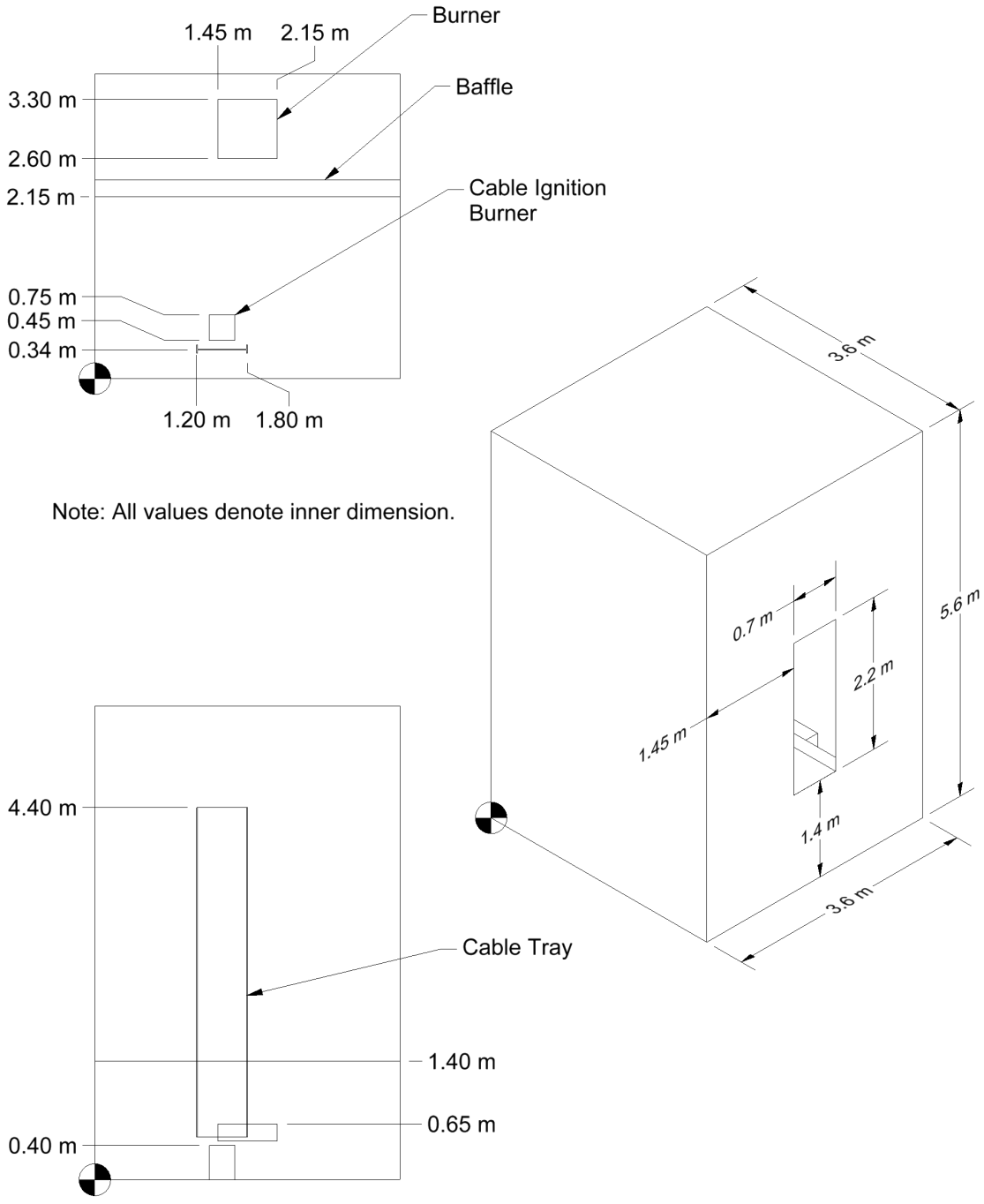

Figure 3-4. Drawing of the iBMB compartment used in Benchmark Exercise #5.

3.1.6 LLNL Enclosure Experiments

Sixty-four experiments were conducted by Lawrence Livermore National Laboratory (LLNL) in 1986 to study the effects of ventilation on enclosure fires (Foote, 1987).

Geometry: The test enclosure was 6 m (19.7 ft) long, 4 m (13.1 ft) wide, and 4.5 m (14.8 ft) high (Figure 3-5). For some of the experiments, the compartment was divided into a 3 m high (9.8 ft high) lower space and a 1.5 m high (4.9 ft high) upper plenum space.

Heat Release Rate: A methane burner was placed directly in the center of the enclosure. For most of the tests the burner was placed on the floor. The fires varied in size from 50 kW to 400 kW. The burner was 0.57 m (4.9 ft) in diameter and 0.23 m (0.75 ft) in height. The radiative fraction was assumed to be 0.20, typical of low-soot-producing methane fires.

Ventilation: The door was closed and sealed for most tests and air was pulled through the space at rates varying from 100 g/s to 500 g/s. Makeup air was provided through one of two ducts: one supplying the lower compartment and one supplying the upper plenum space. In the numerical simulations, an effective inlet area was calculated based on the reported volume flow rate and pressure drop before the fire was ignited.

Measurements: Two vertical arrays of fifteen thermocouples each were positioned along the length of the compartment to the left and right of the fire. Five of the fifteen TCs were located in the upper plenum. In addition, pressure measurements were made in the upper and lower spaces.

Please see the report “An Experimental Investigation of Internally Ignited Fires in Nuclear Power Plant Control Cabinets” (Foote, 1987) for details concerning the LLNL Enclosure Experiments.

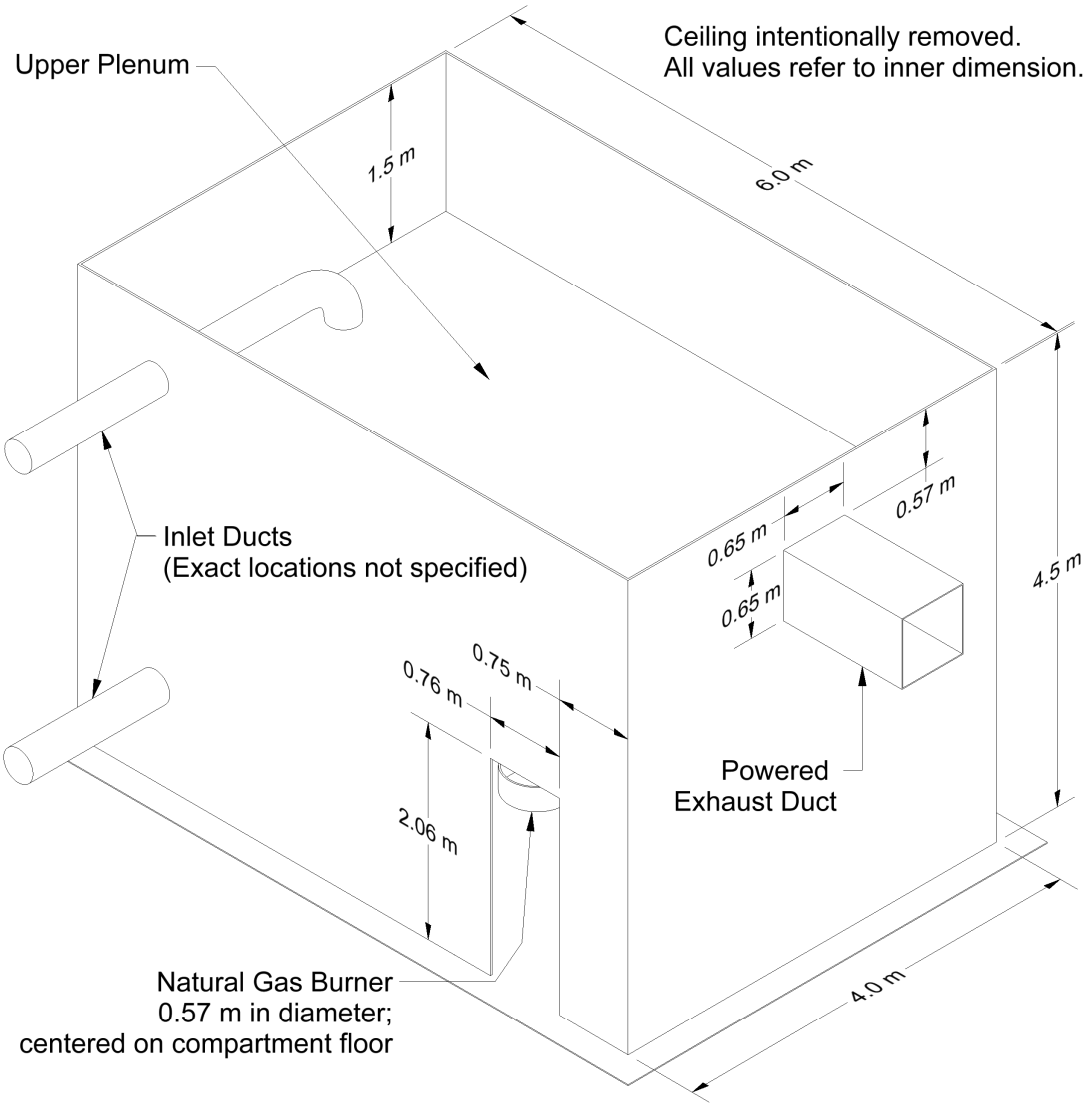

Figure 3-5. Drawing of LLNL compartment.

3.1.7 NBS Multi-Room Experiments

The National Bureau of Standards (NBS), now called the National Institute of Standards and Technology (NIST), conducted an NBS Multi-Room series (consisting of 45 fire experiments and representing 9 different sets of conditions) in a three-room suite. The experiments were conducted in 1985 and are described in detail by Peacock et al. (1988). For the current study, only three of the experiments have been used.

Geometry: The enclosure consisted of two relatively small rooms connected by a relatively long corridor, as shown in Figure 3-6.

Heat Release Rate: A natural gas burner was located against the rear wall of one of the small compartments. Fire tests of 100 kW, 300 kW, and 500 kW were conducted. For the current study, only three 100-kW fire experiments have been used, including Test 100A from Set 1,

Test 100O from Set 2, and Test 100Z from Set 4. These tests were selected because they had been used in prior validation studies and because they had the steadiest values of measured heat-release rate during the steady-burn period. In the two tests for which the door was open, the HRR during the steady-burn period measured by oxygen-consumption calorimetry was 110 kW. It was assumed that the closed-door test (Test 100O) had the same HRR as the open-door tests.

Radiative Fraction: Natural gas was used as the fuel in Test 100A. In Tests 100O and 100Z, acetylene was added to the natural gas to increase the smoke yield, and as a consequence the radiative fraction increased. The radiative fraction of natural gas has been studied previously, whereas the radiative fraction of the acetylene/natural gas mixture has not been studied. The radiative fraction for the natural gas fire was assigned a value of 0.20, whereas a value of 0.30 was assigned for the natural gas/acetylene fires.

Measurements: Only two types of measurements conducted during the NBS test series were used in the evaluation considered here, because there was less confidence in the other measurements. The measurements considered here were the HGL temperature and depth, for which bare-bead TCs were used to make these measurements. Single-point measurements of temperature within the burn room were not used in the evaluation of plume or ceiling jet algorithms. This is because the geometry was not consistent in either case with the assumptions used in the model algorithms of plumes or jets. Specifically, the burner was mounted against a wall, and the room width-to-height ratio was less than that assumed by the various ceiling-jet correlations.

Please see the report “An Experimental Data Set for the Accuracy Assessment of Room Fire Models” (Peacock et al., 1988) for details concerning the NBS Multi-Room Experiments.

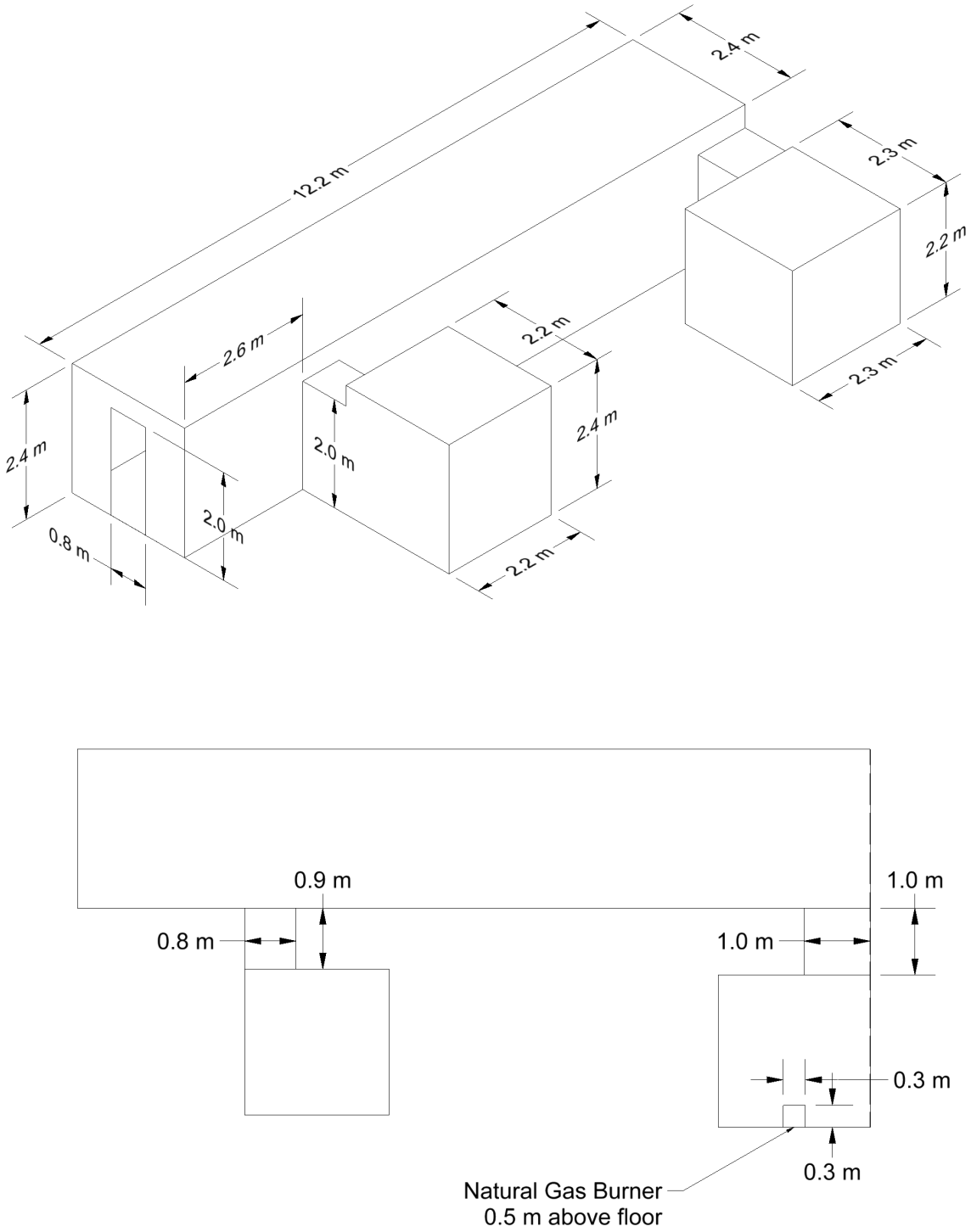

Figure 3-6. Drawing of NBS Multi-Room Experiment.

3.1.8 NIST/NRC Experiments

These experiments, sponsored by the U.S. NRC and conducted at NIST, consisted of 15 large-scale experiments performed in 2003. All 15 tests were included in the validation study. The experiments are documented in NUREG/CR-6905 (Hamins, 2006). Ventilation conditions, fire size, and fire location were varied. Numerous measurements (approximately 350 per test) were made, including gas and surface temperatures, heat fluxes, and gas velocities.

Geometry: The test room had dimensions of 21.7 m (71.2 ft) deep by 7.1 m (23.3 ft) wide by 3.8 m (12.5 ft) high, designed to represent a compartment in a nuclear power plant containing power and control cables (Figure 3-7). The room had one door and a mechanical air-injection and -extraction system.

Wall Linings: The walls and ceiling were covered with two layers of calcium silicate boards, each layer 1.25 cm (0.5 in) thick. The floor was covered with one layer of gypsum board on top of a layer of plywood. Thermophysical and optical properties of the calcium silicate and other materials used in the compartment are given in the test report (Hamins, 2006).

Heat Release Rate: The fire sizes ranged from 350 kW to 2.2 MW. A single nozzle was used to spray liquid hydrocarbon fuels onto a 1 m by 2 m (3.3 ft by 6.6 ft) fire pan that was about 10 cm (4 in) deep. The test plan originally called for the use of two nozzles to provide the fuel spray. Experimental observation suggested that the HRR was steadier using a single nozzle. In addition, it was observed that the actual extent of the liquid pool was well approximated by a 1 m (3.3 ft) circle in the center of the pan. For safety reasons, the fuel flow was terminated when the lower layer's oxygen concentration dropped to approximately 15 percent by volume. The fuel used in 14 of the tests was heptane, while toluene was used for one test (Test 17).

Radiative Fraction: The values of radiative fraction and its expanded (2-sigma) uncertainty were reported as 0.44 ± 0.07 and 0.40 ± 0.09 for heptane and toluene respectively.

Soot Yield: The values of the soot yield and its expanded uncertainty were reported as 0.0149 kg/kg ± 0.0033 kg/kg and 0.195 kg/kg ± 0.052 kg/kg for heptane and toluene respectively.

Natural Ventilation: The compartment had a 2 m (6.6 ft) by 2 m (6.6 ft) door in the middle of the west wall. Some of the tests had a closed door and no mechanical ventilation (Tests 2, 7, 8, 13, and 17), and in those tests the measured compartment leakage was an important consideration. The test report lists leakage areas based on measurements performed before Tests 1, 2, 7, 8, and 13. For the closed-door tests, the leakage area used in the simulations was based on the last available measurement. The chronological order of the tests differed from the numerical order. For Test 4, the leakage area measured before Test 2 was used. For Tests 10 and 16, the leakage area measured before Test 7 was used.

Mechanical Ventilation: The mechanical ventilation system was used during Tests 4, 5, 10, and 16, providing about 5 air changes per hour. The door was closed during Test 4 and open during Tests 5, 10, and 16. The supply duct was positioned on the south wall, about 2 m (6.6 ft) off the floor. An exhaust duct of equal area to the supply duct was positioned on the opposite wall at a comparable location. The flow rates through the supply and exhaust ducts were measured in detail during breaks in the testing, in the absence of a fire. During the tests, the flows were monitored with a single bidirectional probe.

Please see "Report of Experimental Results for the International Fire Model Benchmarking and Validation Exercise 3" (Hamins et al., 2006) for details concerning the NIST/NRC Experiments.

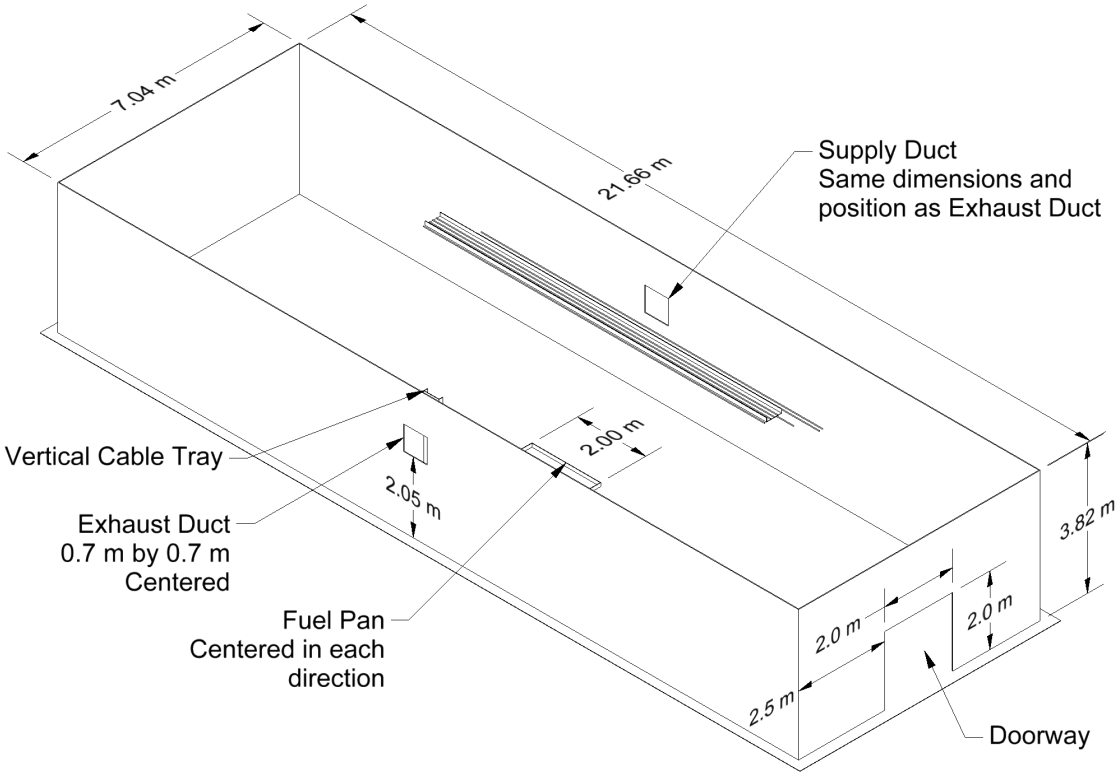

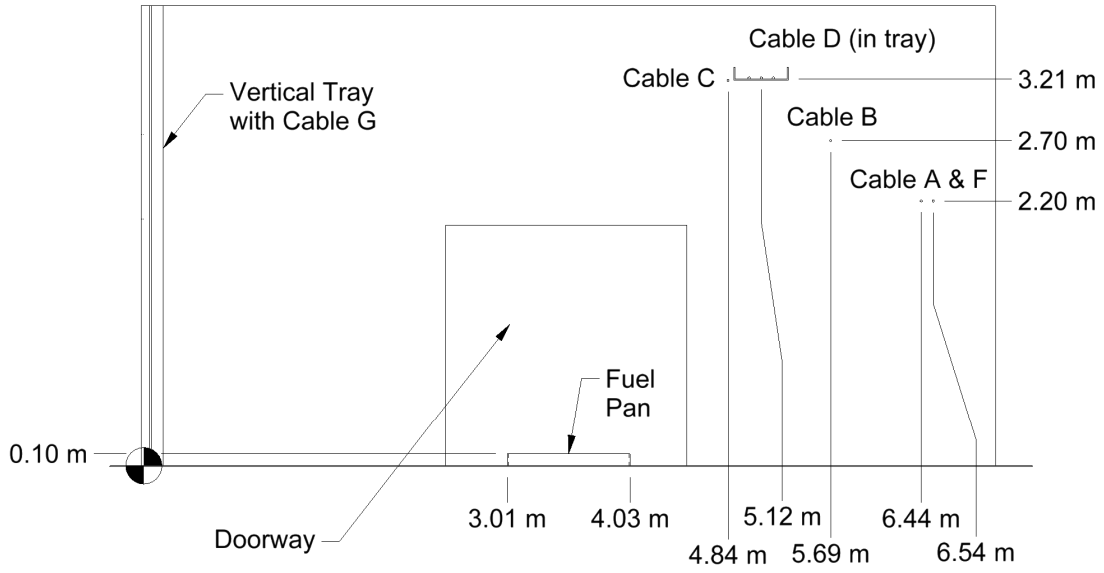

Figure 3-7. Drawing of the NIST/NRC compartment.

3.1.9 NIST Smoke-Alarm Experiments

A series of experiments was conducted by NIST to measure the activation time of ionization and photoelectric smoke alarms in a residential setting (Bukowski et al., 2008). Tests were conducted in actual homes with representative sizes and floor plans, used actual furnishings and household items for fire sources, and tested actual smoke alarms sold in retail stores at that time. Thirty-six tests were conducted in two homes; twenty-seven in a single-story manufactured home, and eight in a two-story home. Eight of the experiments that were conducted in the single-story manufactured home were selected for model validation. Only tests that used a flaming ignition source with a couch or mattress fuel package were considered; the cooking-oil fires and tests that used a smoldering ignition source were not considered.

Geometry: A drawing of the manufactured home is shown in Figure 3-8. The ceiling was peaked on the long axis, reaching a height of 2.4 m (7.9 ft). The outside walls were approximately 2.1 m (6.9 ft) in height. The slope of the ceiling was approximately 8.4°. The doors to Bedroom #3 and the bathroom were closed during all experiments.

Heat Release Rate: Although a load cell was used in the experiments to measure the mass-loss rate of the fuel package, the mass-loss data were not reliable enough to reconstruct the HRR curves for each test. Instead, the HRR curves were determined by approximating the fire growth using a *t*-squared ramp. The parameters for the ramp were calibrated in FDS by using the temperature measured at the highest thermocouple in the tree (2 cm (0.8 in) below the ceiling) in the fire room (Bedroom #1). A time offset was used to align the predicted ceiling thermocouple temperatures with the measured temperatures. This offset is reported as the time at which the *t*-squared ramp begins. The *t*-squared calibration parameters and time offsets for the HRR ramps are shown in Table 3-1. Additionally, the ignition source had a small effect on the measured ceiling thermocouple temperatures. Therefore, the size of the ignition source was approximated as either 3 kW or 7 kW and the time offset of the ignition source was also calibrated by using the measured ceiling thermocouple temperatures.

Measurements: Groups of smoke alarms were located in the room of fire origin, at least one bedroom, and in a central location. Five stations (Station A through Station E) containing smoke-alarm arrays were mounted parallel to the ceiling.

Please see the report “Performance of Home Smoke Alarms Analysis of the Response of Several Available Technologies in Residential Fire Settings” (Bukowski et al., 2008) for details concerning the NIST Smoke-Alarm Experiments.

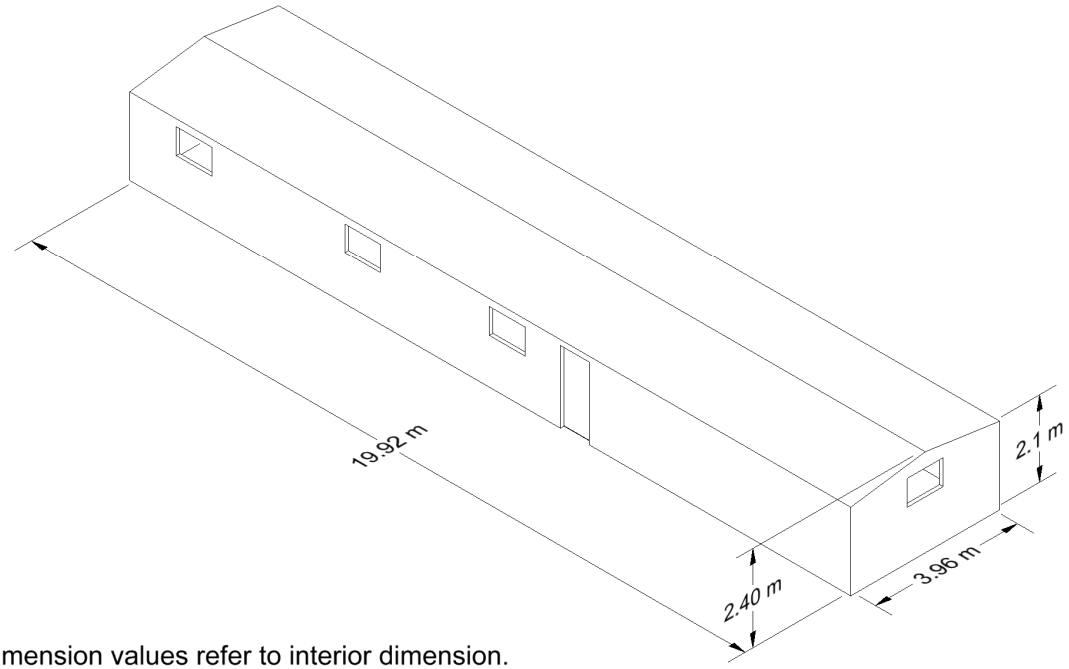

Notes:
1. All dimension values refer to interior dimension.
2. The letters A-E refer to detector locations.
3. All walls are 10 cm thick.
4. All exterior doors and windows were closed during testing.
5. Doors to Bath and Bedroom #3 closed during testing.

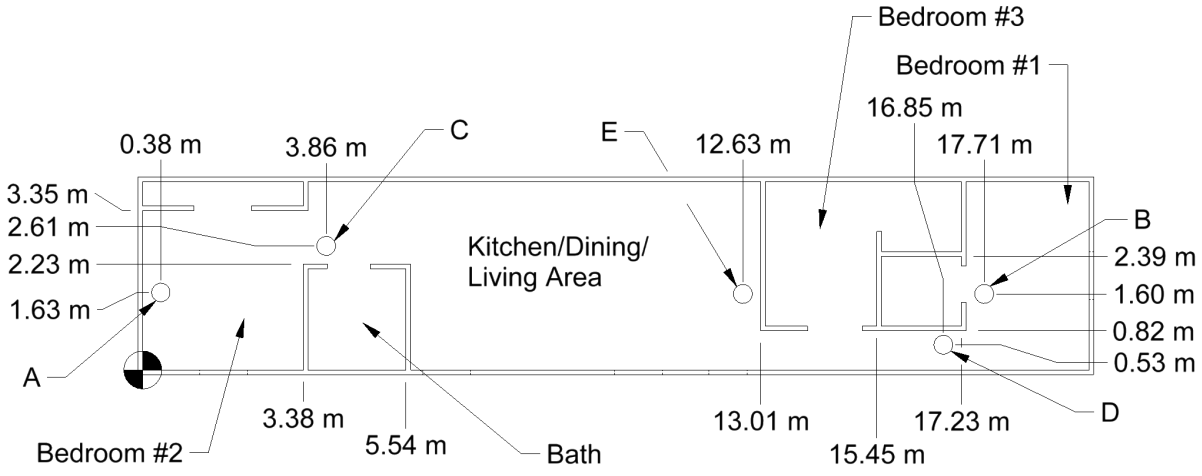

Figure 3-8. Drawing of the manufactured home used in the NIST Smoke-Alarm Tests.

Table 3-1. Parameters for the NIST Home Smoke-Alarm Experiments.

Test No.	Fire Source	Fire Location	HRR (kW)	Ramp Time (s)	Time Offset (s)
SDC02	Chair	Living Room	150	180	20
SDC05	Mattress	Bedroom #1	200	180	20
SDC07	Mattress	Bedroom #1	350	180	50
SDC10	Chair	Living Room	150	180	40
SDC33	Chair	Living Room	100	180	10
SDC35	Chair	Living Room	100	180	10
SDC38	Mattress	Bedroom #1	120	180	25
SDC39	Mattress	Bedroom #1	200	180	25

3.1.10 SP Adiabatic Surface-Temperature Experiments

In 2008, three compartment experiments were performed at SP Technical Research Institute of Sweden under the sponsorship of Brandforsk, the Swedish Fire Research Board (Wickström et al., 2009). The objective of the experiments was to demonstrate how plate thermometer measurements in the vicinity of a simple steel beam can be used to supply the boundary conditions for a multidimensional heat-conduction calculation for the beam.

Geometry: The experiments were performed inside a standard compartment designed for corner fire testing. The compartment is 3.6 m (11.8 ft) deep, 2.4 m (7.9 ft) wide and 2.4 m (7.9 ft) high and includes a door opening measuring 0.8 m (2.6 ft) by 2.0 m (6.6 ft) (Figure 3-9). The room was constructed of 20-cm-thick (0.7-ft-thick) lightweight concrete blocks with a density of 600 kg/m^3 ± 100 kg/m^3. A single steel beam was suspended 20 cm (0.7 ft) below the ceiling along the centerline of the compartment.

Heat Release Rate: The fire was fueled by a propane burner with a constant HRR of 450 kW. The top of the burner, with a square opening measuring 0.3 m (1 ft) by 0.3 m (1 ft), was placed 0.65 m (2.1 ft) above the floor, 2.5 cm (1 in) from the walls. The radiative fraction was assumed to be 0.35.

Measurements: There were three measurement stations along the beam at lengths of 0.9 m (2.9 ft) (Position A), 1.8 m (5.9 ft) (Position B), and 2.7 m (8.9 ft) (Position C) from the far wall where the fire was either positioned in the corner (Tests 1 and 2) or the center (Test 3). The beam in Test 1 was a rectangular steel tube filled with an insulation material. The beam in Tests 2 and 3 was an I-beam.

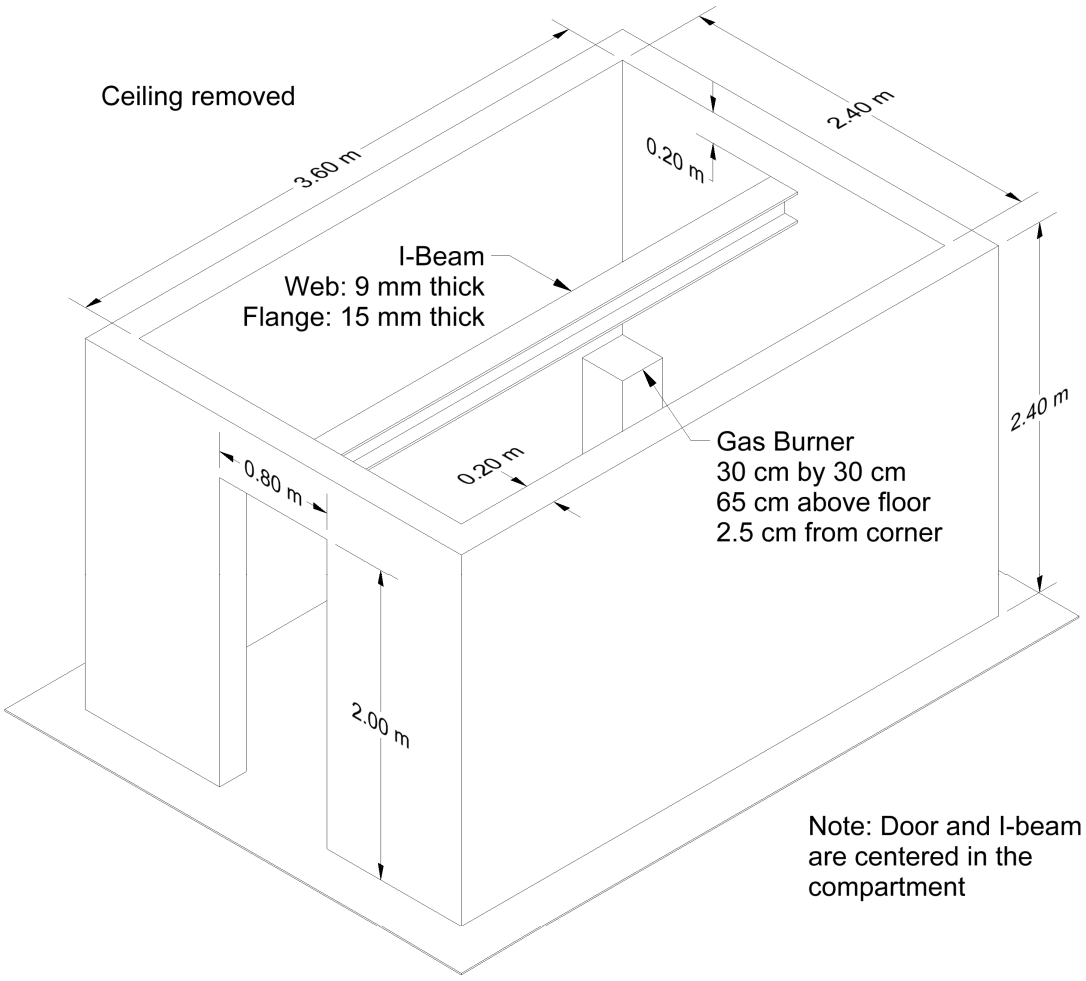

Figure 3-9. Drawing of SP AST Experiment.

A second series of experiments involving plate thermometers was carried out in 2011 (Sjöström et al., 2012). A vertical steel column 6 m (19.7 ft) long and 0.2 m (0.7 ft) in diameter was positioned in the center of 1.1 m (3.6 ft) and 1.9 m (6.2 ft) diesel-fuel and 1.1 m (3.6 ft) heptane pool fires. Gas, plate thermometer, and surface temperatures were measured at heights of 1 m (3.3 ft), 2 m (6.6 ft), 3 m (9.8 ft), 4 m (13.1 ft), and 5 m (16.4 ft) above the pool surface. These experiments are notable because the column is partially engulfed in flames.

Please see the reports “Verification Fire Tests on Using the Adiabatic Surface Temperature for Predicting Heat Transfer” (Wickström et al., 2009) and “Large Scale Test on Thermal Exposure to Steel Column Exposed to Pool Fires” (Sjöström et al., 2012) for details concerning the SP Adiabatic Surface-Temperature Experiments.

3.1.11 Steckler Compartment Experiments

Steckler, Quintiere, and Rinkinen (1979) performed a set of 55 compartment fire tests at NBS in 1979.

Geometry: The compartment was 2.8 m (9.2 ft) by 2.8 m (9.2 ft) by 2.13 m (7 ft) high, with a single door of various widths, or alternatively a single window with various heights (Figure 3-10).

Wall Linings: The test report does not include a detailed description of the compartment. However, an internal report by the test sponsor, Armstrong Cork Company, reports that the compartment floor was composed of 19 mm (0.75 in) calcium silicate board on top of 12.7 mm (0.5 in) plywood on wood joists. The walls and ceiling consisted of 12.7 mm (0.5 in) ceramic fiber insulation board over 0.66-mm (0.03 in) aluminum sheet attached to wood studs.

Heat Release Rate: A methane burner 0.3 m (1 ft) in diameter was used to generate fires with heat-release rates of 31.6 kW, 62.9 kW, 105.3 kW, and 158 kW. The radiative fraction was assumed to be 0.20.

Measurements: Vertical profiles of velocity and temperature were measured in the doorway, along with a single vertical profile of temperature within the compartment.

Please see the report “Flow Induced by Fire in a Compartment” (Steckler et al., 1979) for details concerning the Steckler Compartment Experiments.

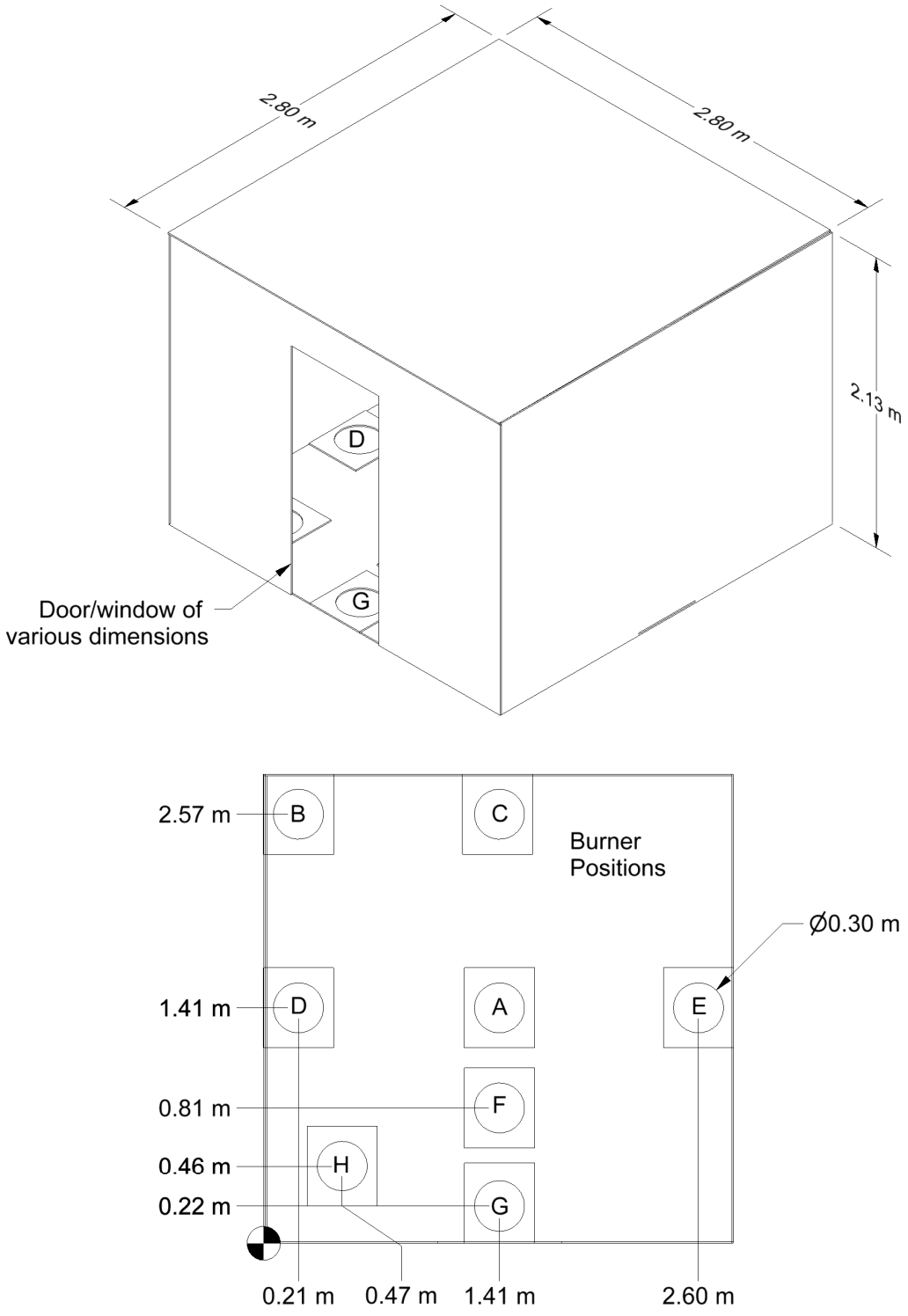

Figure 3-10. Drawing of Steckler Compartment.

3.1.12 UL/NIST Vent Experiments

In 2012, the Fire Fighting Technology Group at NIST conducted experiments at Underwriters Laboratories (UL®) in Northbrook, Illinois, to assess the change in compartment temperature caused by the opening of one or two 1.2 m (3.9 ft) square ceiling vents (Opert, 2012).

Geometry: The 6.1 m (20 ft) by 4.3 m (14.1 ft) by 2.4 m (7.9 ft) compartment with a single door opening is shown in Figure 3-11. Two vents, nominally 1.3 m (4.3 ft) by 1.3 m (4.3 ft), were positioned side by side at the center of the ceiling.

Heat Release Rate: The natural-gas fires ranged in size from 500 kW to 2 MW. The radiative fraction was assumed to be 0.25, typical of large natural-gas fires.

Ventilation: The two vents were opened and closed in such a way that during the four experiments there were 31 discrete time intervals in which model predictions could be compared to quasi-steady conditions.

Measurements: The compartment contained two vertical arrays of thermocouples; the door and vents were instrumented with thermocouples and bidirectional velocity probes. Only the thermocouple measurements were used to assess the HGL and ceiling-jet temperatures and HGL depth.

Please see the report “Assessment of Natural Vertical Ventilation for Smoke and Hot Gas Layer Control in a Residential Scale Structure” (Opert, 2012) for details concerning the UL/NIST Vent Experiments.

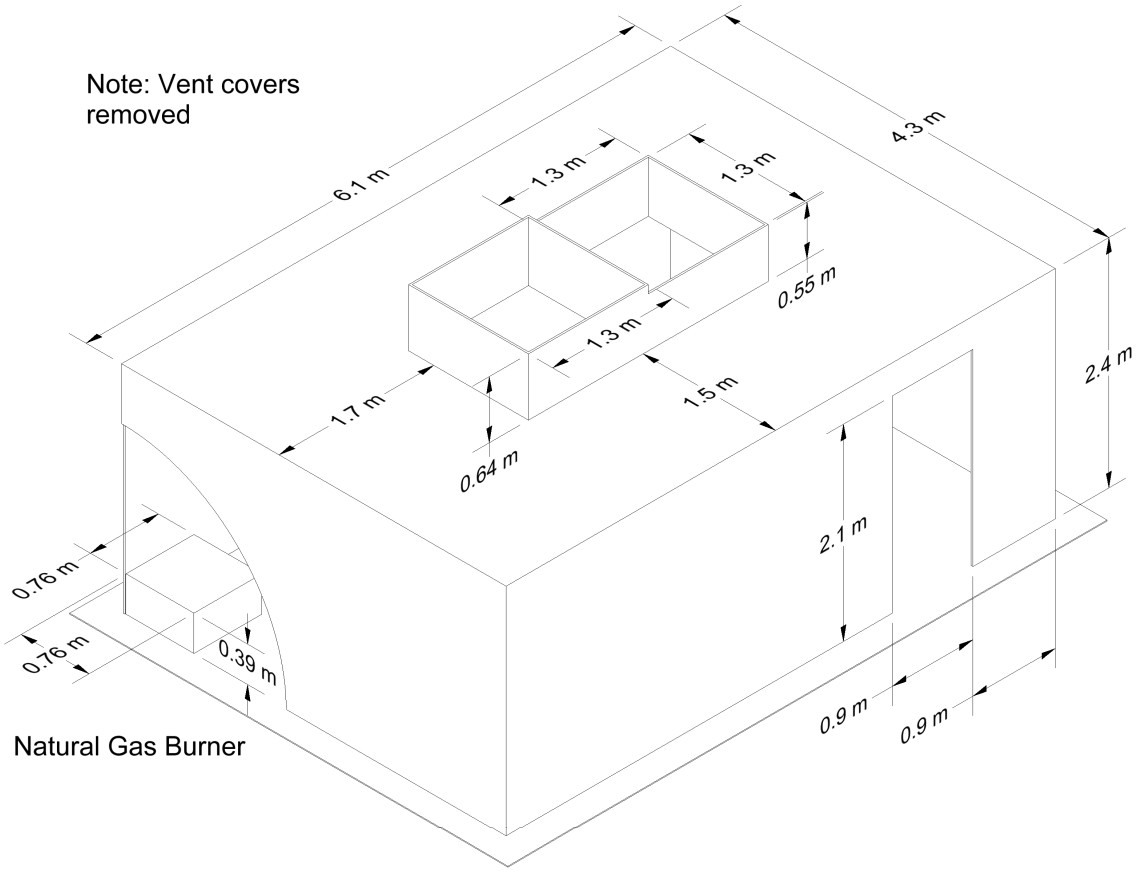

Figure 3-11. Drawing of UL/NIST Experiment.

3.1.13 UL/NFPRF Sprinkler, Vent, and Draft Curtain Experiments

In 1997, a series of 34 heptane spray burner experiments was conducted at the Large Scale Fire Test Facility at Underwriters Laboratories (UL) in Northbrook, Illinois (Sheppard and Steppan, 1997). The experiments were divided into two test series. Series I consisted of twenty-two 4.4 MW fire experiments. Series II consisted of twelve 10 MW fire experiments. The objective of the experiments was to characterize the temperature and flow field for fire scenarios with a controlled heat-release rate in the presence of sprinklers, draft curtains, and smoke and heat vents.

Geometry: The Large Scale Fire Test Facility at UL contains a 37 m (120 ft) by 37 m (120 ft) main fire test cell, equipped with a 30.5 m (100 ft) by 30.5 m (100 ft) adjustable height ceiling. The ceiling was raised to a height of 7.6 m (24.9 ft) and instrumented with thermocouples and other measurement devices. Sheet metal, 1.2 mm (0.05 in) thick and 1.8 m (5.9 ft) deep, was suspended from the ceiling for 16 of the 22 Series I tests, enclosing an area of about 450 m^2 (4850 ft^2) and 49 sprinklers. The curtains were in place for all of the Series II tests.

Wall Linings: The ceiling was constructed of 0.6 m (2 ft) by 1.2 m (3.9 ft) by 1.6 cm (0.6 in) UL fire-rated Armstrong Ceramaguard® (Item 602B) ceiling tiles. The manufacturer reported the

thermal properties of the material to be: specific heat 753 J/(kg·K), thermal conductivity 0.0611 W/(m·K), and density 313 kg/m^3.

Heat Release Rate: The heptane spray burner consisted of a 1 m (3.3 ft) by 1 m (3.3 ft) square of 1.3 cm (0.5 in) pipe supported by four cement blocks 0.6 m (2 ft) off the floor. Four atomizing spray nozzles were used to provide a free spray of heptane that was then ignited. For all but one of the Series I tests, the total heat-release rate from the fire was manually ramped up following a *t*-squared curve to a steady-state in 75 s (150 s was used in Test I-16). The fire was ramped to 10 MW in 75 s for the Series II tests. The fire growth curve was followed until a specified fire size was reached or the first sprinkler activated. After either of these events, the fire size was kept at that level until conditions reached roughly a steady state (i.e., the temperatures recorded near the ceilings remained steady and no more sprinkler activations occurred).

The heat release rate from the burner was confirmed by placing it under the large product calorimeter at UL, ramping up the flow of heptane in the same manner as in the tests, and measuring the total and convective heat-release rates. It was found that the convective heat-release rate was 0.65 ± 0.02 of the total. This corresponds to a radiative fraction of 0.35.

Sprinklers: Central ELO-231 (Extra Large Orifice) uprights were used for all the tests. The orifice diameter of this sprinkler is reported by the manufacturer to be nominally 1.6 cm (0.6 in); the reference activation temperature is reported by the manufacturer to be 74°C (165°F). The RTI (Response Time Index) and C-factor (Conductivity factor) were reported by UL to be 148 $(m \cdot s)^{0.5}$ and 0.7 $(m/s)^{0.5}$ respectively. When installed, the sprinkler deflector was located 8 cm (3 in) below the ceiling. The thermal element of the sprinkler was located 11 cm (4 in) below the ceiling. The sprinklers were installed with nominal 3 m by 3 m (exact 10 ft by 10 ft) spacing in a system designed to deliver a constant 0.34 L/(s·m^2) discharge density when supplied by a 131-kPa (19-psi) discharge pressure.

Ventilation: UL listed double-leaf fire vents with steel covers and a steel curb were installed in the adjustable-height ceiling. Each vent was designed to open manually or automatically. The vent doors were recessed into the ceiling by about 0.3 m (1 ft).

Please see the report “An Experimental Data Set for the Accuracy Assessment of Room Fire Models” (McGrattan et al., 1998) for details concerning the UL/NFPRF Sprinkler, Vent, and Draft Curtain Experiments.

3.1.14 U.S. Navy High-Bay Hangar Experiments

The U.S. Navy (USN) sponsored a series of 33 experiments within two hangars examining fire detection and sprinkler activation in response to spill fires in large enclosures. Experiments were conducted using JP-5 and JP-8 fuels in two Navy high-bay aircraft hangars located in the Naval Air Stations in Barber’s Point, Hawaii, and Keflavik, Iceland (Gott et al., 1997). Eleven experiments were conducted in Hawaii, twenty-two in Iceland.

Geometry: The Hawaii experiments were conducted in a 15 m high (49 ft high) hangar measuring 97.8 m (321 ft) in length and 73.8 m (242 ft) in width. The Iceland experiments were conducted under a 22 m (72 ft) barrel-vault ceiling in a hangar measuring 45.7 m (150 ft) by 73.8 m (242 ft).

Heat Release Rate: The fires in Hawaii were fueled by jet fuel in pans ranging from 0.09 m^2 (1 ft^2) to 4.9 m^2 (52.7 ft^2) in area with heat-release rates varying from 100 kW to 7.7 MW. The burner was placed in the center of the room on a scale. The fires in Iceland were fueled by JP-5

and JP-8, ranging in size from 0.06 m^2 (0.6 ft^2) to 20.9 m^2 (225 ft^2) and the heat release rates ranged from 100 kW to approximately 33 MW. The radiative fraction was assumed to be 0.35.

Measurements: Both facilities were equipped with a number of detection devices, including thermocouples, electronic smoke and spot heat detectors, projected-beam smoke detectors, combination UV/IR optical flame detectors, and line-type heat detectors, as well as sprinklers. Measurements were recorded at a large number of locations, allowing a thorough profile of compartment behavior.

Please see the report "Analysis of High Bay Hanger Facilities for Fire Detection Sensitivity and Placement" (Gott et al., 1997) for details concerning the U.S. Navy High Bay Hangar Experiments.

3.1.15 Vettori Ceiling Sprinkler Experiments

Vettori (1998) analyzed a series of 45 experiments conducted at NIST that were intended to compare the effects of different ceiling configurations on the activation times of quick-response residential pendent sprinklers. The test parameters consisted of two ceiling configurations, three fire-growth rates, and three burner locations—a total of 18 unique test configurations with sets of two or three replicates each.

Geometry: A diagram of the test structure is displayed in Figure 3-12. The ceiling was either obstructed, with parallel beams 3.8 cm (1.5 in) wide by 0.24 m (0.8 ft) deep placed 0.41 m (1.3 ft) on center, or smooth, in which the beams were covered by a sheet of gypsum board.

Heat Release Rate: The fire was fueled by a computer-controlled methane gas burner to mimic a standard *t*-squared fire-growth rate with either a slow, medium, or fast ramp-up. Tests were conducted with the burner placed in a corner of the room, against an adjacent wall, or in a location removed from any wall.

Measurements: Measurements were taken to record sprinkler activation time, temperatures at varying heights and locations within the room, and ceiling-jet velocities at several other locations.

Vettori (2003) analyzed a similar set of sprinkler experiments involving ceilings of various slopes. Because the empirical correlations and zone models lack the necessary physics to model these experiments, only the FDS results are included in this study.

Please see the reports "Effect of a Beamed, Sloped, and Sloped Beamed Ceiling on the Activation Time of a Residential Sprinkler" (Vettori, 1998) and "Effect of an Obstructed Ceiling on the Activation Time of a Residential Sprinkler" (Vettori, 2003) for details concerning the Vettori Flat Ceiling Sprinkler Experiments.

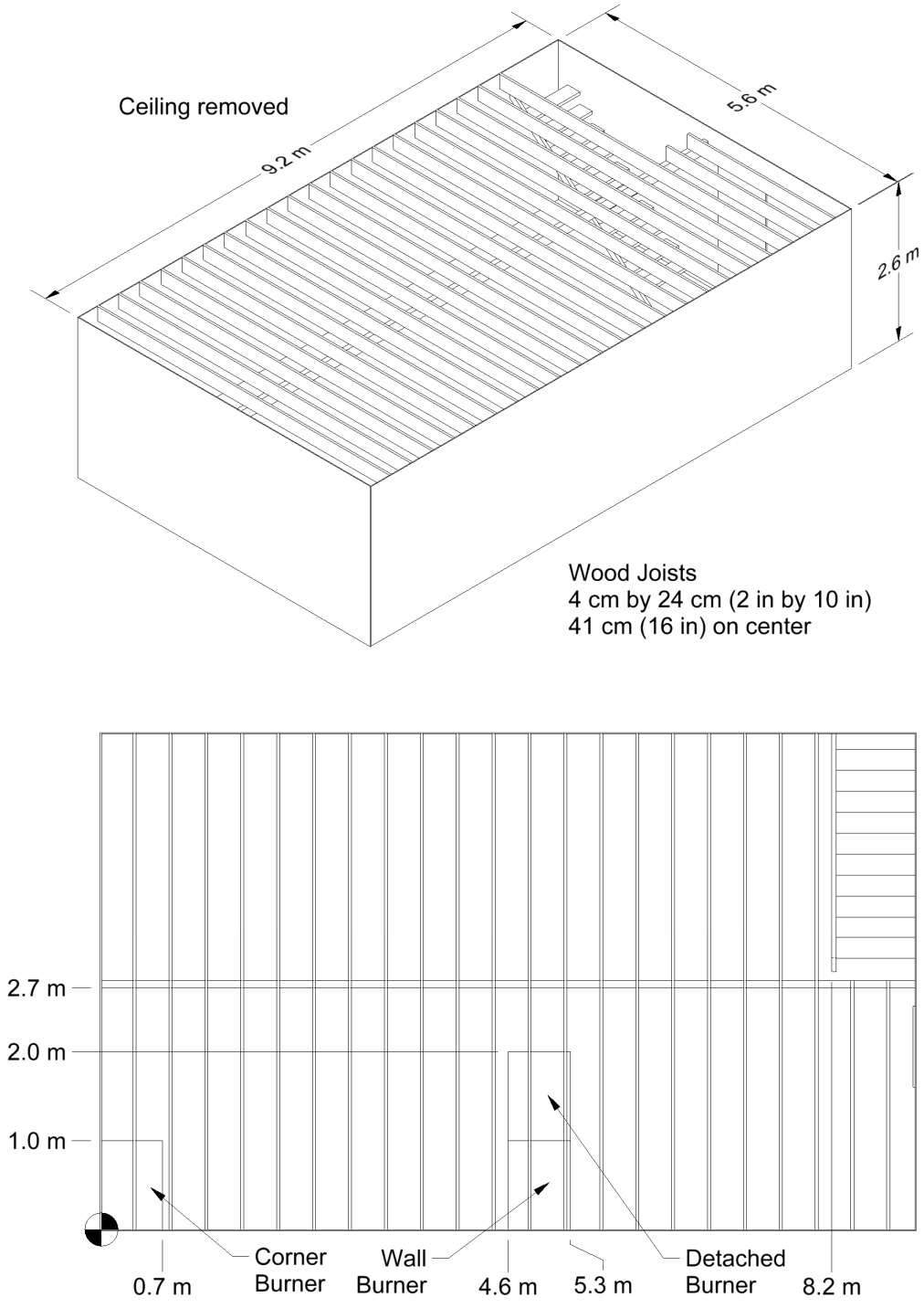

Figure 3-12. Drawing of Vettori Flat Ceiling Sprinkler Experiments.

3.1.16 VTT Large Hall Experiments

Hostikka et al. (2001) studied the movement of smoke in a large hall with a sloped ceiling.

Geometry: The tests were conducted inside the VTT Technical Research Centre of Finland Fire Test Hall, with dimensions of 19 m (62 ft) high by 27 m (87 ft) long by 14 m (46 ft) wide (Figure 3-13). The walls and ceiling of the test hall consisted of a 1-mm-thick (0.04-in-thick) layer of sheet metal on top of a 5 cm (2 in) layer of mineral wool. The floor was constructed of concrete. The report does not provide thermal properties of these materials.

Heat Release Rate: The fires were fueled by a single circular pan of heptane with its center located 16 m (52.5 ft) from the west wall and 7.2 m (23.6 ft) from the south wall. The HRR ranged from 2 MW to 4 MW. The pan had a diameter of 1.2 m (3.9 ft) for Case 1 and 1.6 m (5.2 ft) for Cases 2 and 3. In each case, the fuel surface was 1 m (3.3 ft) above the floor. The trays were placed on load cells and the HRR was calculated from the mass-loss rate. The radiative fraction was assumed to be 0.35, typical of liquid hydrocarbon fires.

Natural Ventilation: In Cases 1 and 2, all doors were closed and ventilation was restricted to infiltration through the building envelope. Precise information on air infiltration during these tests is not available. Personnel who conducted the experiments recommend a leakage area of about 2 m^2 (21.5 ft^2), distributed uniformly throughout the enclosure. By contrast, in Case 3, the doors located in each end wall (Doors 1 and 2 respectively) were open to the external ambient environment. These doors were each 0.8 m (2.6 ft) wide by 4 m (13.1 ft) high and were located in such a way that their centers were 9.3 m (30.5 ft) from the south wall.

Mechanical Ventilation: The test hall had a single mechanical exhaust duct, located in the roof space, running along the center of the building. This duct had a circular section with a diameter of 1 m (3.3 ft), and opened horizontally to the hall at a distance of 12 m (39.4 ft) from the floor and 10.5 m (34.4 ft) from the west wall. Mechanical exhaust ventilation was operational for Case 3, with a constant-volume flow rate of 11 m^3/s (388 ft^3/s) drawn through the exhaust duct.

Measurements: Three vertical arrays of thermocouples, plus two thermocouples in the plume, were used to measure the HGL temperature, HGL height, and plume temperature. The HGL temperature and height were reduced from an average of the three thermocouple arrays.

Please see the report “Experimental Study of the Localized Room Fires” (Hostikka, et al., 2001) for details concerning the VTT Large Hall Experiments.

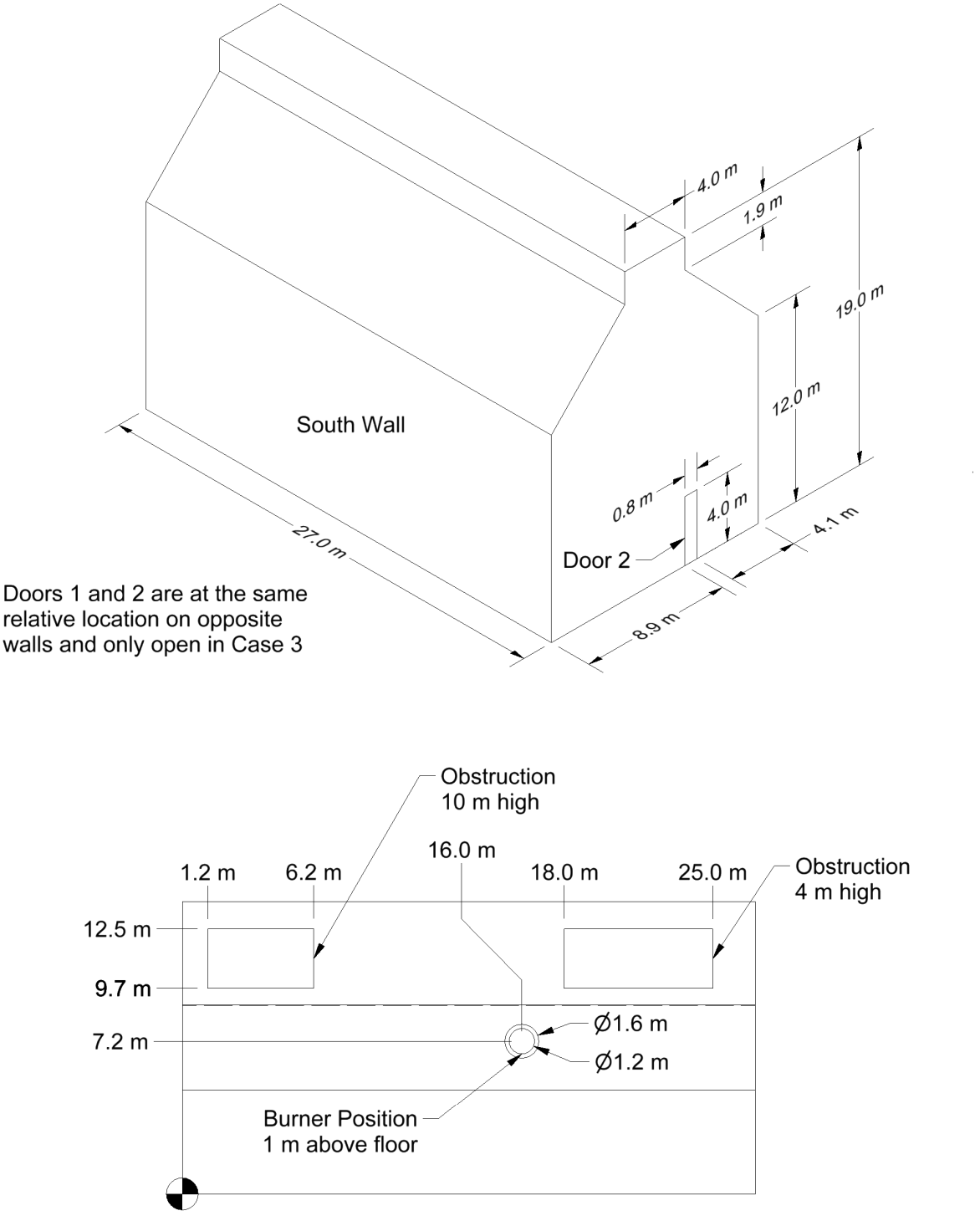

1

2 **Figure 3-13. Drawing of VTT Test Hall.**

3.1.17 WTC Spray Burner Experiments

As part of its investigation of the World Trade Center (WTC) disaster, the Building and Fire Research Laboratory at NIST conducted several series of fire experiments both to gain insight into the observed fire behavior and to validate FDS for use in reconstructing the fires. The first series of experiments involved a relatively simple compartment with a liquid spray burner and various structural elements with varying amounts of sprayed fire-resistive materials (Hamins et al., 2005).

Geometry: A diagram of the compartment is shown in Figure 3-14. The overall enclosure was rectangular, as were the vents and most of the obstructions. The compartment walls and ceiling were made of 2.5 cm (1 in) thick calcium silicate board. The manufacturer provided the thermal properties of the material used in the calculation. The density was 737 kg/m^3 and the conductivity was 0.12 W/m/K. The specific heat ranged from 1.17 kJ/kg/°K at 93°C (200°F) to 1.42 kJ/kg/°K at 425°C (800°F). This value was assumed for higher temperatures. The steel used to construct the column and truss flanges was 0.6 cm (0.25 in) thick. The density of the steel was assumed to be 7,860 kg/m^3 and its specific heat was assumed to be 0.45 kJ/kg/°K.

Heat Release Rate: Spray nozzles were used to inject liquid fuel downward into a 1 m (3.3 ft) by 2 m (6.6 ft) steel pan. Two fuels were used in the experiments. The properties of the fuels were obtained from measurements made on a series of unconfined burns that are cited in the test report. The first fuel was a blend of isomers of heptane, C_7H_{16}. Its soot yield was measured to be 1.5 percent. The second fuel was a mixture (40 percent to 60 percent by volume) of toluene, C_7H_8, and heptane. The radiative fraction for the heptane blend was 0.44; for the heptane/toluene mixture it was 0.39.

Ventilation: The compartment was naturally ventilated by way of openings at either end of the compartment. The air moved from the lower towards the higher openings.

Measurements: The instrumentation consisted of vertical arrays of thermocouples, gas sampling probes for oxygen, carbon dioxide, and carbon monoxide concentrations, smoke concentration, unprotected and protected steel temperatures, exterior and interior wall temperatures, heat flux, and velocity.

Please see the report “Federal Building and Fire Safety Investigation of the World Trade Center Disaster; Experiments and Modeling of Structural Steel Elements Exposed to Fire” (Hamins et al., 2005) for details concerning the WTC Spray Burner Experiments.

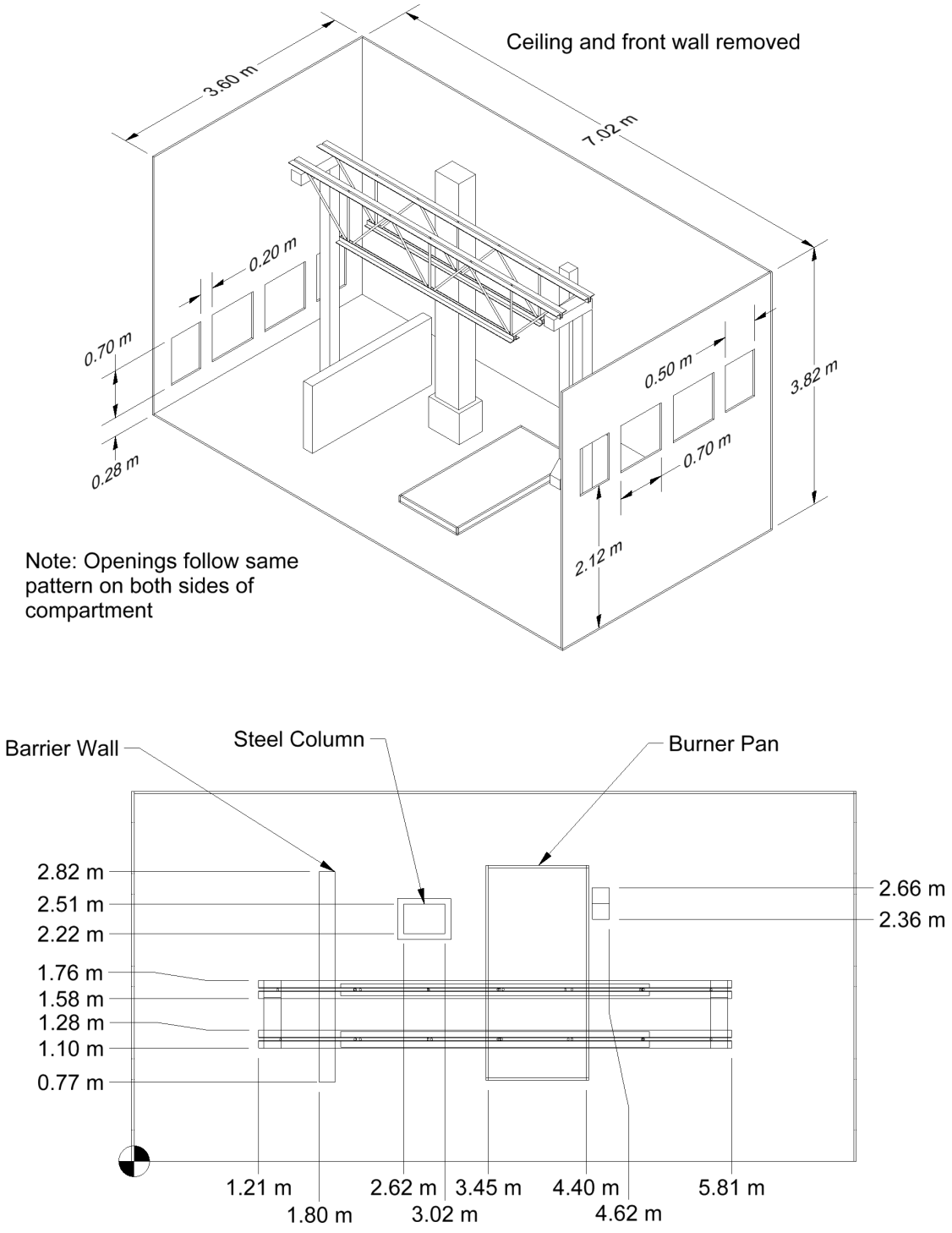

Figure 3-14. Drawing of the WTC Experiment.

3.2 Summary of Experimental Parameters

Table 3-2 provides a summary of the major parameters for all the experiments used in the validation study. The basic parameters are defined as follows:

- $\dot{Q}$ The heat release rate of the fire (kW)
- D The diameter of the fire (m); for non-circular burners, $D \cong \sqrt{4A/\pi}$
- H The height of the compartment (m)
- L The length of the compartment (m); i.e., the longer lateral dimension
- W The width of the compartment (m); i.e., the shorter lateral dimension
- L_f The length of the flame (m)
- r_{cj} The radial distance from the plume centerline to a ceiling target or detector (m)
- r The distance between the fire and a target (m)
- φ Equivalency ratio, which relates the energy release of the fire to the energy release that can be supported by the mass flow rate of oxygen into the compartment

To characterize the range of applicability of the validation study, Table 3-3 lists various normalized parameters that can be used to determine whether a modeled fire scenario fits within the range of the experimental parameters. These parameters express, for instance, the size of the fire relative to the size of the room or the relative distance from the fire to critical equipment. This information is important because typical fire models are not designed for fires that are very small or very large in relation to the volume of the compartment or the ceiling height. For a given set of experiments and NPP fire scenarios, the user can calculate the relevant normalized parameters. These parameters will either be inside, outside, or on the margin of the validation parameter space.

Table 3-2. Summary of major experiment parameters.

Experiment	Experiment Parameters									
	$\dot{Q}$ (kW)	D (m)	H (m)	$\dot{Q}^*$	L_f/H	φ	W/H	L/H	r_{cj}/H	r/D
ATF Corridors	50 to 500	0.5	2.4	0.3 to 3.3	0.3 to 0.9	0.0 to 0.1	0.8	7.1	0.8 to 6.0	N/A
Fleury	100 to 300	0.3 to 0.6	Open	0.3 to 5.5	Open	Open	Open	Open	Open	0.8 to 8
FM/SNL	470 to 2000	0.9	6.1	0.6 to 2.4	0.3 to 0.6	0.0 to 0.2	2.0	3.0	0.2 to 0.3	N/A
iBMB*	3500, 400	1.13, 0.79	5.7, 5.6	2.4, 0.7	0.8, 0.3	0.6, 0.1	0.6	0.6	N/A	N/A
LLNL	50 to 400	0.6	4.5	0.2 to 1.5	0.1 to 0.4	0.1 to 0.4	0.9	1.3	0.3 to 1.0	N/A
NBS Multi-Room	110	0.3	2.4	1.5	0.5	0.0	1.0	5.1	N/A	N/A
NIST/NRC	350 to 2200	1.0	3.8	0.3 to 2.0	0.3 to 1.0	0.0 to 0.3	1.9	5.7	0.3 to 2.1	2 to 4
SP AST	450	0.3	2.4	6.1	0.9	0.1	1.0	1.5	N/A	N/A
Steckler	32 to 158	0.3	2.1	0.8 to 3.8	0.3 to 0.7	0.0 to 0.5	1.3	1.3	N/A	N/A
UL/NFPRF	4400 to 10,000	1.0	7.6	4.0 to 9.1	0.7 to 1.0	N/A	4.9	4.9	0.6 to 3.9	N/A
UL/NIST Vents	500 to 2000	0.9	2.4	0.7 to 2.6	0.8 to 1.6	0.2 to 0.6	1.8	2.5	1.0 to 2.3	N/A
USN Hawaii	100 to 7700	0.3 to 2.5	15	0.7 to 1.3	0.1 to 0.4	N/A	4.9	6.5	0 to 1.2	N/A
USN Iceland	100 to 15,700	0.3 to 3.4	22	0.7 to 1.3	0.0 to 0.3	N/A	2.1	3.4	0 to 1.0	N/A
Vettori Flat	1055	0.7	2.6	2.5	1.1	0.3	2.1	3.5	0.8 to 2.9	N/A
Vettori Sloped	1055	0.7	2.5	2.5	1.2	0.3	2.2	2.9	N/A	N/A
VTT Hall	1860 to 3640	1.2 to 1.6	19	1.0 to 1.1	0.2	0 to 0.09	1.0	1.4	0 to 0.6	N/A
WTC	1970 to 3240	1.6	3.8	0.6 to 0.9	0.8 to 1.1	0.3 to 0.5	0.9	1.8	0 to 0.8	0.3 to 1.3

* Where two values are present, the first is for the test from Benchmark Exercise #4 and the second is for the test from Benchmark Exercise #5.

Table 3-3. Summary of normalized experimental parameters

Quantity	Normalized Parameter	Definition	Experiment Range
Fire Froude Number	$\dot{Q}^* = \dfrac{\dot{Q}}{\rho_\infty c_p T_\infty D^2 \sqrt{gD}}$	Ratio of inertial and buoyancy-induced velocities. A typical accidental fire has a Froude number of order 1. Momentum-driven fire plumes, like jet flares, have relatively high values. Buoyancy-driven fire plumes have relatively low values.	0.2 to 9.1
Flame Length Ratio	$\dfrac{H_\mathrm{f} + L_\mathrm{f}}{H}$ $\dfrac{L_\mathrm{f}}{D} = 3.7\,\dot{Q}^{*2/5} - 1.02$	A convenient parameter for expressing the "size" of the fire relative to the height of the compartment. A value of 1 means that the flames reach the ceiling.	0.0 to 1.6
Ceiling-Jet Distance Ratio	$\dfrac{r_\mathrm{cj}}{H}$	Ceiling-jet temperature and velocity correlations use this ratio to express the horizontal distance from target to plume.	0.0 to 6.0
Equivalence Ratio	$\varphi = \dfrac{\dot{Q}}{\Delta H_{\mathrm{O}_2} \dot{m}_{\mathrm{O}_2}}$ $\dot{m}_{\mathrm{O}_2} = \begin{cases} 0.23 \times \dfrac{1}{2} A_0 \sqrt{H_0}\ \text{(Natural)} \\ 0.23\,\rho_\infty \dot{V}\ \text{(Mechanical)} \end{cases}$	The equivalence ratio relates the energy release rate of the fire to the energy release that can be supported by the mass flow rate of oxygen into the compartment, $\dot{m}_{\mathrm{O}_2}$. The fire is considered over- or underventilated based on whether φ is less than or greater than 1 respectively.	0.0 to 0.6
Compartment Aspect Ratio	L/H or W/H	This parameter indicates the general shape of the compartment.	0.8 to 7.1
Radial Distance Ratio	$\dfrac{r}{D}$	This ratio is the relative distance from a target to the fire. It is important when calculating the radiative heat flux.	0.3 to 8

3.3 Experimental Uncertainty

The difference between a model's prediction and an experiment's measurement is a combination of three components: (1) uncertainty in the measurement of the predicted quantity, (2) uncertainty in the model input parameters, and (3) uncertainty in the model physics and numerics. The first two components are related to uncertainty in the measured input and output quantities. For example, consider the HGL temperature. First, the thermocouple measurements used to calculate the HGL temperature have uncertainty. Second, the measurement of the heat-release rate of the fire has uncertainty, and this uncertainty affects the predicted HGL temperature. Third, the model itself, including its physical assumptions and numerical approximations, has uncertainty. The objective of the validation study is to quantify this third component, the *model uncertainty*. To do this, the first two components of uncertainty related to the experimental measurements must be quantified. The combination of these two, the *experimental uncertainty*, is the objective of this section.

For many of the test series considered in this report, the uncertainty of the measurements was not documented in the experiment reports. Instead, estimates of measurement uncertainty are made based on those few experiments that do include uncertainty estimates, and this information is supplemented by engineering judgment.

In the following two subsections, each component of the experimental uncertainty is considered separately. First, the uncertainty in the measurement of the predicted quantity of interest, such as the surface temperature of the compartment, is considered. Second, the uncertainties of the most important input parameters are propagated through simple models to quantify their effect on the predicted quantity. Then, the uncertainties are combined through simple quadrature to estimate the total experimental uncertainty.

Note that in this report, all uncertainties are expressed in relative form, as a percentage. The uncertainty of a measurement is a combination of the *epistemic uncertainty* associated with the various underlying measurements and assumptions and the *aleatory uncertainty* associated with random variations in the experiment. Following the recommended guidelines for evaluating and expressing the uncertainty of measurements (Taylor and Kuyatt, 1994), the epistemic and aleatory uncertainty values are combined through quadrature resulting in a *combined relative standard uncertainty*.

3.3.1 Measurement Uncertainty

Because most of the experiments described in Section 3.1 were reported with little or no information about the uncertainty of the measurements, much of this section is based on the uncertainty analysis contained in the test report of the NIST/NRC Compartment Fire Experiments, NUREG/CR-6905 (2003). The types of measurements described in this report are the ones most commonly used in large-scale fire experiments. They include thermocouples for gas- and surface-temperature measurements, heat-flux gauges, smoke and gas analyzers, and pressure sensors.

Note that the experimental uncertainties reported in NUREG/CR-6905 are reported in the form of 95 percent confidence intervals, or two standard deviations of the reported value. In this report, however, the uncertainty of all measurements and model predictions are reported as a single standard deviation.

3.3.1.1 Thermocouples

Thermocouples are used to measure both gas and surface temperatures. They come in a variety of sizes and are constructed of different types of metals. Some are shielded or aspirated to limit the influence of thermal radiation from remote sources. In NUREG/CR-6905 (2003), Hamins et al. estimate the uncertainty of the various thermocouple measurements. Estimates of the combined relative standard uncertainty fall in a range between 2.5 percent and 7.5 percent. Because it is not possible to analyze the thousands of thermocouple measurements made in the experiments reported in Section 3.1, the relative standard uncertainty applied to all thermocouple measurements is 5 percent.

3.3.1.2 Heat Flux Gauges

For the NIST/NRC Compartment Fire Experiments (NUREG/CR-6905, 2003), four types of heat-flux gauges were used, some of which measured the total heat flux and others of which measured only the radiation heat flux. The uncertainty associated with a heat-flux measurement depends on many factors, including gauge characteristics and the calibration conditions and accuracy, as well as the incident flux modes (convective, radiative, and/or conductive) (Bryant et al., 2003). Typically, the reported relative standard uncertainty of heat-flux gauges varies from about 2.5 percent to 5 percent, with the measurement uncertainty dominated by uncertainty in the calibration and repeatability of the measurement. For all of the experiments described in Section 3.1, a combined relative standard uncertainty of 5 percent is suggested.

3.3.1.3 Gas Analyzers

Gas concentrations were measured in two sets of experiments conducted at NIST, the NIST/NRC experiments (NUREG/CR-6905, 2003) and the WTC experiments (Hamins et al., 2005). The volume fractions of the combustion products, carbon monoxide (CO) and carbon dioxide (CO_2), were measured using gas sampling in conjunction with non-dispersive infrared analyzers, while the oxygen (O_2) volume fraction was typically measured using a paramagnetic analyzer. Gases were extracted through stainless steel or other types of lines and were pumped from the compartment and passed through the analyzers. For several reasons, water in the sample was typically filtered, so the reported results are denoted as “dry”. Analyzers were calibrated through the use of standard gas mixtures, with low relative uncertainties. Problems with the technique might involve instrument drift, analyzer response, incomplete and partial drying of sample gases, or (in the case in which drying is not used) undetermined amounts of water vapor in the oxygen cell, which result in inaccurate readings.

For the NIST/NRC experiments, the species were measured in both the upper and lower layers. The relative standard uncertainty in the measured values was about 2 percent for both the O_2 depletion and the CO_2 measurements. The largest contributors were the uncertainty in the composition of the calibration gas and the possibility of an undetermined amount of water vapor in the sample.

3.3.1.4 Smoke Light Extinction Calculation

The smoke concentration was measured in the NIST/NRC experiments (NUREG/CR-6905, 2003) using laser transmission at 632.8 nm. The reported mass concentration of smoke, m_s''', was computed using the following expression:

$$m_s''' = \frac{\ln(I_0/I)}{\varphi_s L} \tag{3-1}$$

where L is the path length, I and I_0 are the laser signal and reference signal respectively, and φ_s is the specific extinction coefficient, which has a nearly universal value of 8.7 m^2/g ± 5 percent for hydrocarbons (Mulholland and Croakin, 2000). The epistemic uncertainty of this measurement was reported to be 9 percent in NUREG/CR-6905, with the dominant contribution to the uncertainty coming from drift in the laser measurement. Repeatability of the smoke measurement was investigated for the NIST/NRC experiments. The mean difference between replicate measurements was about 11 percent. Therefore, combining the epistemic and aleatory uncertainties through quadrature leads to a relative standard uncertainty of 14 percent.

3.3.1.5 Pressure Gauges

The uncertainty in pressure measurements is typically small, but depends on the sensor type and calibration. In NIST/NRC experiments, the differential pressure gauge used was temperature-compensated, highly linear, and very stable. An estimate of the epistemic uncertainty was given as 0.5 percent.

3.3.1.6 Oxygen-Consumption Calorimeters

For all of the experiments described in Section 3.1, the HRR is determined either by oxygen-consumption calorimetry or by the mass-loss rate multiplied by the fuel heat of combustion. The accuracy of each method varies roughly between 2.5 percent, where the fire is small and the fuel stoichiometry is well understood, and 13 percent, where the fire is large or the smoke is not completely captured or the fuel stoichiometry is not well understood. In NUREG/CR-6905, the relative standard uncertainty of a 2-MW heptane spray fire is estimated to be 7.5 percent. It is assumed that the uncertainty of the HRR for the other experiments is comparable.

3.3.1.7 Sprinkler and Detector Activation Times

There are a variety of ways to measure the time at which a sprinkler actuates, a cable shorts, or a detector alarms. For example, a thermocouple registers a rapid decrease in temperature when a sprinkler opens. Changes in the electrical response of a detector or cable are essentially instantaneous. For these reasons, the uncertainty in the reported activation or failure time of various devices is, for all practical purposes, zero.

3.3.2 Propagation of Input Parameter Uncertainty

The empirical correlations described in Section 4.1 provide a convenient way to assess the propagation of the uncertainty of the model input parameters. The more complex fire models might require dozens of physical and numerical input parameters for a given fire scenario. However, only a few of these parameters, when varied over their plausible range of values, significantly impact the results. For example, the thermal conductivity of the compartment walls

does not significantly affect a predicted cable surface temperature, but the HRR of the fire does. The relatively simple empirical models identify the key parameters that impact the predicted quantity and they provide the means to quantify the functional relationship between model inputs and outputs.

3.3.2.1 Gas and Surface Temperatures

According to the McCaffrey, Quintiere, and Harkleroad (MQH) correlation, the HGL temperature rise, $T - T_0$, in a compartment fire is proportional to the HRR, $\dot{Q}$, raised to the two-thirds power:

$$T - T_0 = C\dot{Q}^{2/3} \tag{3-2}$$

Here, C is related to the geometry and thermal properties of the compartment and T_0 is a reference temperature, typically ambient temperature. Taking the first derivative of T with respect to $\dot{Q}$ and writing the result in terms of differentials yields:

$$\frac{\Delta T}{T - T_0} \cong \frac{2}{3}\frac{\Delta \dot{Q}}{\dot{Q}} \tag{3-3}$$

This is a simple formula with which one can readily estimate the relative change in the model output quantity, $\Delta T/(T - T_0)$, caused by the relative change in the model input parameter $\Delta \dot{Q}/\dot{Q}$. In subsection 3.3.1.6, the uncertainty in the HRR of the validation experiments, $\Delta \dot{Q}/\dot{Q}$, was estimated to be 7.5 percent. Equation (3-3) indicates that a 7.5 percent increase in the HRR should lead to a 5 percent increase in the HGL temperature.

3.3.2.2 HGL Depth

Most of the experiments for which the HGL depth was predicted had at least one open door or window that effectively determined the steady-state HGL depth. Unlike all of the other predicted quantities, the HGL depth is relatively insensitive to the fire's HRR. It is largely determined by the height of the opening, and for this reason there is essentially no uncertainty associated with the model inputs that affect the layer depth.

3.3.2.3 Gas and Smoke Concentration

Most fire models assume that combustion product gases and soot, once beyond the flaming region of the fire, are passively transported throughout the compartment. The major products of combustion, such as CO_2 and water vapor, plus the major reactant, O_2, are generated or consumed in direct proportion to the burning rate of the fuel, which is directly proportional to the HRR. The mass fraction of any species in the HGL is directly proportional to the product of its yield and the HRR.

For the experiments described in Section 3.1, the yields of the major product gases such as O_2 and CO_2 from pure fuels such as methane gas and heptane liquid are known from the basic stoichiometry to a high level of accuracy. Thus, the relative uncertainty in the concentration of major product gases is the same as that of the HRR, 7.5 percent. The uncertainty in the smoke concentration, however, is a combination of the uncertainty of the HRR and the soot yield. The relative standard uncertainty of the soot yield of heptane reported in NUREG/CR-6905 is 11 percent. The uncertainties for HRR and soot yield are combined through quadrature and the resulting expanded relative uncertainty is $(0.075^2 + 0.11^2)^{1/2} = 0.133$, or 13 percent.

3.3.2.4 Pressure

In a closed and ventilated compartment, the average pressure, p (Pa), is governed by the following equation:

$$\frac{\mathrm{d}p}{\mathrm{d}t} = \frac{\gamma - 1}{V}\left(\dot{Q} - \dot{Q}_{\mathrm{loss}}\right) + \frac{\gamma p}{V}\left(\dot{V} - \dot{V}_{\mathrm{leak}}\right) \tag{3-4}$$

where γ is the ratio of specific heats (about 1.4), V is the compartment volume (m^3), $\dot{Q}$ is the HRR (kW), $\dot{Q}_{\mathrm{loss}}$ is the sum of all heat losses to the walls (kW), $\dot{V}$ is the net ventilation rate into the compartment (m^3/s), and $\dot{V}_{\mathrm{leak}}$ is the leakage rate out of the compartment (m^3/s). The leakage rate is a function of the compartment overpressure:

$$\dot{V}_{\mathrm{leak}} = A_{\mathrm{leak}}\sqrt{\frac{2(p - p_\infty)}{\rho_\infty}} \tag{3-5}$$

where A_{leak} is the leakage area (m^2), p_∞ is the ambient pressure (Pa), and ρ_∞ is the ambient air density (kg/m^3). The maximum compartment pressure is achieved when the pressure-rise term in Eq. (3-4) is set to zero. Rearranging terms yields an estimate for the maximum pressure:

$$(p - p_\infty)_{\max} \cong \frac{\rho_\infty}{2}\left(\frac{(\gamma - 1)\left(\dot{Q} - \dot{Q}_{\mathrm{loss}}\right) + \gamma p_\infty \dot{V}}{\gamma p_\infty A_{\mathrm{leak}}}\right)^2 \tag{3-6}$$

The test report for the NIST/NRC experiments (NUREG/CR-6905) contains estimates of the uncertainty in the HRR, ventilation rate, and leakage area. To calculate the uncertainty in the maximum pressure rise resulting from the uncertainty in these three parameters, the pressure-rise estimate in Eq. (3-6) was calculated using 1000 randomly selected sets of values of the HRR, ventilation rate, and leakage area. These parameters were assumed to be randomly distributed with mean values of 1000 kW, 1 m^3/s, and 0.06 m^2 and relative standard uncertainties of 75 kW, 0.1 m^3/s, and 0.0021 m^2. The mean values of these parameters were typical of the NIST/NRC experiments, and the uncertainties were reported in the test report. The resulting relative standard uncertainty in the pressure is 21 percent.

3.3.2.5 Heat Flux

The heat flux to a target or wall is a combination of direct thermal radiation from the fire and convective and thermal radiation from the HGL. If the heat flux is predominantly caused by the thermal radiation of the fire, it can be approximated using the point-source radiation model:

$$\dot{q}'' = \frac{\chi_{\mathrm{r}}\dot{Q}}{4\pi r^2} \tag{3-7}$$

Where $\dot{q}''$ is the heat flux (kW/m^2), χ_{r} is the radiative fraction, $\dot{Q}$ is the HRR (kW), and r is the distance from the fire (m). The relative standard uncertainty of the heat flux is a combination of the uncertainty in the radiative fraction and the HRR:

$$\frac{\delta\dot{q}''}{\dot{q}''} \cong \frac{\delta\dot{Q}}{\dot{Q}} + \frac{\delta\chi_{\mathrm{r}}}{\chi_{\mathrm{r}}} \tag{3-8}$$

NUREG/CR-6905 estimates the relative standard uncertainty of the radiative fraction of a heptane pool fire to be 8 percent. Combined with the 7.5 percent uncertainty in the HRR (through quadrature) yields an 11 percent relative standard uncertainty in the heat flux directly from a fire.

The heat flux, $\dot{q}''$ (kW/m^2), to a cold surface resulting from the exposure to hot gases and not necessarily the fire itself is the sum of radiative and convective components:

$$\dot{q}'' = \varepsilon\sigma\left(T_{\text{gas}}^4 - T_\infty^4\right) + h\left(T_{\text{gas}} - T_\infty\right) \tag{3-9}$$

where ε is the surface emissivity, σ is the Stefan-Boltzmann constant, T_{gas} is the gas temperature, T_∞ is the ambient temperature, and h is the convective heat-transfer coefficient. From the discussion above, the relative standard uncertainty in the gas temperature rise above ambient is 5 percent (resulting from an estimated uncertainty in the HRR of 7.5 percent). There is also uncertainty in the convective heat-transfer coefficient, but this is attributed to the model, not the experimental measurements. Thus, the uncertainty in the heat flux is largely a function of the uncertainty in the gas temperature, which is largely a function of the HRR. As was done for the pressure, 1000 randomly selected values of gas temperature with a mean of 300°C above ambient and a relative uncertainty of 5 percent resulted in a corresponding uncertainty of 9 percent in the heat flux.

In actual compartment fires, the heat flux to surfaces is a combination of direct thermal radiation from the fire and indirect radiation and convection from the hot gases. Given that the calculation of the former incurs a 11 percent relative standard uncertainty and the latter 9 percent, to simplify the analyses, a value of 10 percent is used for all heat-flux predictions.

3.3.2.6 Sprinkler Activation Time

The uncertainty in the reported sprinkler activation times is mainly because of uncertainties in the measured HRR, RTI (Response-Time Index), and activation temperature. There is a negligible uncertainty in the measured activation time itself, which is typically determined with a pressure transducer. To determine the effect of the uncertainties in the HRR, RTI, and activation temperature, consider the ordinary differential equation governing the temperature, T_{d}, of a sprinkler (Custer et al., 2008):

$$\frac{\text{d}T_{\text{d}}}{\text{d}t} = \frac{\sqrt{u}}{\text{RTI}}\left(T_{\text{gas}} - T_{\text{d}}\right) \tag{3-10}$$

Here, u and T_{gas} are the respective velocity and the temperature of the ceiling jet. According to Alpert's ceiling-jet correlation, the ceiling-jet temperature and velocity are proportional to the HRR raised to the power of 2/3 and 1/3 respectively. Given the relative standard uncertainty in the HRR of 7.5 percent, the uncertainties in the ceiling-jet temperature and velocity are thus 5 percent and 2.5 percent respectively. As for the RTI and activation temperature, these values are measured experimentally and the uncertainties differ depending on the test procedure. Vettori (1998) reports that the RTI of the sprinklers used in his experiments is 56 $(\text{m}\cdot\text{s})^{0.5}$ with a relative standard uncertainty of 11 percent and that the activation temperature is 68°C ± 2.4°C. This latter uncertainty estimate is assumed to represent one standard deviation. Assuming an ambient temperature of approximately 20°C, the relative standard uncertainty in the activation temperature is assumed to be 5 percent.

Equation (3-10) was integrated 1000 times using random selections of the ceiling-jet temperature and velocity, RTI, and activation temperature. The mean ceiling-jet temperature was increased linearly at rates varying from 0.5°C/s to 2°C/s, which are consistent with the variety of growth rates measured by Vettori. The mean ceiling-jet velocity was assumed to be 1 m/s. This procedure yielded a relative standard uncertainty in the sprinkler activation time of 6 percent.

The activation times recorded by Vettori include two or three replicates for each configuration. The standard deviation of the 45 measured activation times, normalized by the mean of each set of replicates, was 6 percent, which is consistent with the result obtained above.

3.3.2.7 Cable Failure Time

The uncertainty in the reported cable failure times is mainly because of uncertainties in the measured exposing temperature, cable diameter, and jacket thickness. The uncertainty in the measured mass per unit length of the cable is assumed to be negligible. To determine the uncertainty in the cable failure time, the heat-conduction equation in the THIEF model was solved numerically using 10,000 random selections of the exposing temperature, cable diameter, and jacket thickness. The cable diameter was varied from 16.25 mm to 16.35 mm and the jacket thickness was varied from 1.45 mm to 1.55 mm. The uncertainty in the exposing temperature of the cylindrical heater was assumed to be 2.5 percent, the lower bound of the range of uncertainty estimates for thermocouple measurements given in subsection 3.3.1.1. The mass per unit length of the cable was assumed to be 0.529 kg/m and the ambient temperature was assumed to be 20°C. This procedure yielded an estimated relative standard uncertainty in the cable failure time of 12 percent.

3.3.2.8 Smoke Detector Activation Time

There is a single set of experiments with which to evaluate model predictions of smoke-detector activation time, the NIST Home Smoke Alarm Experiments. The test report (Bukowski et al., 2008) does not include detailed information about the alarm mechanism within the various smoke detectors used in the experiments. Thus, from a modeling standpoint, these devices are “black boxes” and their activation can only be discerned from a variety of empirical techniques, the most popular of which is to assume that the smoke detector behaves like a sprinkler or heat detector whose activation is governed by Eq. (3-10) with a low activation temperature and RTI. Bukowski and Averill (1998) suggest that an activation temperature of 5°C is typical of many residential smoke alarms. The propagated uncertainty of this estimate is difficult to determine because temperature rise is not particularly well correlated with smoke concentration within the sensing chamber of the detector. Nevertheless, the relative standard deviation of the normalized activation times[4] for the NIST Home Smoke-Alarm Experiments is 34 percent. Without more detailed information about the activation criteria, the models cannot predict the activation times more accurately than this value.

[4] To determine this value, the activation times of multiple detectors at the same location were averaged and the activation times were normalized by the average value. Then, the standard deviation of the normalized activation times was calculated to produce the relative standard deviation of 34 percent.

3.3.3 Summary of Experimental Uncertainty Estimates

Table 3-4 summarizes the estimated uncertainties for all of the output quantities for which the models are to be evaluated. The rightmost column in the table represents the total experimental uncertainty, denoted as $\tilde{\sigma}_E$, a combination of the uncertainty in the measurement of the output quantity itself, along with the propagated uncertainties of the key measured input quantities. This total experimental uncertainty is obtained by taking the square root of the sum of the squares of the measurement and propagation uncertainties that have been estimated in the previous two subsections. It is assumed that the two forms of uncertainty are independent.

Table 3-4. Summary of the experimental uncertainty estimates.

Measured/Predicted Quantity	Measurement Uncertainty (%)	Key Input Parameters; Corresponding Relative Uncertainty (%); Power Dependence			Input Parameter Propagation Uncertainty (%)	Total Experimental Uncertainty, $\tilde{\sigma}_E$ (%)
HGL, Plume, Ceiling Jet, Surface, and Target Temperatures	5	HRR	7.5	2/3	5	7
HGL Depth	5	Door Height	0	-1	0	5
Gas Concentration	2	HRR	7.5	1	7.5	8
Smoke Concentration	14	HRR Soot Yield	7.5 11	1 1	13	19
Pressure	1	HRR Leak Area Vent. Rate	7.5 3.5 10	2 -2 2	21	21
Heat Flux	5	HRR Rad. Frac.	7.5 8	1 1	10	11
Sprinkler Activation Time	0	HRR RTI Act. Temp.	7.5 11 5	2/3 1 1	6	6
Cable Failure Time	0	Temp. Diameter Thickness	2.5 0.6 6.7	-	12	12
Smoke Detector Activation Time	0	Response Mechanism	-	-	34	34

4
MODEL DESCRIPTIONS

Numerous fire models have been developed and maintained by various organizations to predict fire-generated conditions. This study selects the following five of these fire models, which represent a wide range of capabilities and mathematical and computational sophistication:

1. NRC's Fire Dynamics Tools (FDT^s Version 1805.1)
2. EPRI's Fire-Induced Vulnerability Evaluation (FIVE-Rev2)
3. NIST's Consolidated Model of Fire Growth and Smoke Transport (CFAST Version 6.3.1)
4. EdF's MAGIC (Version 4.1.3)
5. NIST's Fire Dynamics Simulator (FDS Version 6.0.0)

These particular models were chosen based on the fact that most of them (a) have been used to calculate fire conditions in NPP fire protection applications or (b) were developed by stakeholders within the nuclear industry for NPP fire protection applications.

The results of the model validation study presented in Chapter 5 are based on these particular versions of the models. The validation results do not apply to earlier versions of the models.

4.1 Empirical Correlations: FDT^s and FIVE

The FDT^s are a set of empirical correlations in the form of Microsoft® Excel® spreadsheets. For the most part, the correlations in the FDT^s library are closed-form algebraic expressions programmed in spreadsheets to provide a user-friendly interface that reduces input and computational errors. Technical details are available in NUREG-1805 and in Supplement 1 to NUREG-1805. In addition to describing corrections and improvements of the original FDT^s spreadsheets, the supplement documents the implementation of the Thermally Induced Failure (THIEF) model for electrical cables (Volume 3 of NUREG/CR-6931, 2007) as Chapter 19.

FIVE is another library of engineering calculations in the form of Excel® spreadsheets. FIVE consists of functions programmed in Visual Basic, the programming language within Excel®. Technical details are available in EPRI 3002000830. To verify that the correlations work as programmed, the FDT^s and FIVE have been checked according to the verification cases listed in NIST SP 1169 (2013).

HGL Temperature, Natural Ventilation

For a compartment with natural ventilation, the correlation of McCaffrey, Quintiere, and Harkleroad (MQH) (Walton, 2008) predicts the HGL temperature rise.

HGL Temperature, Forced Ventilation

For a compartment with forced ventilation, the correlation of Foote, Pagni, and Alvares (FPA) or the correlation of Deal and Beyler (DB) (Walton, 2008) predicts the HGL temperature rise.

HGL Temperature, No Ventilation

For a compartment with no ventilation, the correlation of Beyler (Walton, 2008) predicts the HGL temperature rise.

HGL Depth

For a compartment with no ventilation and constant HRR, the available safe egress time (ASET) correlation (Walton, 1985; Milke, 2008) predicts the HGL interface height. An alternative method is presented by Yamana and Tanaka (Tanaka, 1985).

Plume Temperature

Correlations by Heskestad (2008) and McCaffrey (1979) estimate the increase in the centerline plume temperature.

Cable Failure Time

The Thermally Induced Electrical Failure (THIEF) of a cable can be predicted using a simple one-dimensional heat transfer calculation, under the assumption that the cable can be treated as a homogeneous cylinder (NUREG/CR-6931, 2007). Cable failure is assumed when the cable temperature exceeds an empirically determined critical temperature.

Steel Temperature

The temperature rise of an unprotected or protected steel member exposed to fire can be predicted using heat transfer analysis on the steel member (Milke, 2008). There are different formulations for unprotected steel and protected steel (both neglecting and accounting for the thermal capacity of the insulation layer).

Point Source Radiation Heat Flux

The point source radiation model assumes that radiative energy is concentrated at a point located within a flame (Beyler, 2008) and can be used to calculate the radiation heat flux on a target or surface.

Solid Flame Radiation Heat Flux

The solid flame radiation model predicts the heat flux to a target based on the effective emissive power from a flame and a view factor calculation (Beyler, 2008).

Ceiling Jet Temperature

For a steady-state fire, the correlation of Alpert (2008) predicts the ceiling jet temperature rise from a fire plume.

Sprinkler Activation Time

For a steady-state fire, the correlation of Alpert (2008) along with a heat transfer analysis on the sprinkler link (Budnick, Evans, and Nelson, 1997) can be used to predict the activation time of a sprinkler.

Smoke Detector Activation Time

Smoke detector activation time is sometimes modeled in the same way as the activation time of a sprinkler with a low activation temperature and RTI. Heskestad and Delichatsios (1977) correlated smoke detector activation to a particular temperature rise that depends on the type of fuel.

4.2 Zone Fire Models: CFAST and MAGIC

This section provides qualitative background information on two zone-fire models included in the V&V study, CFAST and MAGIC, including their development and use. Zone-fire models (also referred to as two-zone models) are modeling programs developed under the assumption that a fire will generate two distinct zones with uniform thermal properties.

4.2.1 Basic Description of Zone Fire Models

Zone fire models such as CFAST and MAGIC predict the fire induced environment as a function of time for single- or multi-compartment scenarios. Each compartment is divided into two zones (or volumes) in order to numerically solve differential equations, and the two volumes are assumed to be uniform in temperature and species concentration. The approximate solution of the conservation equations for each zone, together with the ideal gas law and the equation of heat conduction into the walls, is used in attempts to simulate the environmental conditions generated by a fire.

CFAST (Peacock et al., 2013) is a two zone fire model that predicts the environment that arises within compartments as a result of a fire prescribed by the user. CFAST was developed and is maintained by NIST's Fire Research Division. CFAST predicts the average temperatures of the upper and lower gas layers within each compartment; flame height; ceiling, wall, and floor temperatures within each compartment; flow through vents and openings; visible smoke and gas species concentrations within each layer; target temperatures; heat transfer to targets; sprinkler activation time; and the impact of sprinklers on the fire's HRR. Version 6.3.1 was used for the current study.

MAGIC (Gay et al. 2012b) is a two-zone fire model developed and maintained by EdF. It is available through EPRI to its members. In terms of modeling capabilities, MAGIC predicts (1) environmental conditions in the room (such as hot gas layer temperature and oxygen/smoke concentrations), (2) heat ransfer-related outputs to walls and targets (such as incident, convective, radiated, and total heat fluxes), (3) fire intensity and flame height, and (4) flow velocities through vents and openings. Version 4.1.3 was used for the current study.

The models use similar, but not identical assumptions, governing equations, and engineering correlations. Significant similarities and differences are highlighted in the sections that follow.

4.2.2 Developers of Zone Fire Models

The CFAST model was developed, and is maintained, by the Fire Research Division of NIST. The developers include Walter Jones, Richard Peacock, Glenn Forney, Rebecca Portier, Paul Reneke, John Hoover, and John Klote.

MAGIC was developed and is maintained by Electricité de France (EdF).

4.2.3 Documentation of Zone Fire Models

Relevant publications concerning CFAST include the CFAST Technical Reference Guide (Peacock et al., 2013), User's Guide (Peacock et al., 2013a), and Model Evaluation Guide (Peacock et al., 2013b). The Technical Reference Guide describes the underlying physical principles, provides a comparison with experimental data, and describes the limitations of the model. The User's Guide describes how to use the model.

MAGIC is supported by three EdF publications, including (1) the technical manual, which provides a mathematical description of the model (Gay and Wizenne 2012b); (2) the user's manual, which details how to use the graphical interface (Gay and Wizenne 2012a); and (3) the validation studies, which compare MAGIC's results with experimental measurements (Gay and Wizenne 2012c). These three proprietary publications are available through EPRI to EPRI members.

4.2.4 Governing Equations and Assumptions for Zone Fire Models

The general equations solved by both CFAST and MAGIC include conservation of mass and energy. The models do not explicitly solve the momentum equation, except for use of the Bernoulli equation for the flow velocity at vents. These equations and the ideal gas law are solved to obtain fire-generated conditions in the selected control volumes.

Zone models are implemented based on two general assumptions: (1) two zones per compartment provide a reasonable approximation of the scenario being evaluated, and (2) the complete momentum equation is not needed to solve the set of equations associated with the model. Consequently, the two zones have uniform properties. That is, the temperature and gas concentrations are assumed to be constant throughout the zone; the properties only change as a function of time.

Chapter 3 of the CFAST Technical Reference Guide (Peacock et al., 2013) fully describes the equations and assumptions associated with the CFAST model. A complete technical description of the MAGIC algorithms and sub-models is provided in the MAGIC documentation (Gay and Wizenne, 2012).

4.2.5 Input Data for Zone Fire Models

All of the data required to run a zone model (CFAST or MAGIC) reside in a primary data file, which the user creates. Some instances might require databases of information on objects, thermophysical properties of boundaries, and sample prescribed fire descriptions. In general, the data files contain the following information:

- Compartment dimensions (height, width, and length). The compartment (or each compartment in a multi-room scenario) is assumed to have a rectangular floor base and flat ceiling.
- Construction materials of the compartment (e.g., concrete and gypsum), including material properties (e.g., thermal conductivity, specific heat, density, thickness, and heat of combustion). Depending on the selected material, this information might be available in databases supplied by the model developers.
- Dimensions and positions of horizontal and vertical flow openings such as doors, windows, vents, and leakage paths.
- Mechanical ventilation specifications (injection and extraction rates, vent elevations, and time to start/stop the system).
- Fire properties (e.g., heat-release rate, heat of combustion, lower oxygen limit, species-production rates as a function of time, radiative fraction, and fuel composition).
- Fire location (lateral position, elevation, and position relative to a wall or corner).
- Footprint area of the fire: For CFAST, this is specified as an area of no particular shape. For MAGIC, the specification includes whether the fire is circular in shape (e.g., pool fires specified by the diameter) or rectangular (e.g., bounded pool fires or fires in electrical cabinets specified by length and width).

- Sprinklers and detectors are characterized by their location within the compartment and their response characteristics, which include activation temperature and response-time index.
- Two sets of parameters (thermophysical properties and location) describe targets. Thermophysical properties include the density, specific heat, and thermal conductivity of the material. Location refers to where the target is with respect to the fire (expressed with three-dimensional coordinates).

Many of these properties are commonly available in fire protection engineering and materials handbooks. Experimentally determined property data might also be available for certain scenarios. However, depending on the application, properties for specific materials might not be readily available. A small file distributed with the CFAST and MAGIC software contains a database with thermal properties of common materials. These data are given as examples; users should verify the accuracy and appropriateness of the data.

The CFAST User's Guide (Peacock et al., 2013a) provides a complete description of the required input parameters. Some of these parameters have default values included in the model, which are intended to be representative for a range of fire scenarios. Unless explicitly noted, default values were used for parameters not specifically included in this validation study.

The MAGIC User's Guide (Gay and Wizenne, 2012a) provides a complete description of the input parameters required to run MAGIC.

4.2.6 Output Quantities of Zone-Fire Models

Once the simulation is complete, CFAST produces an output file containing all of the solution variables. Typical outputs include (but are not limited to) the following:

- environmental conditions in the room (such as hot gas layer temperature; oxygen and smoke concentration; and ceiling, wall, and floor temperatures)
- heat transfer related outputs to walls and targets (such as incident, convective, radiated, and total heat fluxes)
- fire intensity and flame height
- flow velocities through vents and openings
- sprinkler activation time

MAGIC has an extensive library of output values. Once a given simulation is completed, MAGIC generates an output file with all of the solution variables. Through a "post-processor" interface, the user selects the relevant output variables for the analysis. Typical outputs include (but are not limited to) the following examples:

- environmental conditions in the room (such as hot gas layer temperature, oxygen concentration, and smoke concentration)
- heat transfer related outputs to wall and targets (such as incident, convective, radiated, and total heat fluxes)
- oxygen effects on heat-re ease rate and flame height
- flow velocities through vents and openings
- target temperatures (including sprinkler bulb temperature and gas temperature measured by the detectors)

4.2.7 Verification of Zone-Fire Models

This section documents the mathematical and numerical robustness of CFAST and MAGIC, which involves verifying that the implementation of the model matches the stated documentation. Specifically, ASTM E1355 suggests the following analyses to address the mathematical and numerical robustness of models:

- Analytical tests involve testing the correct functioning of the model. In other words, these tests use the code to solve a problem with a known mathematical solution. However, there are relatively few situations for which analytical solutions are known.

- "Code checking" refers to verifying the computer code on a structural basis. This verification can be achieved manually or by using a code-checking program to detect irregularities and inconsistencies within the computer code.

- Numerical tests investigate the magnitude of the residuals from the solution of a numerically solved system of equations (as an indicator of numerical accuracy) and the reduction in residuals (as an indicator of numerical convergence).

Analytical Tests: General analytical solutions do not exist for most fire problems. Nonetheless, it is possible to test specific aspects of the model in typical situations.

Certain CFAST sub-models address phenomena that have analytical solutions; for example, one-dimensional heat conduction through a solid or pressure increase in a sealed or slightly leaky compartment as a result of a fire or fan. The developers of CFAST routinely use analytical solutions to test sub-models to verify the correctness of the coding of the model as part of its development. Such routine verification efforts are relatively simple and the results might not always be published or included in the documentation. Two additional types of verification are possible. The first type involves validating individual algorithms against experimental work. The second involves simple experiments, especially for conduction and radiation, for which the results are asymptotic (e.g., for a simple single-compartment test case with no fire, all temperatures should equilibrate asymptotically to a single value). Such comparisons are included in the CFAST model evaluation guide (Peacock et al., 2013b).

Some studies have been performed to control the correct behavior of the following sub-models of MAGIC:

- conduction into the wall: comparison to other models and analytic solutions

- target and cable thermal behavior: consistency of the behavior in typical situations

- plumes model: comparison with the theoretical model

- vent and opening: comparison to other zone and field models

- room pressure: comparison with pressure estimated by the perfect gas law and simplified energy equation

These studies are EdF's proprietary material.

Code Checking:

Standard programs have been used to check the CFAST model structure and language. Specifically, FLINT, LINT, and Forcheck have been applied to the entire model to verify the correctness of the interface, undefined or incorrectly defined (or used) variables and constants, and completeness of loops and threads.

The CFAST code has also been checked by compiling and running the model on a variety of computer platforms. Because FORTRAN and C are implemented differently for various computers, this represents both a numerical check as well as a syntactic check. CFAST has been compiled for the Sun® (Solaris), SGI® (IRIX®), and Concurrent computer platforms, as well as PCs running Microsoft Windows® (Lahey, Digital (Compaq®), and Intel® FORTRAN). Within the precision afforded by the various hardware implementations, the answers are identical.[5]

The source code for MAGIC is tested with the following methods:

- First, to control robustness, the code may be compiled in several different platforms and software applications. The MAGIC code has been compiled under Microsoft Windows 2000, Windows XP, Windows Vista, and Windows 7, with a variety of compilers, including Absoft® Pro FORTRAN, Visual FORTRAN, and G77 (gfortran). In addition, a global update of the FORTRAN sources was performed in 2004 (Benmamoun, 2004), and aspects such as code documentation, variable glossary, and source cleanup were addressed.
- In terms of code quality, two tools have been used to control the language:
  - FOR_STUDY® from Cobalt Blue
  - *plus*FORT from Polyhedron Software

  These tools confirm the consistency of variables and constants (undefined and incorrectly or redundantly declared) and use of good FORTRAN syntax.

The software quality-assurance system (Gautier, 1996) provides a process to fix detected anomalies concerning the interface of the code. Maintenance of MAGIC is based on observation forms, which identify problems; modification forms, which describe the problem analysis and proposed solutions; and correction forms, which explain the chosen solution and implementation features. The project manager decides on the implementation of the correction in future versions.

Numerical Tests: Two components of the numerical solutions of CFAST must be verified. The first is the differential-algebraic equation (DAE) solver called DASSL, which has been tested for a variety of differential equations and is widely used and accepted (Barnett, 1990). The radiation and conduction routines have also been tested against known solutions for asymptotic results.

The second component is the coupling between algorithms and the general solver. The structure of CFAST provides close coupling that avoids most errors. The error attributable to numerical solution is far less than that associated with the model assumptions. Also, CFAST is designed to use 64-bit precision for real-number calculations to minimize the effects of numerical error. CFAST includes a number of numerical tests in the CFAST Evaluation Guide (Peacock et al., 2013b).

[5] Typically, an error limit of one part in 10^6.

For each new MAGIC version, a set of tests is used to ensure that the calculation is correct. These tests come from previous case studies. The convergence and speed of the calculation is the first step of control. Main results from the original study are then compared, and significant differences are analyzed. These studies are EdF proprietary material.

Specific tests are performed in the maintenance process when new models are implemented in MAGIC or when existing models are corrected or improved. Those tests are not systematically conducted for new versions, but they are available in case problems arise with the model under study. The tests are mentioned in the correction report (Gautier, 1996) which is kept for each code correction. These reports are EdF proprietary material and not published.

4.2.8 Limitations of Zone Fire Models

Zone models have been developed for use in solving practical fire problems in fire protection engineering, while also providing a tool to study fundamental fire dynamics and smoke spread. They are intended for use in system modeling of buildings and building components. They are not intended for detailed study of flow within a compartment, such as is needed for detailed smoke detector placement. Both CFAST and MAGIC include the activation of sprinklers and fire suppression by water droplets.

The most extensive use of the models is for fire and smoke spread in complex buildings. Their efficiency and computational speed are inherent in the few computation cells needed for the implementation of a zone model. These models are used for the design and reconstruction of timelines for fire and smoke spread in residential, commercial, and industrial fire applications. Some applications of the models have been for design of smoke-control systems.

Compartments: Zone models are generally limited to situations in which the compartment volumes are strongly stratified. However, in order to facilitate the use of the model for preliminary estimates when a more sophisticated calculation is ultimately needed, there are algorithms for corridor flow, smoke-detector activation, and detailed heat conduction through solid boundaries. CFAST does permit modeling of non-rectangular compartments, although the application is intended to be limited to relatively simple spaces. There is no intent to include complex geometries in which a complex flow field is a driving force. For these applications, computational fluid dynamics (CFD) models are appropriate.

Gas Layers: There are also limitations inherent in the assumption of stratification of the gas layers. The zone model concept, by definition, implies a sharp boundary between the upper and lower layers, whereas in reality the transition is typically over about 10 percent of the height of the compartment and can be larger in weakly stratified flow. For example, a burning cigarette in a normal room is not within the purview of a zone model. While it is possible to make predictions within 5 percent of the actual temperatures of the gas layers, this is not the optimum use of the model. It is more properly used to make estimates of fire spread (not flame spread), smoke detection and contamination, and life safety calculations.

Heat Release Rate: There are limitations inherent in the assumptions used in the application of the empirical models. As a general guideline, the heat release should not exceed about 1 MW/m^3. This is a limitation on the numerical routines attributable to the coupling between gas flow and heat transfer through boundaries (conduction, convection, and radiation). The inherent two-layer assumption is likely to break down well before this limit is reached.

Heat Transfer: Both models include radiation, convection, and conduction sub-models that include the interaction between the fire, gas layers, and compartment surfaces. MAGIC additionally includes the impact of radiation through vents to other compartments or the

outdoors; CFAST does not include this effect. Both models include calculation of heat transfer to user-placed targets within compartments.

Ventilation and Leakage: The vent flow algorithms in both CFAST and MAGIC assume that the size of an individual vent is small compared to the total surface area of the connecting compartments. With larger vents, some additional uncertainty in the calculated flows can be expected. An important limitation arises from the uncertainty in the scenario specification. For example, leakage in buildings is significant, and this affects flow calculations especially when wind is present and for tall buildings. These effects can overwhelm limitations on accuracy of the implementation of the model. The overall accuracy of the model is closely tied to the specificity, care, and completeness with which the data are provided.

Thermal Properties: The accuracy of the model predictions is limited by how well the user can specify the thermophysical properties. For example, the fraction of fuel which ends up as soot has an important effect on the radiation absorption of the gas layer and, therefore, the relative convective versus radiative heating of the layers and walls, which in turn affects the buoyancy and flow. The level of uncertainty of the predictions is higher if the properties of real materials and real fuels are unknown or difficult to obtain or if the physical processes of combustion, radiation, and heat transfer are more complicated than their mathematical representations in a zone model.

4.3 CFD Fire Model: FDS

This section contains information about the Fire Dynamics Simulator (FDS), its development, and its use in fire-protection engineering. Most of the information has been extracted from the FDS Technical Reference Guide (McGrattan et al., 2013), which contains a comprehensive description of the governing equations and numerical algorithms used to solve them.

4.3.1 FDS Basic Description

FDS is a computational fluid dynamics (CFD) model of fire-driven fluid flow. The model numerically solves a form of the Navier-Stokes equations appropriate for low-speed thermally driven flow with an emphasis on smoke and heat transport from fires. The partial derivatives of the conservation equations of mass, momentum, and energy are approximated as finite differences and the solution is updated in time on a three-dimensional rectilinear grid. Thermal radiation is computed using a finite volume technique on the same grid as the flow solver. Lagrangian particles are used to simulate smoke movement and sprinkler sprays. Smokeview is a companion program that produces images and animations of the FDS calculations.

Version 1 of FDS/Smokeview was publicly released in February 2000, The present version of FDS/Smokeview is Version 6, which was released in September 2013. Changes in the version number correspond to major changes in the physical model or input parameters. For minor changes and bug fixes, incremental versions are released, cited according to fractions of the integer version number. Version 6.0.0 was used for the current study.

4.3.2 FDS Developers

FDS was developed, and is currently maintained, by the Fire Research Division at NIST. A substantial contribution to the development of the model was made by VTT Building and Transport in Finland.

4.3.3 FDS Documentation

FDS is documented by two publications, the Technical Reference Guide (McGrattan et al., 2013) and the FDS User's Guide (McGrattan et al., 2013b). The FDS User's Guide describes how to use the model. The Technical Reference Guide consists of four volumes. Volume 1 discusses the mathematical formulation of the model. Volume 2 documents the verification of the model algorithms. Volume 3 documents the validation of the model. Volume 4 is the configuration-management plan; that is, the process of model development and maintenance.

NIST has developed a public Web site to distribute FDS and Smokeview and support users of the programs. The web site (http://fire.nist.gov/fds/) also includes documents that describe various parts of the model in detail.

4.3.4 FDS Governing Equations and Assumptions

Hydrodynamic Model: FDS numerically solves a form of the Navier-Stokes equations appropriate for low-speed thermally driven flow with an emphasis on smoke and heat transport from fires. The core algorithm is an explicit predictor-corrector scheme and is second-order accurate in space and time. Turbulence is treated by means of large eddy simulation (LES). It is possible to perform a direct numerical simulation (DNS) if the underlying numerical grid is fine enough.

Combustion Model: For most applications, FDS assumes that combustion is mixing-controlled and that the reaction of fuel and oxygen is infinitely fast.

Radiation: Radiation heat transfer is included in the model through the solution of the radiation transport equation for a non-scattering gray gas. In a limited number of cases, a wideband model can be used in place of the gray gas model. The radiation equation is solved using a technique similar to a finite volume method for convective transport, so the name given to it is "the finite volume method."

Geometry: FDS approximates the governing equations on one or more rectilinear grids. The user prescribes rectangular obstructions that are forced to conform to the underlying grid.

Boundary Conditions: All solid surfaces are assigned thermal boundary conditions, as well as information about the burning behavior of the material. Usually, material properties are stored in a database and invoked by name. Heat and mass transfer to and from solid surfaces is usually handled with empirical correlations.

Sprinklers and Detectors: The activation of sprinklers and heat and smoke detectors is modeled using fairly simple correlations based on thermal inertia (in the case of sprinklers and heat detectors) and the lag in smoke transport through smoke detectors. Sprinkler sprays are modeled by Lagrangian particles that represent a sampling of the water droplets ejected from the sprinkler.

4.3.5 FDS Input Data

All of the input parameters required by FDS to describe a particular scenario are conveyed in one text file created by the user. This file contains information about the numerical grid, ambient environment, building geometry, material properties, combustion kinetics, and desired output quantities. The numerical grid is one or more rectilinear meshes with (usually) uniform cells. All geometric features of the scenario have to conform to this numerical grid. An obstruction that is

smaller than a single grid cell is either approximated as a single cell or rejected. The building geometry is input as a series of rectangular obstructions. Materials are defined by their thermal conductivity, specific heat, density, thickness, and burning behavior. This information is conveyed in various ways depending on the desired level of detail. A significant part of the FDS input file directs the code to output various quantities in various ways. Much as in an actual experiment, the user must decide before the calculation begins what information to save. There is no way to recover information after the calculation is over if it was not requested at the start. A complete description of the input parameters required by FDS can be found in the FDS User's Guide (McGrattan et al., 2013b).

A number of material properties are needed as inputs for FDS, most related either to solid objects or the fuel. In many fire scenarios, the solid objects are the fuel. For solid surfaces, FDS needs the density, thermal conductivity, specific heat, and emissivity. Note that FDS does not distinguish between walls and various other solid objects, sometimes regarded as "targets" in simpler models.

For the fuel, FDS needs to know whether it is a solid, liquid, or gas; its heat of combustion; its heat of vaporization (liquids and solids); the stoichiometric coefficients of the ideal reaction; the soot and carbon monoxide (CO) yields; and the fraction of energy released in the form of thermal radiation. The radiative fraction is not an inherent property of the fuel, but rather a measured quantity that varies with the size and geometric configuration of the fire. It can be computed directly by FDS, but it is often input directly because it cannot be predicted reliably with the present form of the combustion model.

Some of the property data needed by FDS are commonly available in fire-protection engineering and materials handbooks. Depending on the application, properties for specific materials might not be readily available (especially burning behavior at different heat fluxes). A small file distributed with the FDS software contains a database with thermal properties of common materials. These data are given as examples; users should verify the accuracy and appropriateness of the data.

4.3.6 FDS Output Quantities

FDS computes the temperature, density, pressure, velocity, and chemical composition within each numerical grid cell at each discrete time step. There are typically hundreds of thousands to several million grid cells and thousands to hundreds of thousands of time steps. In addition, FDS computes at solid surfaces the temperature, heat flux, mass-loss rate, and various other quantities. Typical output for the gas phase includes the following quantities:

- gas temperature
- gas velocity
- gas species concentration (water vapor, carbon dioxide (CO_2), CO, and nitrogen (N_2))
- smoke concentration and visibility estimates
- pressure
- heat release rate per unit volume
- mixture fraction (or air/fuel ratio)
- gas density
- water droplet mass per unit volume

On solid surfaces, FDS predicts additional quantities associated with the energy balance between gas and solid phases, including the following examples:

- surface and interior temperature
- heat flux, both radiative and convective
- burning rate
- water droplet mass per unit area

In addition, the program records the following global quantities:

- total heat release rate (HRR)
- sprinkler and detector activation times
- mass and energy fluxes through openings or solids

Time histories of various quantities at a single point in space or global quantities such as the fire's heat-release rate (HRR) are saved in simple comma-delimited text files that can be plotted using a spreadsheet program. However, most field or surface data are visualized with a program called Smokeview, a tool specifically designed to analyze data generated by FDS.

4.3.7 FDS Verification

The verification of FDS is documented in Volume 2 of the FDS Technical Reference Guide (McGrattan et al., 2013). This document describes a set of several hundred test cases that fall into three basic categories:

Analytical Tests: These involve comparison of the computed solutions with closed-form solutions of the governing equations. There are no closed-form mathematical solutions for the fully turbulent, time-dependent Navier-Stokes equations. CFD provides an approximate solution for the nonlinear partial differential equations by replacing them with discretized algebraic equations that can be solved using a powerful computer. Certain sub-models address phenomena that have analytical solutions. The developers of FDS routinely use analytical solutions to test sub-models to verify the correctness of the coding of the model. With each new release of FDS, the entire set of verification calculations is run to ensure that no new errors have been introduced into the source code. Some of these include the following examples:

- heat conduction into a semi-infinite solid
- evaporation of water droplets in uniform temperature environment
- radiation heat transfer from a hot object with a uniform temperature
- pressure increase in a sealed or slightly leaky compartment attributable to a fire or fan
- idealized reaction of fuel and oxygen in an adiabatic chamber

The common thread in all of these exercises is the well-defined initial and final states, which test the basic conservation laws.

Code Checking: This involves verification of the basic structure of the computer code, either manually or automatically with a code-checking program, to detect irregularities and inconsistencies. FDS has been compiled and run on computers manufactured by several companies and run under various operating systems, including Unix, Linux, Microsoft Windows, and Apple® OS X®. Various Fortran compilers have been used as well. Each combination of hardware, operating system, and compiler involves a slightly different set of compiler and run-time options. Compliance with the Fortran standard of the International Organization for Standardization (ISO) and American National Standards Institute (ANSI) improves the portability of the program. By adhering to the standard, the code is streamlined and outdated or potentially

harmful code is removed. FDS version 6 is fully compliant with the Fortran 2003 ISO/ANSI standard.

Numerical Tests: These involve assessment of the magnitude of the residuals from the solution of a numerically solved system of equations (as an indicator of numerical accuracy) and the reduction in residuals (as an indicator of numerical convergence). The use of finite differences to approximate spatial and temporal partial derivatives introduces error into the FDS calculation. This numerical error depends on the grid size. As the numerical grid is refined, the numerical error decreases. If the grid is refined to about 1 mm or less, the simulation becomes a direct numerical simulation (DNS), where no assumptions about the underlying turbulence need to be made. While DNS simulations are too costly for practical fire calculations, they can be useful in checking the numerical algorithm because there exist in the literature a variety of small-scale fluid flow and combustion experiments that can be simulated in great detail. Numerous comparisons between small-scale experiments and DNS solutions using FDS have shown that the hydrodynamic solver is robust and without serious flaws.

4.3.8 FDS Limitations

Although FDS can address most fire scenarios, there are limitations in all of its various algorithms. Some of the more prominent limitations of the model are listed here. More specific limitations are discussed as part of the description of the governing equations in the FDS Technical Reference Guide (McGrattan et al., 2013).

Low-Speed Flow Assumption: The use of FDS is limited to low-speed flow (having a Mach number less than about 0.3) with an emphasis on smoke and heat transport from fires. This assumption rules out using the model for any scenario involving flow speeds approaching the speed of sound, such as explosions, choke flow at nozzles, and detonations.

Rectilinear Geometry: The efficiency of FDS is attributable to the simplicity of its rectilinear numerical grid and the use of fast, direct solvers for the pressure field. This can be a limitation in some situations in which certain geometric features do not conform to the rectangular grid, although most building components do. For most practical large-scale simulations, the increased grid resolution afforded by the fast pressure solver offsets the approximation of a curved boundary by small rectangular grid cells.

Fire Growth and Spread: FDS was originally intended for design scenarios in which the heat release rate of the fire is specified and the transport of heat and exhaust products is the principal aim of the simulation. However, for fire scenarios in which the heat release rate is predicted rather than prescribed, the uncertainty of the model is higher. There are several reasons for this: (1) properties of real materials and real fuels are often unknown or difficult to obtain; (2) the physical processes of combustion, radiation, and solid-phase heat transfer are more complicated than their mathematical representations in FDS; and (3) the results of calculations are sensitive to both the numerical and physical parameters.

Combustion: For most applications, FDS assumes that combustion is mixing-controlled and that the reaction of fuel and oxygen is infinitely fast, regardless of the temperature. For large-scale well-ventilated fires, this is a good assumption. However, if a fire is in an under-ventilated compartment, or if a suppression agent such as water mist or CO_2 is introduced, fuel and oxygen might mix but might not burn. Also, a shear layer with high strain rate separating the fuel stream from an oxygen supply can prevent combustion from taking place. The physical mechanisms underlying these phenomena are complex, and even simplified models still rely on an accurate prediction of the flame temperature and local strain rate.

Sub-grid scale modeling of gas phase suppression and extinction is still an area of active research in the combustion community. Until reliable models can be developed for building-scale fire simulations, simple empirical rules can be used that prevent burning from taking place when the atmosphere immediately surrounding the fire cannot sustain the combustion.

Radiation: Radiative heat transfer is included in the model through the solution of the radiation transport equation for a non-scattering gray gas and (in some limited cases) through using a wideband model. The equation is solved using a technique similar to finite volume methods for convective transport; thus, the name given to it is “the finite volume method.” The model has several limitations. First, the absorption coefficient for the smoke-laden gas is a complex function of its composition and temperature. Because of the simplified combustion model, the chemical composition of the smoky gases, especially the soot content, can affect both the absorption and emission of thermal radiation. Second, the radiation transport is discretized through approximately 100 solid angles. For targets far away from a localized source of radiation, like a growing fire, the discretization can lead to a non-uniform distribution of the radiant energy. This can be seen in the visualization of surface temperatures, where “hot spots” show the effect of the finite number of solid angles. The problem can be lessened by the inclusion of more solid angles, but at a price of longer computing times. In most cases, the radiative flux to far-field targets is not as important as those in the near-field, where coverage by the default number of angles is much better.

5
VALIDATION RESULTS

This chapter describes the results of the validation study, including a description of the metrics used to quantify the model uncertainty.

5.1 Model Uncertainty Metrics

The accuracy of each model in predicting a particular quantity is summarized with a scatter plot like the one shown in Figure 5-1. The measured values are represented by the horizontal axis and the predicted values by the vertical. If a particular prediction and measurement are the same, the resulting point falls on the solid diagonal line. To better make use of these results, two statistical parameters are calculated for each model and each predicted quantity. The first parameter, δ, is the *bias factor*. It indicates the extent to which the model, on average, under- or overpredicts the measurements of a given quantity. For example, the bias factor for the data shown in Figure 5-1 is 0.98. This means that the model has been shown to slightly underestimate the ceiling-jet temperatures by 2 percent, on average, and this is shown graphically by the red line just below the diagonal. The second parameter is the *relative standard deviation* of the model, $\tilde{\sigma}_M$. This indicates the variability of the model. Referring again to Figure 5-1, there are two sets of off-diagonal lines. The first set, shown as dashed black lines, indicate the uncertainty of the experimental measurements in terms of a relative standard deviation, $\tilde{\sigma}_E$. It is assumed that the experiments are unbiased; that is, the bias factor for the experimental measurements is 1. The slopes of the dashed black lines are $1 \pm 2\tilde{\sigma}_E$, representing the 95 percent confidence intervals. The set of red dashed lines indicate the model's relative standard deviation, $\tilde{\sigma}_M$. The slopes of these lines are $\delta \pm 2\tilde{\sigma}_M$. If the model were as accurate as the measurements against which it is compared, the two sets of off-diagonal lines would merge. The extent to which the data scatters outside the experimental bounds is an indication of the degree of model uncertainty.

The derivation of the relevant uncertainty statistics has previously been presented by McGrattan and Toman (2011) and is summarized here. The calculation of δ and $\tilde{\sigma}_M$ uses a weighted[6] set of measured and predicted values, along with an estimate of the experimental relative standard deviation, $\tilde{\sigma}_E$, derived in Section 3.3. Before describing the calculation, a few assumptions must be made:

1. The experimental measurements are assumed to be unbiased, and their uncertainty is assumed to be normally distributed with a constant relative standard deviation $\tilde{\sigma}_E$. The experimental uncertainty is a combination of the uncertainty in the measurement of the given quantity and the uncertainty of various important input parameters propagated

[6] Referring to Figure 5-1, data points are often unevenly distributed over the range of the quantity of interest. For example, dozens of temperatures might be measured in the interval from 0°C to 100°C, while only a few are measured in the interval from 900°C to 1000°C. To correct for this when computing the bias and standard deviation, the data is weighted so that points in a sparsely covered interval are of equal value to the points in a densely covered interval. The entire range (in this case, 0°C to 1000°C) is divided into 10 equal intervals. The data from each interval is weighted so that each interval has equal weight in computing the accuracy metrics.

through the model. Table 5-1 provides estimates of relative experimental uncertainties for the quantities of interest.

2. The true value of the quantity of interest is assumed to be normally distributed about the predicted value divided by a bias factor δ. The relative standard deviation of the distribution is denoted as $\tilde{\sigma}_M$.

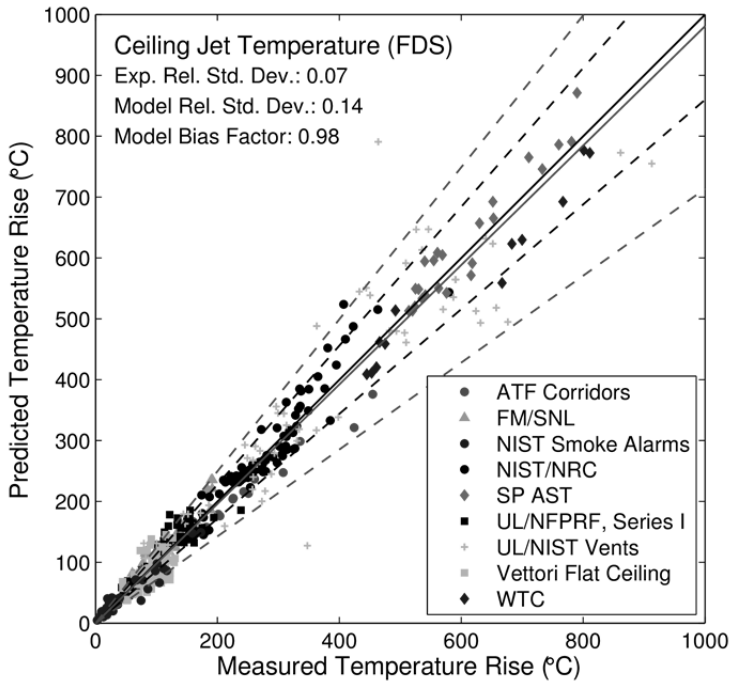

Figure 5-1. Sample result from validation study.

The computation of the estimated bias and scatter associated with model error proceeds as follows. Given a set of n experimental measurements, E_i, and a corresponding set of model predictions, M_i, compute the following:

$$\overline{\ln(M/E)} = \frac{1}{n}\sum_{i=1}^{n} \ln(M_i/E_i) \tag{5-1}$$

The standard deviation of the model error $\tilde{\sigma}_M$ can be computed from the following equation:

$$\sqrt{\tilde{\sigma}_M^2 + \tilde{\sigma}_E^2} \cong \sqrt{\frac{1}{n-1}\sum_{i=1}^{n}\left[\ln(M_i/E_i) - \overline{\ln(M/E)}\right]^2} \tag{5-2}$$

The bias factor is:

$$\delta = \exp\left(\overline{\ln(M/E)} + \frac{\tilde{\sigma}_M^2 - \tilde{\sigma}_E^2}{2}\right) \tag{5-3}$$

For a given model prediction M, the "true" value of the quantity of interest is assumed to be a normally distributed random variable with a mean value of $\mu = M/\delta$ and a standard deviation of $\sigma = \tilde{\sigma}_M(M/\delta)$.

Using these values, the probability of exceeding a critical value x_c is:

$$P(x > x_c) = \frac{1}{2}\mathrm{erfc}\left(\frac{x_c - \mu}{\sigma\sqrt{2}}\right) \tag{5-4}$$

Note that the *complimentary error function* is defined as follows:

$$\mathrm{erfc}(x) = \frac{2}{\sqrt{\pi}}\int_x^\infty e^{-t^2}\, dt \tag{5-5}$$

It is a standard function in mathematical or spreadsheet programs such as Microsoft Excel[7].

5.1.1 Example

As an example of how to use the uncertainty metrics, consider the following example. Suppose that electrical cables within a compartment are assumed to fail if their surface temperature reaches 330°C (626°F). Suppose also that the CFD model FDS predicts that the maximum cable temperature caused by a fire within the compartment is 300°C (572°F). What is the probability that the cables could fail?

Step 1: Subtract the ambient value of the cable temperature, 20°C (68°F), to determine the predicted temperature ***rise***. Refer to this value as the *model prediction, M*:

$$M = 300\ °\mathrm{C} - 20\ °\mathrm{C} = 280\ °\mathrm{C} \tag{5-6}$$

Step 2: Refer to Table 5-1, which indicates that, on average, FDS underpredicts target temperatures with a bias factor, δ, of 0.98. Calculate the *adjusted model prediction*:

$$\mu = \frac{M}{\delta} = \frac{280\ °\mathrm{C}}{0.98} \cong 286\ °\mathrm{C} \tag{5-7}$$

Referring again to Table 5-1, calculate the standard deviation of the distribution:

$$\sigma = \tilde{\sigma}_M\left(\frac{M}{\delta}\right) = 0.18\left(\frac{280\ °\mathrm{C}}{0.98}\right) \cong 51\ °\mathrm{C} \tag{5-8}$$

Step 3: Calculate the probability that the actual cable temperature would exceed 330°C (626°F):

$$P(T > 330\ °\mathrm{C}) = \frac{1}{2}\ \mathrm{erfc}\left(\frac{T - T_0 - \mu}{\sigma\sqrt{2}}\right) = \frac{1}{2}\ \mathrm{erfc}\left(\frac{330\ °\mathrm{C} - 20\ °\mathrm{C} - 286\ °\mathrm{C}}{51\ °\mathrm{C}\sqrt{2}}\right) \cong 0.32 \tag{5-9}$$

[7] Excel 2007 does not evaluate $\mathrm{erfc}(x)$ for negative values of x, even though the function is defined for all real x. In such cases, use the identity $\mathrm{erfc}(-x) = 2 - \mathrm{erfc}(x)$.

The process is shown graphically in Figure 5-2. The area under the "bell curve" for temperatures higher than 330 °C (626 °F) represents the probability that the actual cable temperature would exceed that value.

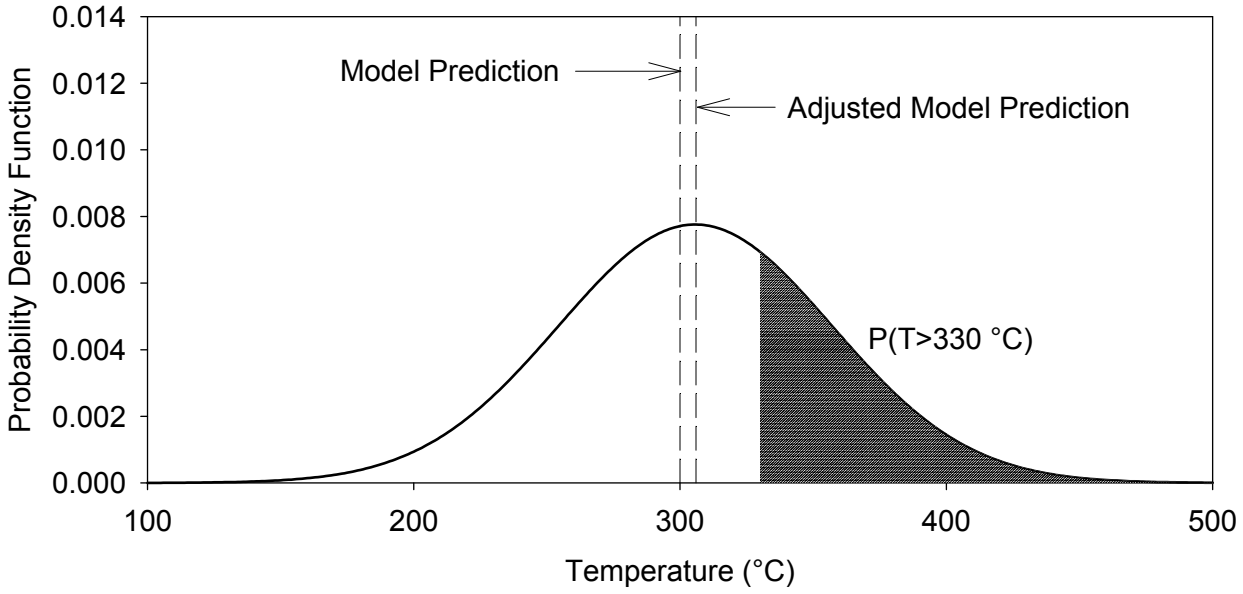

Figure 5-2. Normal distribution of the "true" peak temperature of an electrical cable

5.1.2 Limitation of the Method

The relatively simple method described above for quantifying model uncertainty is based on the assumption that the relative difference between model prediction and experimental measurement is normally distributed. For large data sets, this can be checked qualitatively by visual inspection. For example, for the data shown in Figure 5-1, the quantity $\ln(M/E)$, when presented in the form of a histogram, does appear to be normally distributed. However, in some cases the data do not appear to be normally distributed. Consider, for example, the data shown in Figure 5-3. The model uncertainty bounds (red dashed lines) do not appear to evenly straddle the data. In this case, the data from one set of experiments (UL/NIST Vents) tend to skew the distribution. It might be argued that this data be analyzed using a different assumption about the distribution. However, this would seriously complicate the presentation of the results and make it much more difficult to apply the uncertainty metrics in the way presented above.

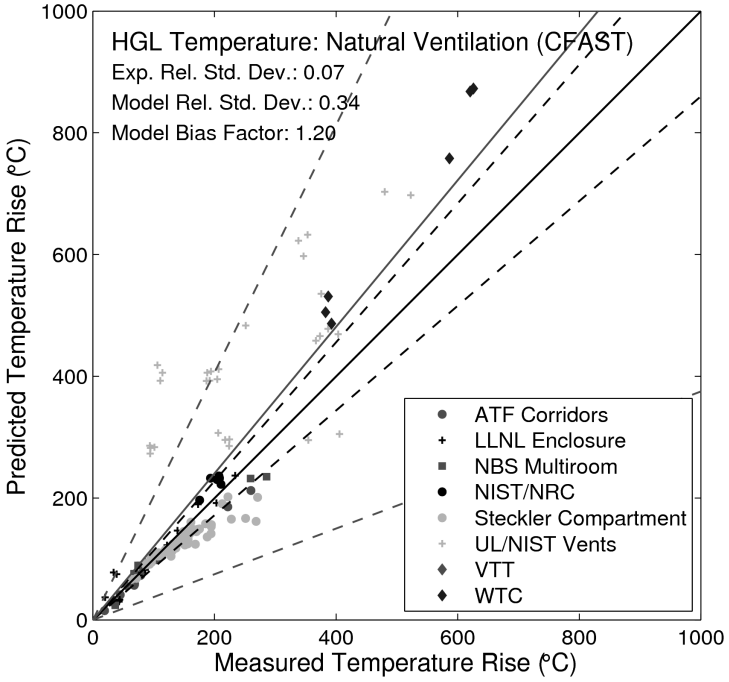

Figure 5-3. Example of data that are non-normally distributed.

5.2 Validation Results for Selected Output Quantities

This section presents the results that summarize the accuracy of the models. For each quantity of interest (e.g., oxygen concentration), the results of the empirical correlations, zone models, and CFD model are discussed separately. While it is not possible to comment on each and every point within the scatter plots, noticeable trends are discussed.

The intent is to compare the models to as much of the experimental data as possible. Because it includes the most detailed physics, the CFD model (FDS) is compared against all of the data. In some cases, the zone and empirical models cannot be applied to all of the data, in which case the specific data or experiments that are excluded are described.

5.2.1 HGL Temperature

The HGL temperature, as discussed in Section 2.2, is particularly important in NPP fire scenarios because it is an indicator of target damage away from the ignition source. For typical electrical cable types (thermoplastic and thermoset), the damage criteria are 205 °C (400 °F) and 330 °C (626 °F) respectively (see Table 8-2 in Volume 2 of NUREG/CR-6850 (EPRI 1011989)). The empirical correlations and zone models typically predict an average HGL temperature, while CFD models predict the local gas temperature in each computational grid cell. For the purpose of comparing all of the models with experimental measurements, both the CFD predictions and experimental measurements of local gas temperatures can be spatially averaged in the form of an HGL temperature.

Because different empirical correlations govern compartments that are naturally ventilated, mechanically ventilated, or unventilated, the results for HGL Temperature are divided into three categories: natural, forced, and no ventilation.

5.2.1.1 Natural Ventilation

Natural ventilation refers to compartments with no HVAC system operational during the test and openings to the outside. The peak measured temperature rise for the naturally ventilated compartment experiments ranges from approximately 0 °C (32 °F) to 700 °C (1292 °F), with most of the data lying at 400 °C (752 °F) or below. This latter temperature range is typical of fires that can potentially damage equipment such as electrical cables.

Empirical Correlation: The results for the MQH correlation are shown in Figure 5-4. The validation results from all of the experiments are within or above experimental uncertainty. There is no indication of systematic underpredictions of HGL temperatures. Note that the correlations only included a subset of the experimental data from the NBS Multiroom Experiments (measurements located in the fire room) because the empirical correlation cannot account for multiple rooms.

Note that the MQH correlation assumes that the ceiling, walls, and floor are composed of a single material. Discussion is provided in Karlsson and Quintiere (2000) to calculate an effective heat-transfer coefficient for compartments with different ceiling, wall, and floor materials as well as materials composed of multiple layers in the MQH correlation. However, the discussion does not provide details on calculating the thermal penetration time through these complex materials. The validation results do not include those of the UL/NIST Vents Experiments (because of the presence of ceiling vents), the ATF Corridors Experiments (because of their multi-story compartment configuration), or the VTT Experiments (because of vents that were located high in the compartment, complex wall lining materials, and irregular geometry).

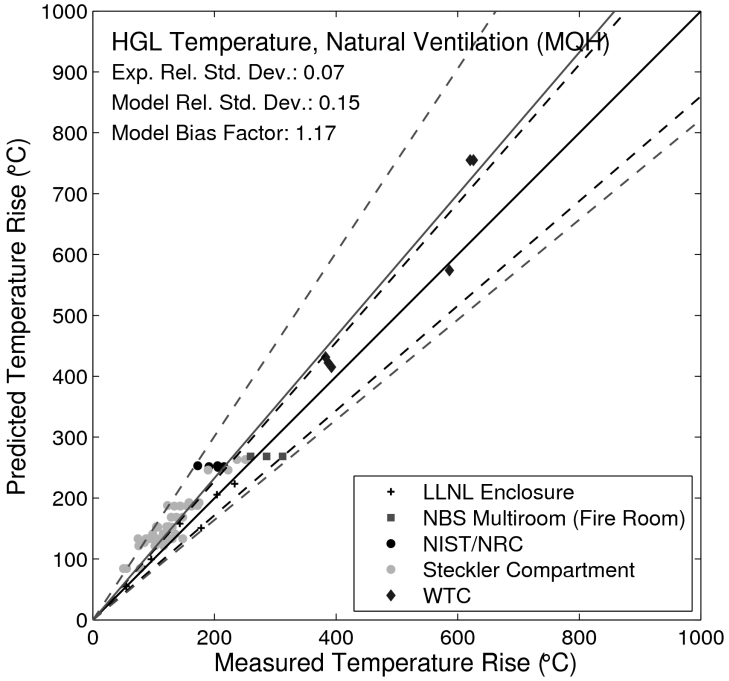

Figure 5-4. HGL Temperature, Natural Ventilation (MQH).

Zone Models: The results for CFAST and MAGIC are shown in Figure 5-5 and Figure 5-6 respectively. Typically, the models slightly overpredict the HGL temperature, particularly for tests with a relatively large fire. This is likely caused by simplifying assumptions for zone models in calculating radiation to layers, to compartment surfaces, and through vents to the outside or other compartments. The UL/NIST Vents experiments are noticeably overpredicted. These tests include large vents in the ceiling of the compartment that might extend beyond the original vent sizes of the empirical correlation used to determine flow through ceiling vents. In addition, the combination of larger HGL temperature and smaller HGL depth compared to the experimental data suggest that part of the difference may be attributed to the reduction method used to estimate layer temperature and position from the individual temperature measurements in the experiments.

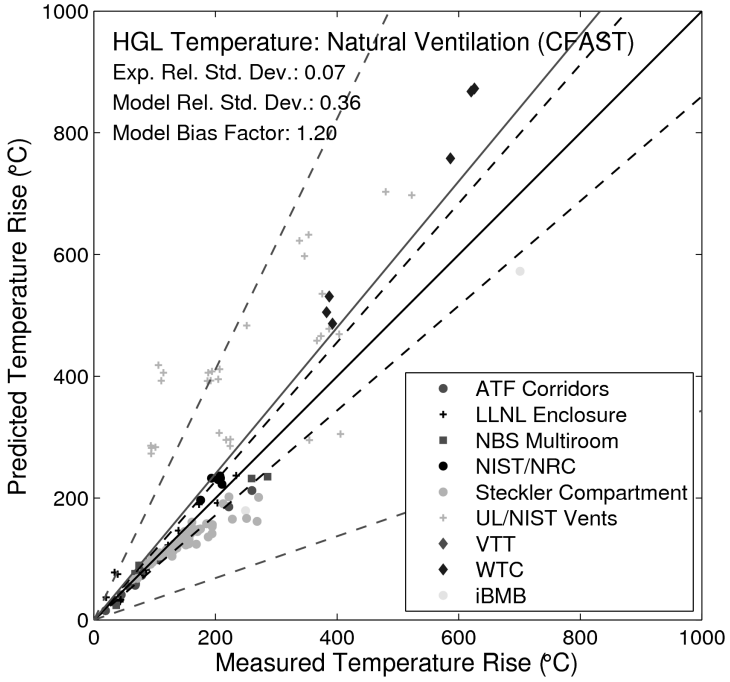

Figure 5-5. HGL Temperature, Natural Ventilation (CFAST).

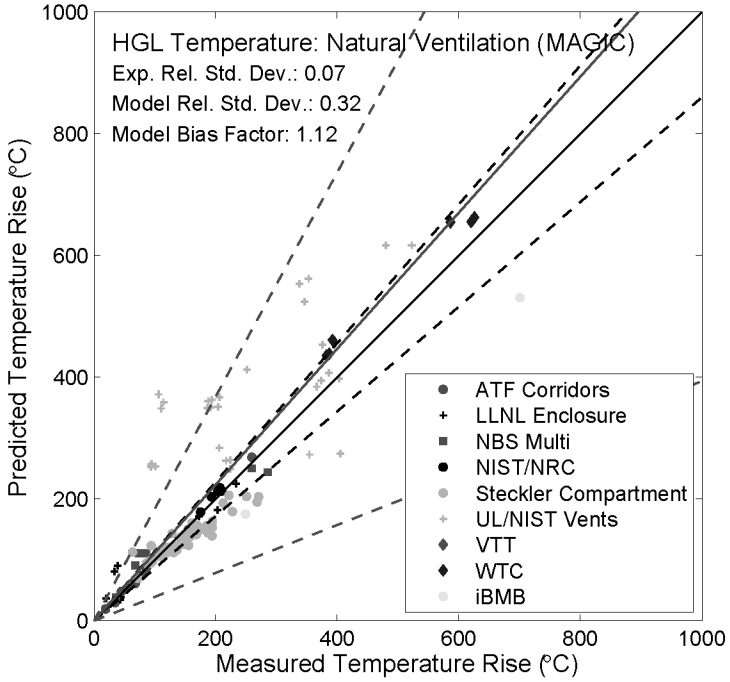

Figure 5-6. HGL Temperature, Natural Ventilation (MAGIC).

CFD Model: The FDS results are shown in Figure 5-7. There is no obvious bias in the model predictions and there are no particular trends in the data. The relatively low bias and model relative standard deviation suggest that FDS HGL predictions are close to experimental uncertainty. FDS does not calculate an HGL temperature directly. Rather, it predicts the gas temperatures at the same locations as the experimental measurements, and the HGL temperature is calculated in the exact same way as it is for the experimental data.

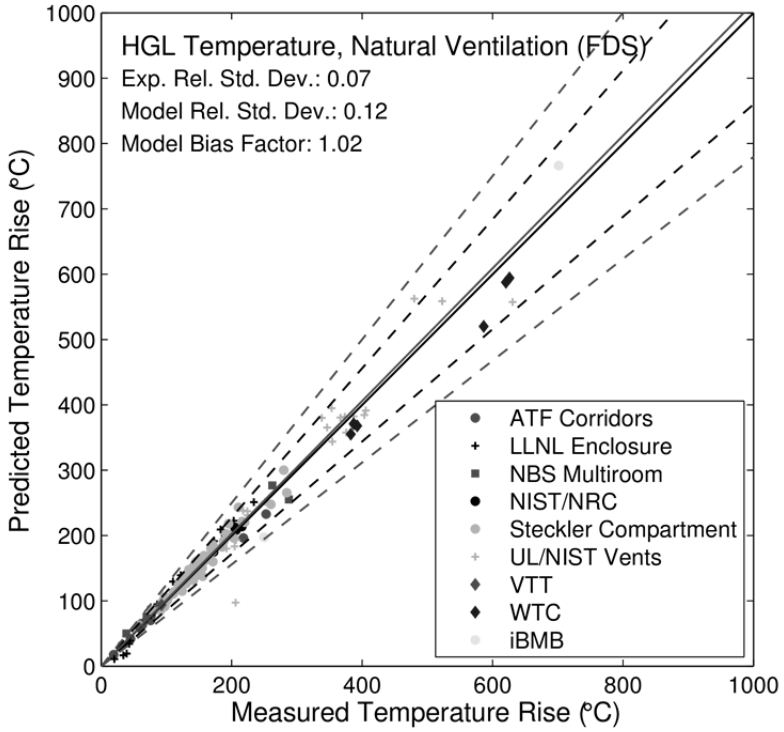

Figure 5-7. HGL Temperature, Natural Ventilation (FDS).

5.2.1.2 Forced Ventilation

The peak measured temperature rise for the forced-ventilation compartment experiments ranges from approximately 0 °C (32 °F) to 300 °C (572 °F).

Empirical Correlation: The results for the FPA and DB correlations are shown in Figure 5-8 and Figure 5-9 respectively. On average, the FPA correlation tends to predict a higher HGL temperature than the DB correlation, which is reflected in the larger model bias factor for the FPA correlation. Note that the predictions for the LLNL Enclosure Experiments are in better agreement with the FPA correlation because they were used to develop the FPA correlation. The validation results do not include the VTT Experiments (because of those experiments' complex wall-lining materials and irregular geometry, as discussed in Section 5.2.1.1).

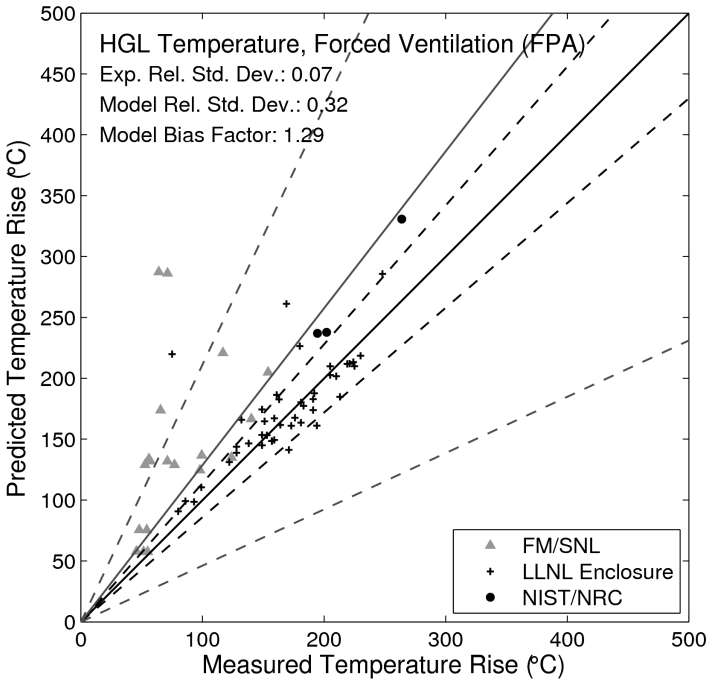

Figure 5-8. HGL Temperature, Forced Ventilation (FPA).

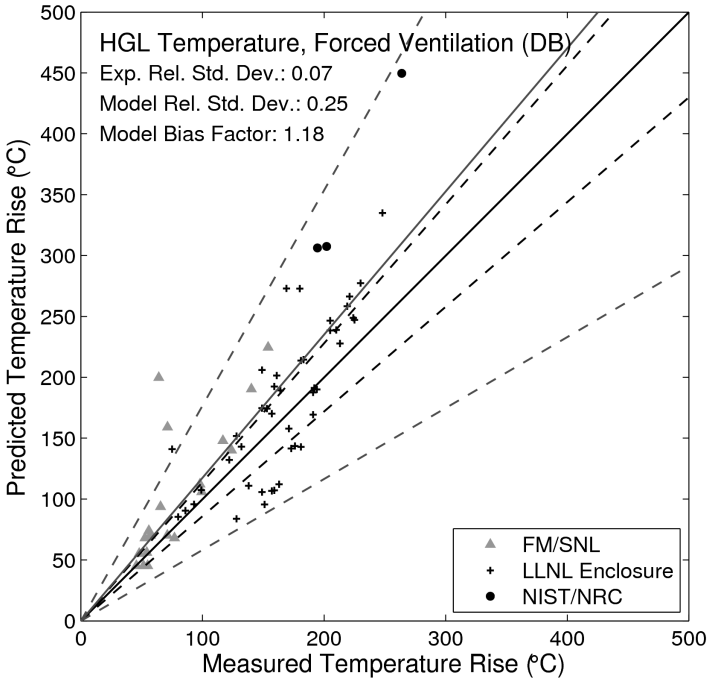

Figure 5-9. HGL Temperature, Forced Ventilation (DB).

Zone Models: The results for CFAST and MAGIC are shown in Figure 5-10 and Figure 5-11 respectively. Typically, the models overpredict the HGL temperature in forced-ventilation tests. The overprediction is likely caused by the simplified mixing assumption applied to the forced-ventilation air that is injected into the upper and lower layer.

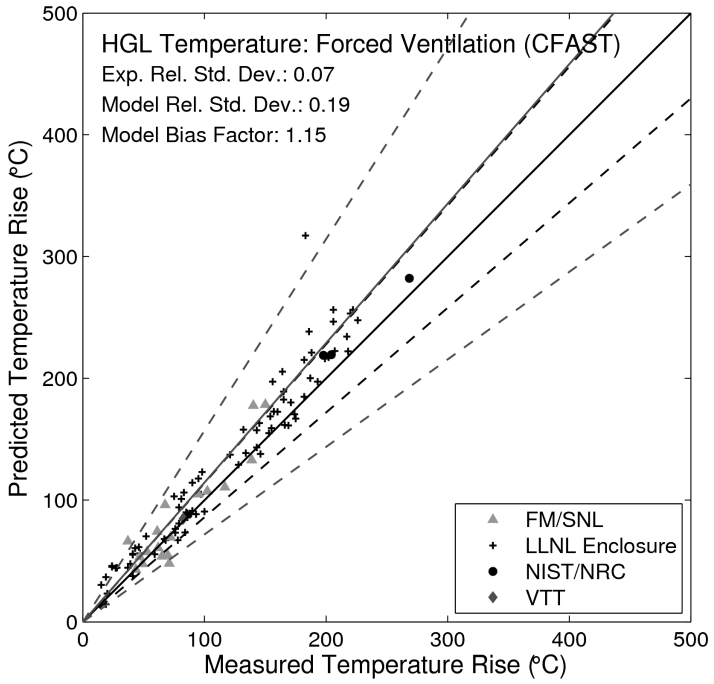

Figure 5-10. HGL Temperature, Forced Ventilation (CFAST).

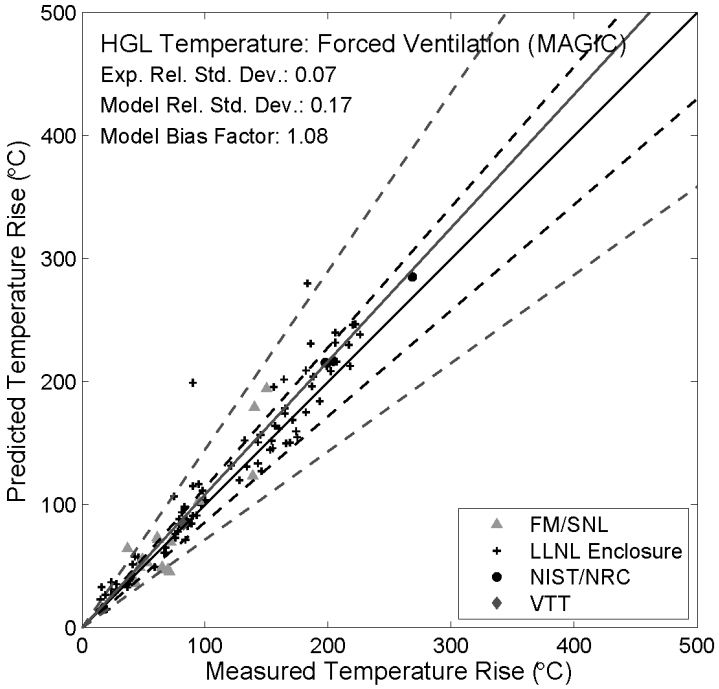

Figure 5-11. HGL Temperature, Forced Ventilation (MAGIC).

CFD Model: The FDS results are shown in Figure 5-12. The FDS results are dominated by the LLNL Enclosure Experiments, which had the largest number of tests. For this data set, the greatest inaccuracies occur for relatively low temperatures on which the effects of the forced ventilation are most pronounced. For higher temperatures, the predictions are more accurate than is implied by the computed model uncertainty.

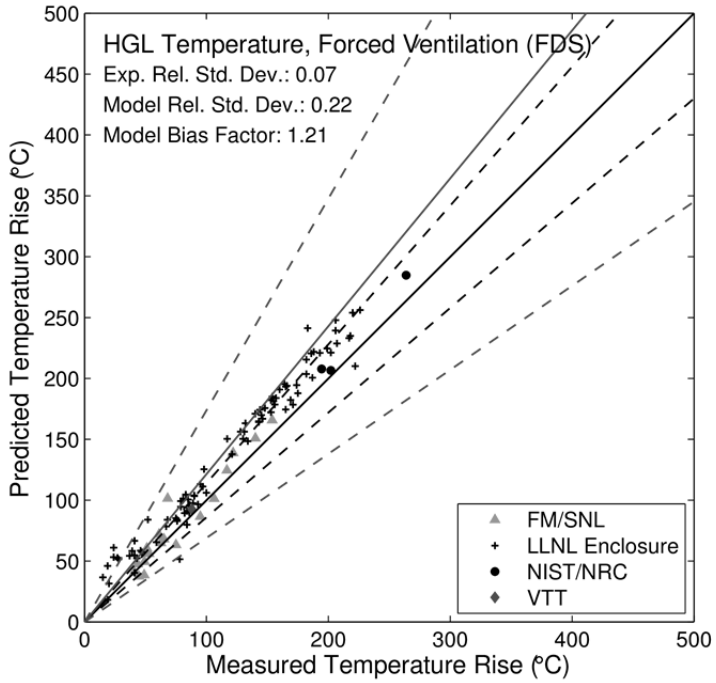

Figure 5-12. HGL Temperature, Forced Ventilation (FDS).

5.2.1.3 No Ventilation

Compartments with no ventilation are typically closed with only leakage paths connecting neighboring compartments or the outside. The peak measured temperature rise for the unventilated compartment experiments ranges from approximately 0 °C (32 °F) to 300 °C (572 °F).

Empirical Correlation

The results for the Beyler correlation are shown in Figure 5-13. The validation results are characterized by a limited set of experiments. The model bias factor might not be an indication of the expected results for a given scenario, and the large model relative standard deviation accounts for the uncertainty associated with the model. The model bias factor is a result of under- and overpredictions from two sets of experiments with very different compartment geometries, which might be the reason for the difference in the results for the two data sets. The validation results do not include those for the NBS Multiroom Experiments (because of the presence of multiple compartments).

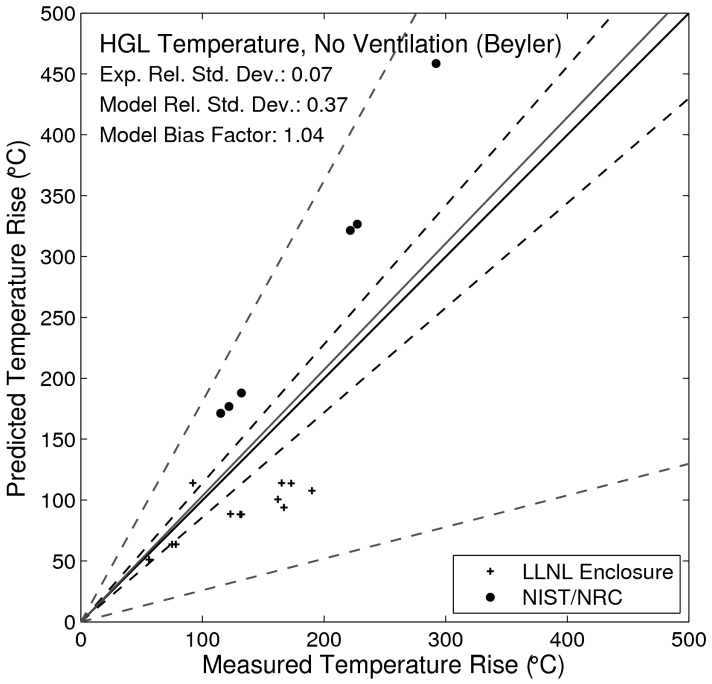

Figure 5-13. HGL Temperature, No Ventilation (Beyler).

Zone Models: The results for CFAST and MAGIC are shown in Figure 5-14 and Figure 5-15 respectively. CFAST predictions of HGL temperature in closed compartments are nearly within experimental uncertainty and reflect the simpler scenarios without vent flows. MAGIC results are comparable to those from CFAST.

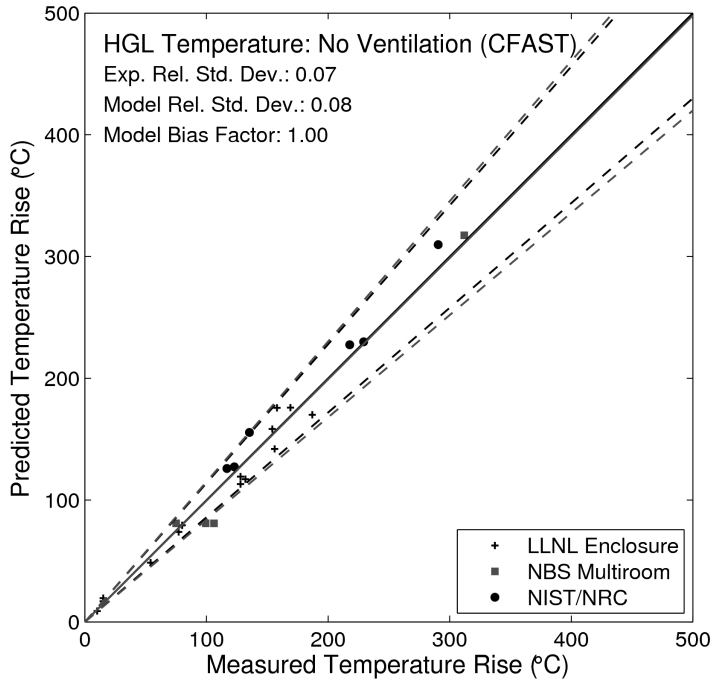

Figure 5-14. HGL Temperature, No Ventilation (CFAST).

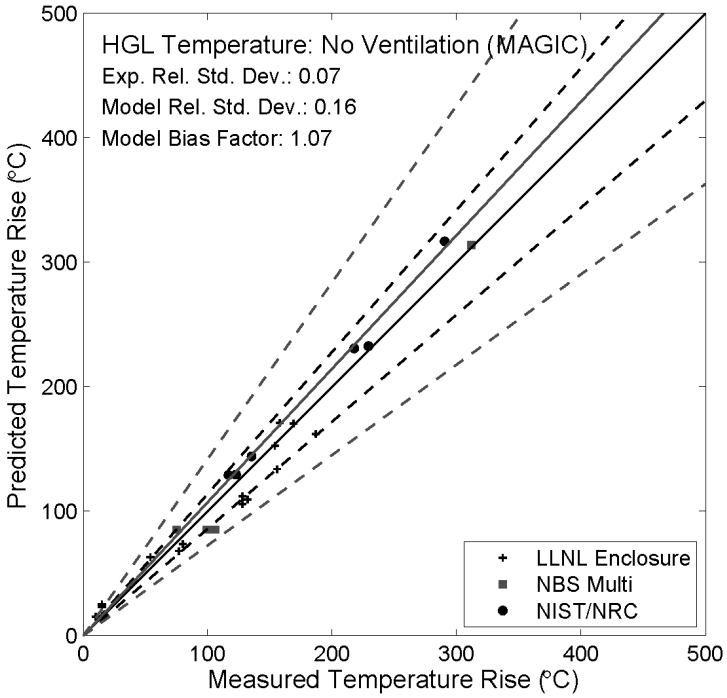

Figure 5-15. HGL Temperature, No Ventilation (MAGIC).

CFD Model: The FDS results are shown in Figure 5-16. The FDS results are most heavily influenced by the LLNL Enclosure Experiments. The NBS and NIST/NRC results do not indicate a particular bias. In the LLNL tests, the experiments were cut short because of the danger posed by a lack of oxygen in a fuel-rich compartment. The temperatures did not reach a steady state before the experiments were ended. The FDS predictions are less accurate during the early stage of the experiments because not enough information was given about the ramp-up of the fuel flow rate.

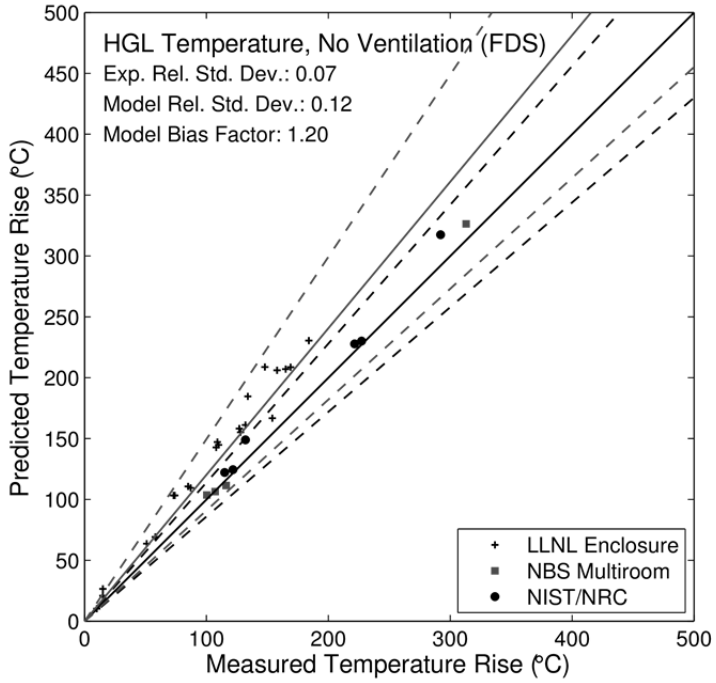

Figure 5-16. HGL Temperature, No Ventilation (FDS).

5.2.2 HGL Depth

The depth of the HGL is also important in NPP fire scenarios because it indicates whether a given target is immersed in high-temperature gases. HGL depth is a direct output of a two-zone model, and it can be calculated from local gas temperatures predicted by a CFD model. The empirical correlations can predict the HGL depth only for very simple closed-compartment geometries.

The range of HGL depth is approximately 1 m (3.3 ft) to 4 m (13.1 ft) with the exception of the VTT experiments, which were conducted in a 19 m (62.3 ft) tall test building.

Zone Models: The results for CFAST and MAGIC are shown in Figure 5-17 and Figure 5-18 respectively. HGL depth is slightly overpredicted by the zone models. Of particular note are the FM/SNL tests, which are closed-compartment experiments with and without forced ventilation. For closed-door tests, visual observations typically show that the HGL fills the entire

compartment volume from floor to ceiling, which is inconsistent with the calculated results for the experimental data. Thus, the calculated experimental values of HGL height for closed-door tests might not be as meaningful as the open-compartment tests for comparison to model results.

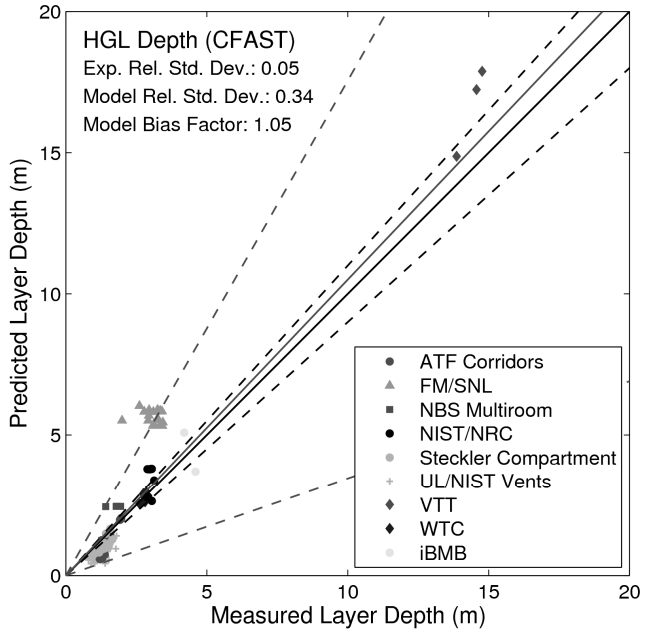

Figure 5-17. HGL Depth (CFAST).

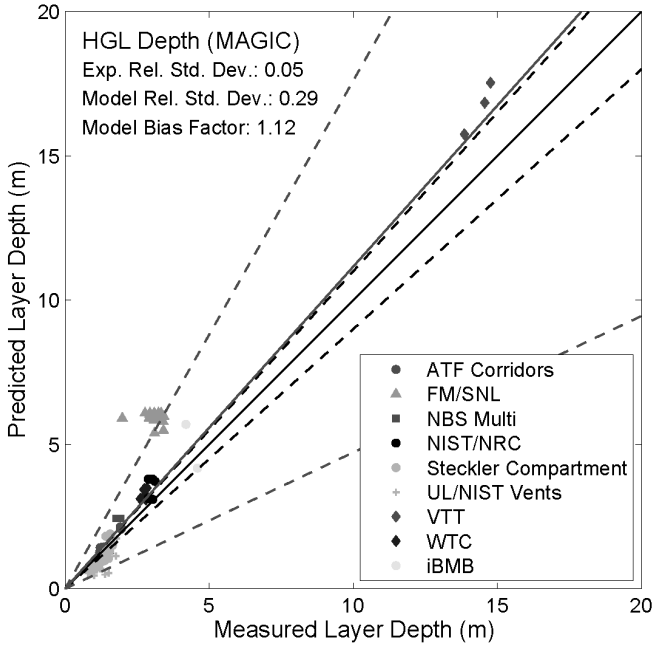

Figure 5-18. HGL Depth (MAGIC).

CFD Model: The FDS results are shown in Figure 5-19. The FDS results are nearly within experimental uncertainty. The reason for this is that the HGL depth is derived from the FDS

temperature predictions in the exact same way as the experimental measurements. Thus, reasonable agreement in the vertical temperature profile leads to a very close match in HGL depth. This is not true of the zone models and empirical correlations; their definitions of HGL depth are not the same as that of the experiments.

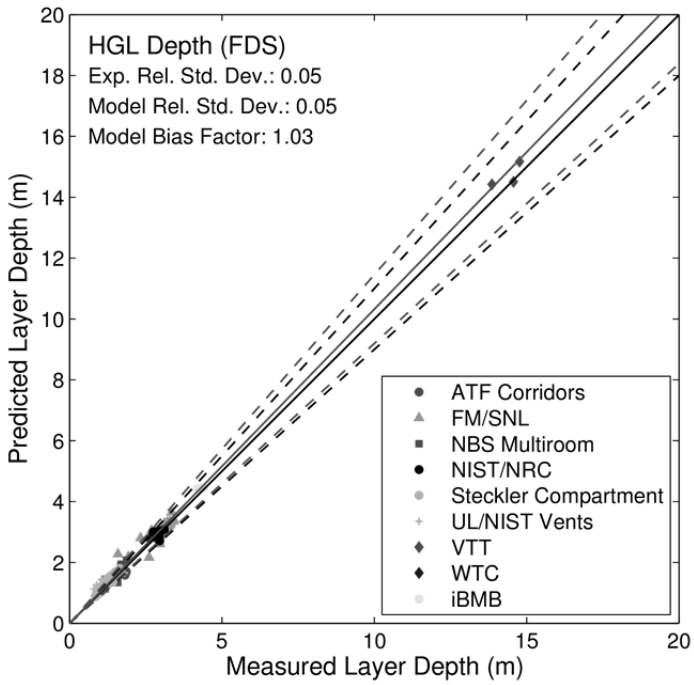

Figure 5-19. HGL Depth (FDS).

5.2.3 Ceiling Jet Temperature

The ceiling jet is the shallow layer of hot gases below the ceiling that spreads radially from the centerline of the fire plume. The ceiling jet has a higher temperature than the overall temperature of the HGL, and therefore it is important in NPP fire scenarios in which targets are located just below the ceiling. A variety of empirical correlations that predict the ceiling jet temperature are embedded in the zone models. CFD models compute the ceiling jet temperature directly from the fundamental equations of fluid motion.

The ceiling-jet temperature measurements range from 0 °C (32 °F) to 900 °C (1652 °F). This upper value is typical of a flashed-over compartment or a compartment in which flames impinge on the ceiling.

Empirical Correlations: Alpert's correlation of ceiling jet temperature was developed for unconfined ceilings against which a hot gas layer is not expected to form. However, it is often applied in compartment fire scenarios in which an HGL does form. The use of the ceiling jet correlation in a compartment with the presence of an HGL can result in an underprediction of the measured ceiling jet temperature by approximately 70 percent. To call attention to this fact, the scatter plots divide the relevant experiments into two categories: Figure 5-20 in which the ceiling is unconfined and Figure 5-21 in which the ceiling is confined and an HGL develops within a compartment.

Figure 5-21 illustrates the underprediction that occurs when the HGL is not accounted for in the ceiling jet temperature calculations. The fact that ceiling jet correlations like Alpert's do not account for the influence of the HGL has been noted by the developers of zone models such as CFAST and MAGIC, which use a modified plume algorithm (Evans, 1985; Cooper, 1988) to account for the entrainment of HGL gases in the upper portion of the plume. Simply adding the ceiling jet temperature rise predicted by the correlation and the predicted HGL temperature rise together to estimate the true ceiling jet temperature has been suggested as an engineering approximation to the results of the more complicated modified plume algorithms (Mowrer, 1992). This strategy was used for the FIVE-Rev1 ceiling jet calculations in the 2007 edition of NUREG-1824 (EPRI 1011999).

The quantification of Table 3-1 from the 2007 edition of NUREG-1824 (EPRI 1011999) that is presented as Table 4-1 in NUREG-1934 (EPRI 1023259) shows a bias factor for the FIVE-Rev1 ceiling jet temperature rise of 1.84. This value indicates that FIVE-Rev1 would overpredict the ceiling jet temperature rise by more than 80 percent as a result of the simplification. For the empirical correlations, this supplement focuses solely on the prediction of ceiling jet temperature rise in an unconfined environment. The prediction of sprinkler or detector activation and ignition of cables exposed to a ceiling jet in a compartment with an HGL are important components of a fire-hazard analysis. Future work will be undertaken to develop empirical correlations that implement appropriate modified plume or other algorithms to calculate ceiling jet temperature rise in a confined environment.

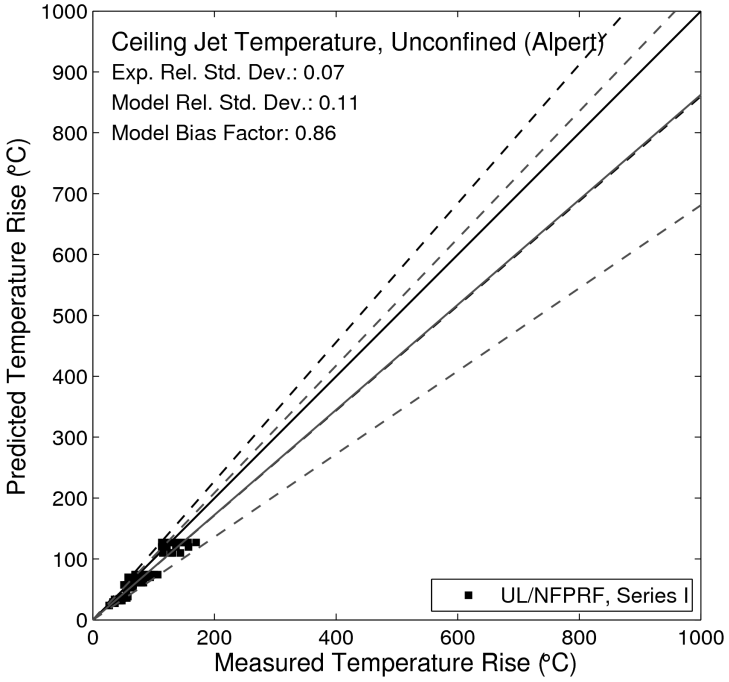

Figure 5-20. Ceiling Jet Temperature, Unconfined Ceiling (Alpert).

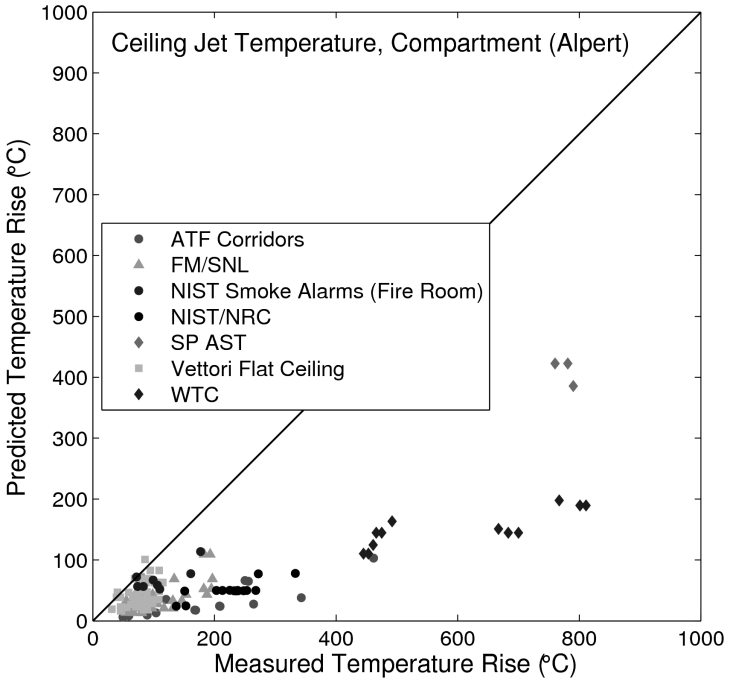

Figure 5-21. Ceiling Jet Temperature, Ceiling of a Confined Compartment (Alpert).

Zone Models: The results for CFAST and MAGIC are shown in Figure 5-22 and Figure 5-23 respectively. Both CFAST and MAGIC predict similar results for ceiling jet temperatures less than about 400 °C (752 °F). At higher temperatures, CFAST predicts higher temperatures than MAGIC. Both models include algorithms to account for the presence of higher gas temperatures near the ceiling surfaces in compartments involved in a fire. The ceiling jet algorithm predicts gas temperature and velocity under a flat, unconstrained ceiling. Limitations of the algorithm can been seen in the predictions for the SP, AST, and WTC tests where the zone mode approximations cluster model predictions together compared to the wider range of experimental measurements. As with the HGL temperature, an overprediction in temperature for the UL/NIST Vents series is seen with the ceiling jet temperature. Because ceiling jet temperatures are calculated as a rise above HGL temperature, this is consistent.

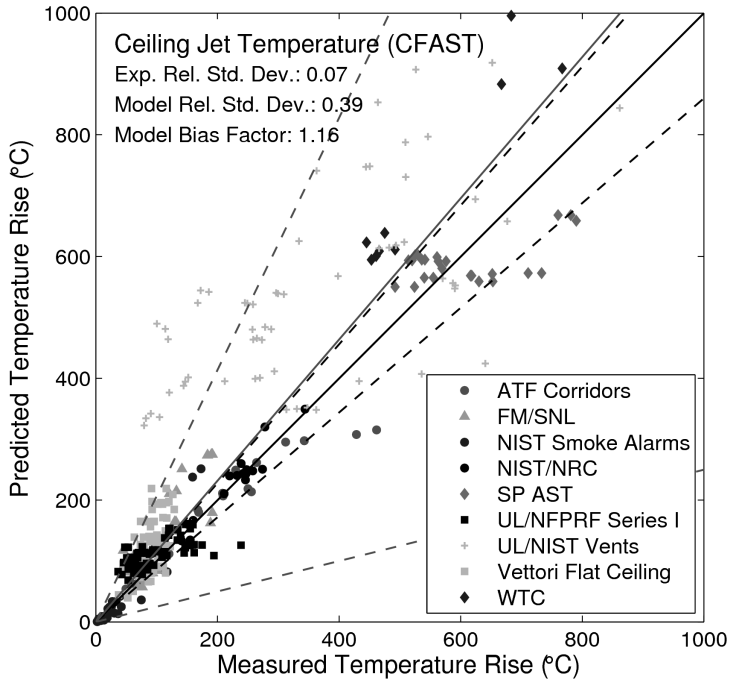

Figure 5-22. Ceiling Jet Temperature (CFAST).

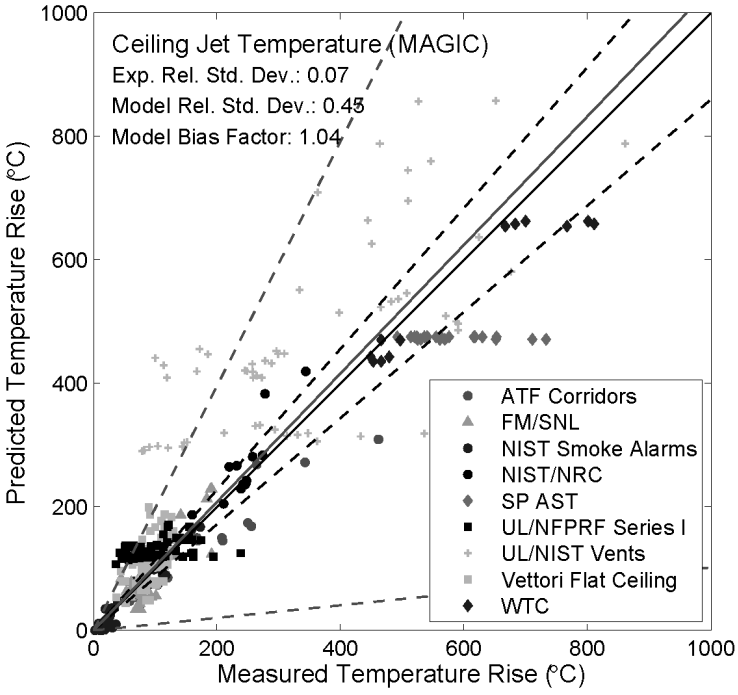

Figure 5-23. Ceiling Jet Temperature (MAGIC).

CFD Model: The FDS results are shown in Figure 5-24. FDS does not have a specific ceiling jet model; it calculates temperatures near the ceiling based on the overall solution of the governing equations. The FDS results do not indicate any particular bias or trend. The model uncertainty is primarily determined by the low-temperature data for which the inaccuracies are expected to be relatively higher because random initial conditions and background motion play more of a role.

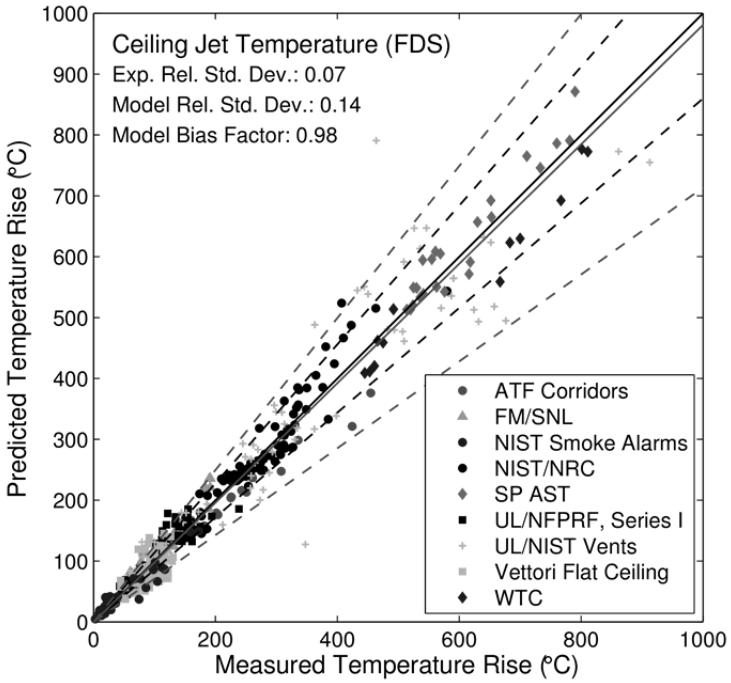

Figure 5-24. Ceiling Jet Temperature (FDS).

5.2.4 Plume Temperature

The fire plume transports hot gases into the HGL. Its temperature is greater than the ceiling-jet and HGL temperature. It is particularly important in NPP fires because of the numerous postulated scenarios that involve targets directly above a potential fire. A variety of empirical correlations that predict the plume temperature are embedded in the zone models. CFD models compute the plume temperature directly from the fundamental equations of motion.

The range of plume temperatures extends nearly to 1000 °C (1832 °F), which is within the flame envelope. This is important when modeling fully immersed targets.

Empirical Correlations: The results for the Heskestad and McCaffrey correlations are shown in Figure 5-25 and Figure 5-26 respectively. Note that the McCaffrey plume temperature correlation includes results at higher temperatures than the Heskestad plume temperature correlation because the Heskestad correlation is only valid above the mean flame height. These correlations do not account for the thermal effects of the hot gas layer.

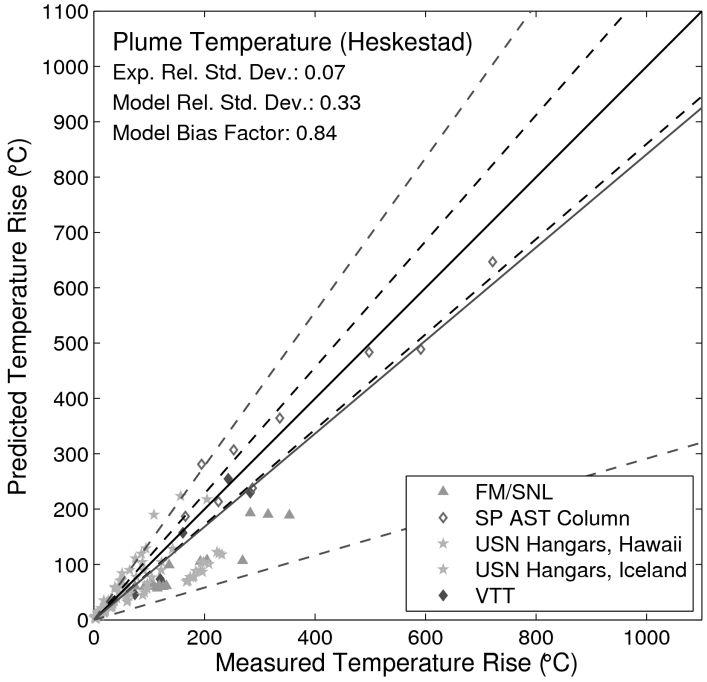

Figure 5-25. Plume Temperature (Heskestad).

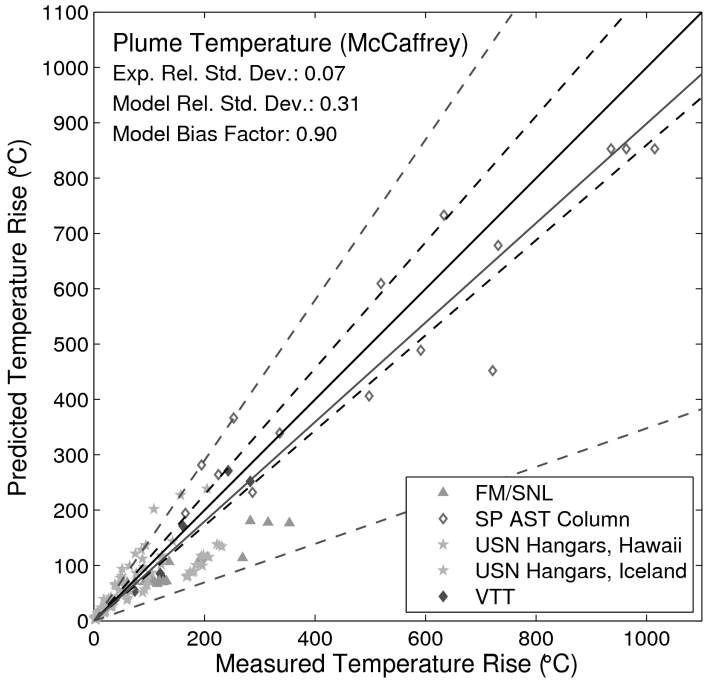

Figure 5-26. Plume Temperature (McCaffrey).

Zone Models: The CFAST and MAGIC results for plume temperature are shown in Figure 5-27 and Figure 5-28 respectively. The zone models have a specific plume sub-model similar to the sub-model they have for ceiling jets. Both models employ the McCaffrey plume correlation supplemented by the HGL temperature. Similar to the cases for HGL and ceiling jet temperature, a slight overprediction of the plume temperature is typical because the plume and HGL temperatures are not purely additive.

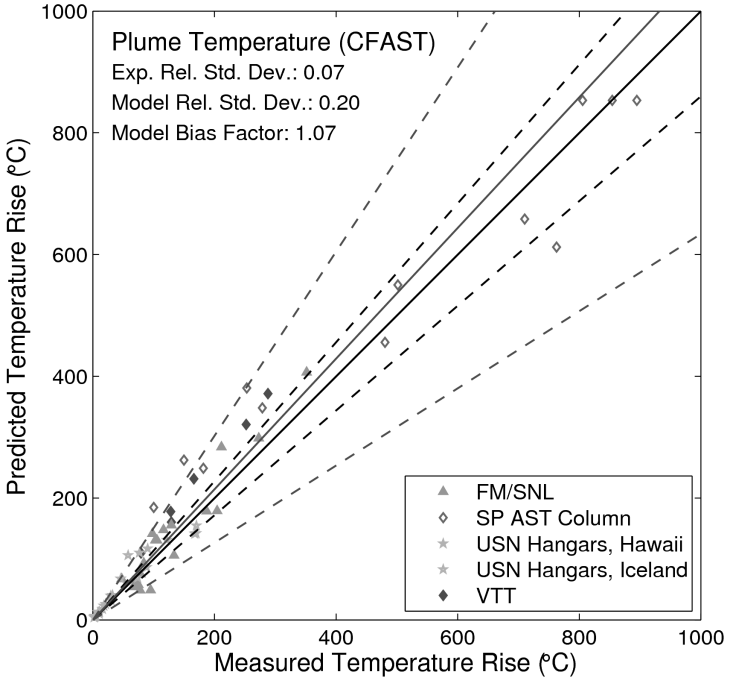

Figure 5-27. Plume Temperature (CFAST).

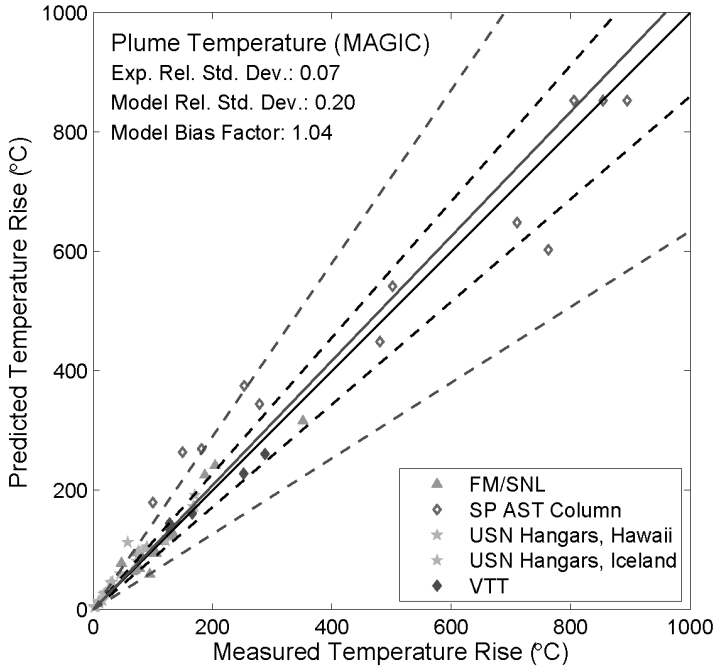

Figure 5-28. Plume Temperature (MAGIC).

CFD Model: The FDS results are shown in Figure 5-29. The uncertainty in the FDS predictions results largely from the USN Hangar experiments in which relatively small fires were lit within very large and drafty aircraft hangars. The HGL temperatures in these experiments were only a few tens of degrees above ambient, and there was a substantial temperature stratification in the hangars which was not included in the model. At the other end of the temperature scale, the SP AST Column predictions are for a fully engulfing hydrocarbon pool fire. Because a single relative uncertainty is applied to the model, the inaccuracy of the USN Hangar results is applied to the entire set of data.

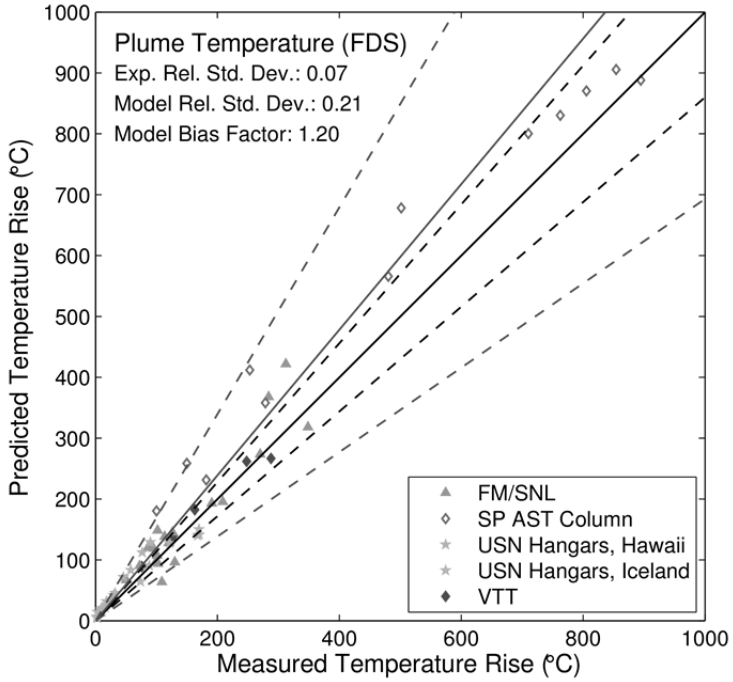

Figure 5-29. Plume Temperature (FDS).

5.2.5 Oxygen Concentration

Oxygen concentration is an indicator of a fire becoming underventilated, which is a precursor to flashover. The zone models calculate the oxygen concentration in the upper and lower layers and CFD models calculate the oxygen concentration in each grid cell. The empirical correlations assessed in this study do not address oxygen concentration.

The measured decrease in oxygen ranges from approximately 3 percent to 12 percent. A decrease in oxygen of approximately 6 percent indicates the start of oxygen-limited fire conditions.

Zone Models: The results for CFAST and MAGIC are shown in Figure 5-30 and Figure 5-31 respectively. Species production in CFAST and MAGIC is based on user-defined product yields, and both the burning rate and the resulting energy and species generation might be limited by the oxygen available for combustion. When sufficient oxygen is available for combustion, the heat-release rate for a constrained fire is the same as for an unconstrained fire. Mass and species concentrations are tracked by the models as gases flow through openings in a structure to other compartments in the structure or to the outdoors.

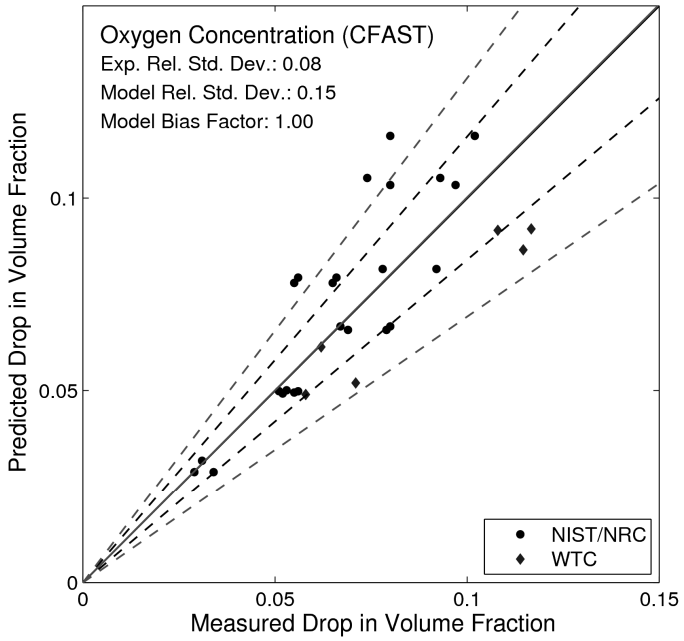

Figure 5-30. Oxygen Concentration (CFAST).

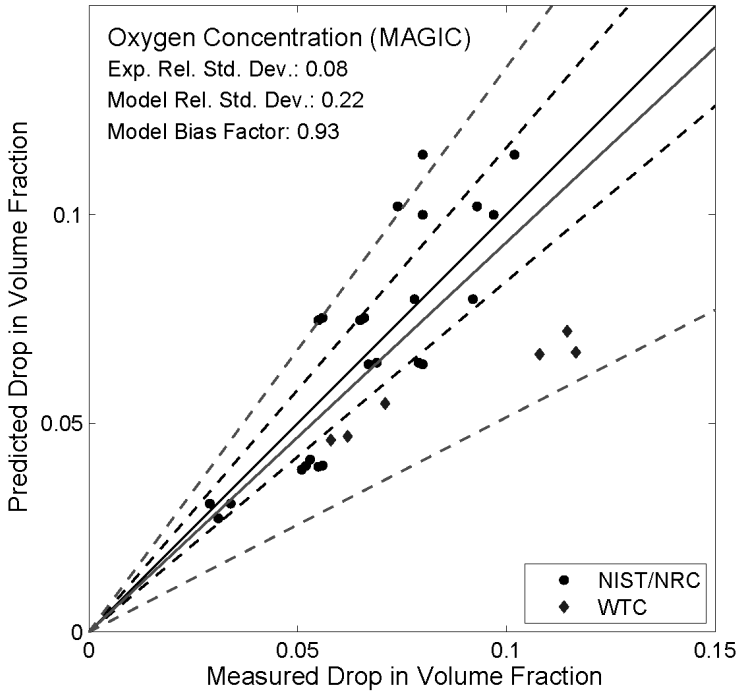

Figure 5-31. Oxygen Concentration (MAGIC).

For most tests, the models show similar results, with MAGIC trending to somewhat higher oxygen concentrations (lower predicted drop in volume fraction), particularly for very large fires (the WTC tests had peak HRR values of up to 3.5 MW). This is likely caused by different calculations for plume entrainment, vent flow mixing, and gas radiation in the two models, leading to additional entrainment by MAGIC and thus somewhat higher oxygen concentrations, lower layer temperatures, and lower heat fluxes to surrounding surfaces.

CFD Model: The FDS results are shown in Figure 5-32. The FDS results do not indicate any particular trend or bias. For both the NIST/NRC and WTC experiments, the fuel was n-heptane, which is predominantly composed of C_7H_{16}. The consumption rate of oxygen is proportional to the burning rate of the fuel, which is specified in the model. Thus, the consumption rate of oxygen is of comparable accuracy to the burning rate of the fuel. Although not shown here, the accuracy of the prediction of CO_2 is comparable to that of the prediction of O_2 because the basic fuel stoichiometry is known. However, the production rates of products of incomplete combustion, such as CO and soot, are not easily predicted; their predicted concentrations are less accurate.

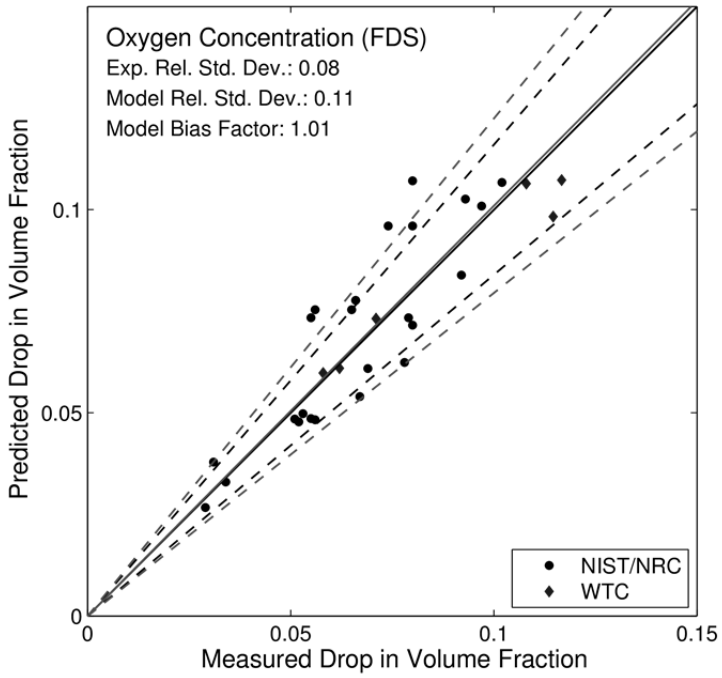

Figure 5-32. Oxygen Concentration (FDS).

5.2.6 Smoke Concentration

Smoke concentration is an important quantity for fire scenarios in areas where operators need to perform certain tasks. Zone and CFD models calculate smoke concentration by calculating the transport of soot from the fire throughout the compartment. Typically the soot yield is a specified model input. Note that the zone models evaluated here assume that soot behaves like the other product gases in that it does not deposit on compartment surfaces. In reality, soot can deposit on surfaces as a result of various deposition mechanisms, which reduces the gas-phase smoke concentration. Soot particles can also agglomerate to form larger particle sizes, which

can increase the soot-deposition rate. The CFD model evaluated here does account for some soot-deposition mechanisms, but does not currently account for soot agglomeration. For these reasons, the models tend to overestimate the smoke concentration (Hamins et al., 2006; Gottuk et al., 2008).

The measured smoke concentrations range from approximately 50 mg/m^3 to 200 mg/m^3. These conditions are typical of sooty fires expected in industrial settings.

The empirical correlation spreadsheets do not contain smoke or visibility estimates.

Zone Models: Zone models treat smoke like other combustion products, with an overall mass balance dependent on user-specified species yields for major combustion species. To model smoke movement, the user prescribes the smoke yield. A simple chemistry combustion scheme in the model then determines the smoke particulate concentration in the form of an optical density.

The results for CFAST and MAGIC are shown in Figure 5-33 and Figure 5-34 respectively. Only the NIST/NRC tests have been used to assess predictions of smoke concentration. For these tests, the smoke yield was specified as one of the test parameters. There are two obvious trends in the results. First, the predicted concentrations are within or near experimental uncertainties in the open-door tests. Second, the predicted concentrations are roughly three to five times the measured concentrations in the closed-door tests. The experimental uncertainty for these measurements has been estimated to be 19 percent.

The difference between model and experiment is far more pronounced in the closed-door tests. Given that the oxygen and carbon dioxide predictions are no worse (and indeed even better) in the closed-door tests, which might be because the smoke is not transported with the other exhaust gases, either the specified smoke yield (which was developed from free-burning experiments) is not appropriate for the closed-door tests or other phenomena are not accounted for in the model. These qualitative differences between the open- and closed-door tests are consistent with the FDS predictions.

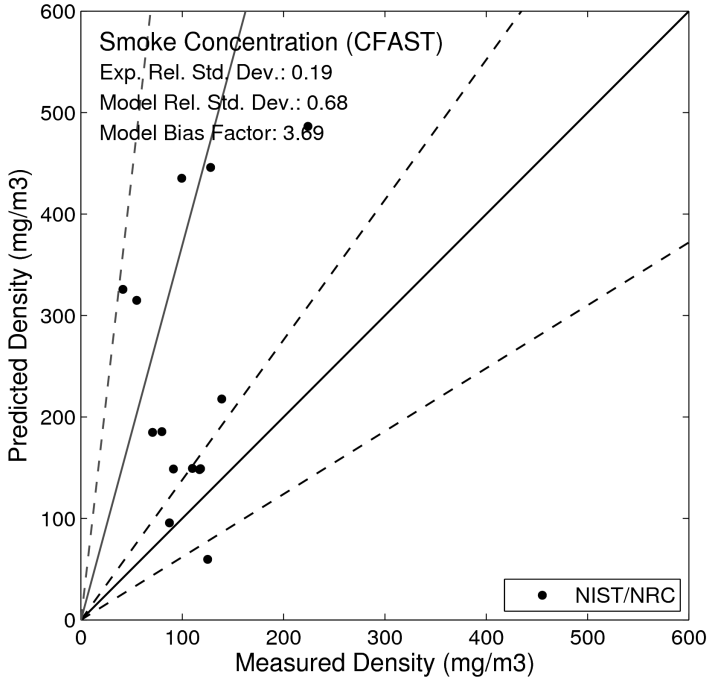

Figure 5-33. Smoke Concentration (CFAST).

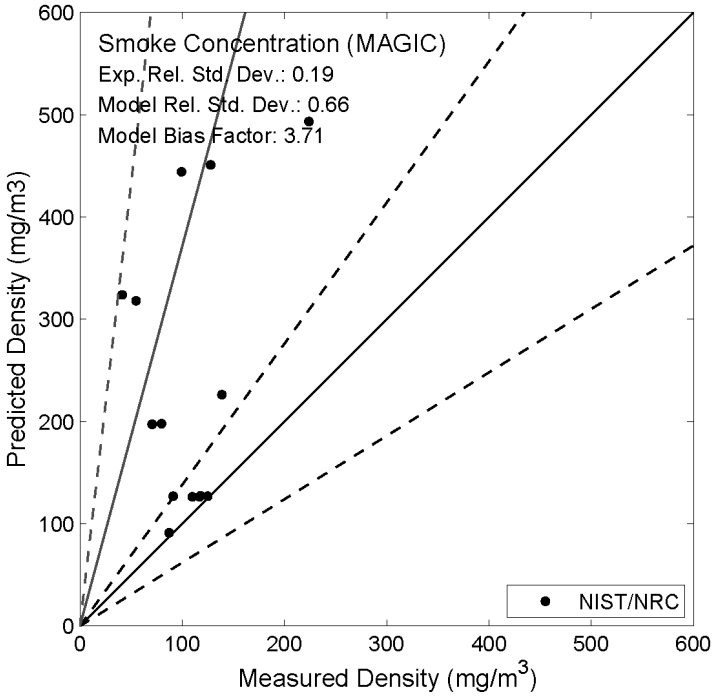

Figure 5-34. Smoke Concentration (MAGIC).

CFD Model: The FDS results are shown in Figure 5-35. The FDS results show an overestimation of the smoke concentration similar to that of the zone models. The overestimation is most pronounced in the closed-door experiments of the NIST/NRC series.

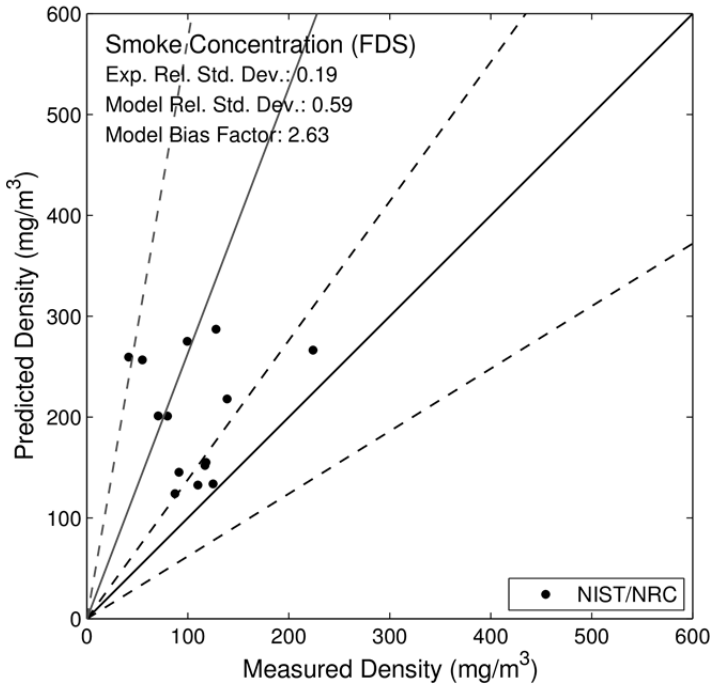

Figure 5-35. Smoke Concentration (FDS).

5.2.7 Pressure

Room pressure is a rarely used quantity in NPP fire modeling. It might be important when it contributes to smoke migration to adjacent compartments. Zone and CFD models calculate room pressure as they solve energy and mass balance equations for individual compartments. Empirical correlations only apply in the simplest of room geometries.

The measured pressures range from approximately 10 Pa to 300 Pa. The lower value is typical of an open compartment; the higher value is typical of a closed compartment with leakage.

Zone Models: The results for CFAST and MAGIC are shown in Figure 5-36 and Figure 5-37 respectively. Prediction of pressure at a specific measurement point is particularly difficult for zone models, which assume that pressure varies only as a function of height within a compartment. The CFAST and MAGIC results are comparable and have a consistently higher uncertainty than the FDS results.

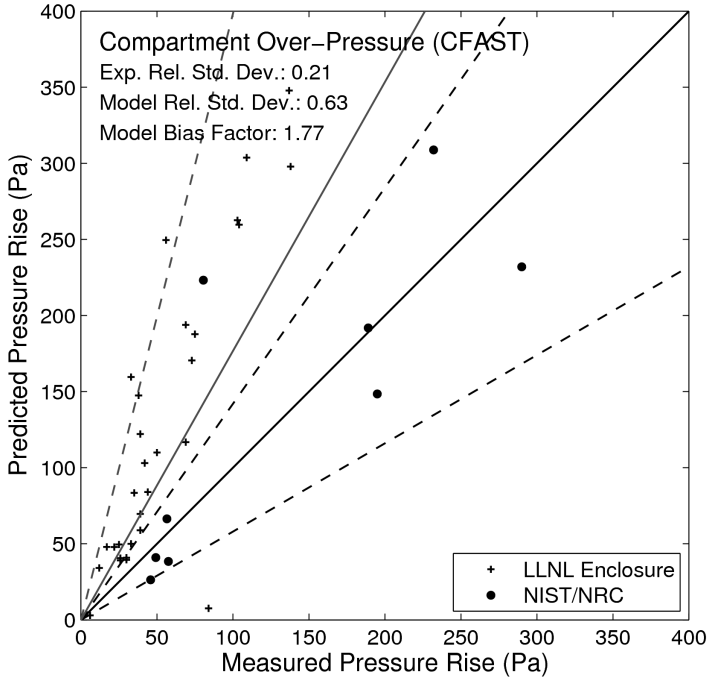

Figure 5-36. Compartment Overpressure (CFAST).

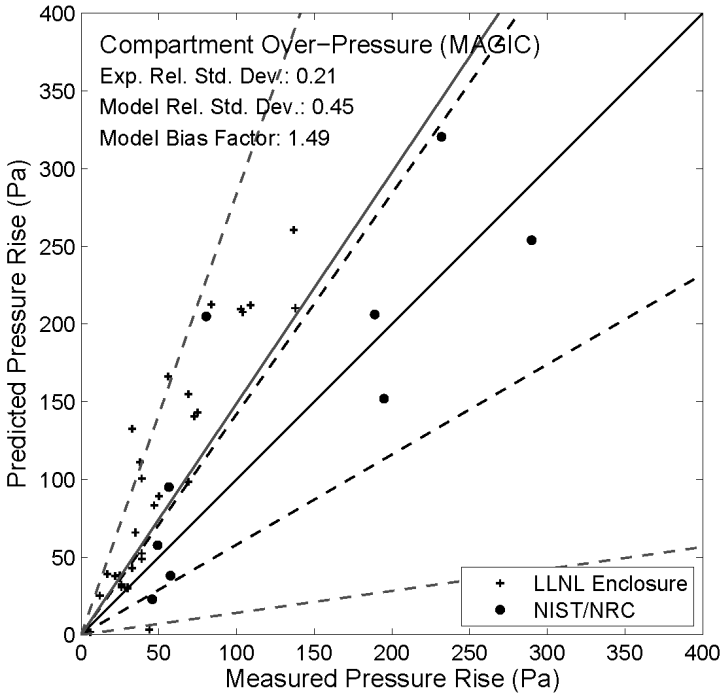

Figure 5-37. Compartment Overpressure (MAGIC).

CFD Model: The FDS results are shown in Figure 5-38; their accuracy is comparable to that of the experimental measurements. This accuracy is based on the fact that FDS conserves mass and energy globally, which along with basic thermodynamic principles assures that the overall compartment pressure will be predicted reasonably well.

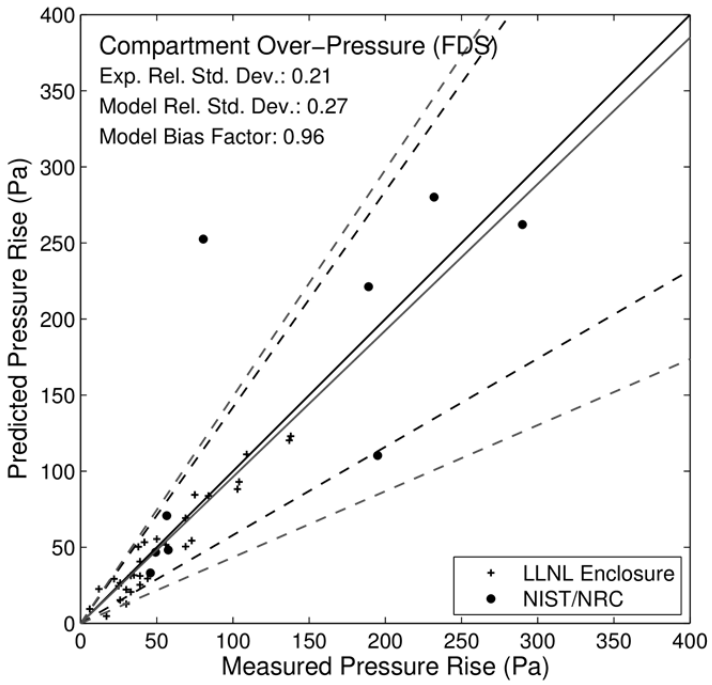

Figure 5-38. Compartment Overpressure (FDS)

5.2.8 Target Temperature

The calculation of target temperature is perhaps the most common objective of fire-modeling analyses. The zone and CFD models calculate the surface temperature of the target as a function of time and consider the heat conducted into the target material.

The range of measured target temperatures varies from model to model because the simpler models were not designed to address all of the target types and locations. The range of the empirical and zone models extends to approximately 800 °C (1472 °F), while the CFD model extends to about 1000 °C (1832 °F), where targets are fully immersed within a large hydrocarbon fuel fire.

Empirical Correlations: The results for the empirical correlations are shown in Figure 5-39. These targets include unprotected and protected steel members. HGL temperatures from the MQH correlation were used as the exposing fire temperature for the SP AST and WTC experiments; plume temperatures from the McCaffrey correlation were used as the exposing fire temperature for the SP AST experiments. In the WTC experiments, the steel members were both protected and unprotected, and only the steel members that were immersed in the HGL were included because the specification of an exposing fire temperature is required. In the protected steel cases, the empirical correlations use different heat transfer models that account

for the insulation material. The validation results do not include the NIST/NRC Experiments because the empirical correlations assessed in this study do not address their scenario.

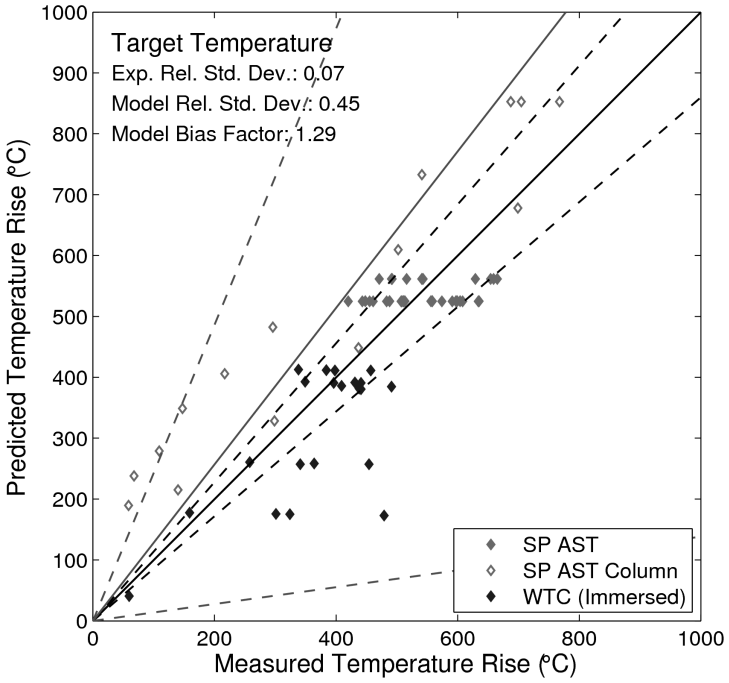

Figure 5-39. Target Temperature (Empirical Correlations)

Zone Models: The results for CFAST and MAGIC are shown in Figure 5-40 and Figure 5-41 respectively. The simplifying assumptions in a zone model are most evident in the prediction of inherently local conditions such as those on a target at a specific location in a compartment. For both zone models, bias and uncertainty are higher for target temperature and heat flux than for other quantities. Predictions for the NIST/NRC tests are often within experimental uncertainty, but predictions for the WTC tests, in which conditions were more extreme, show a far broader scatter.

Both models show a horizontal banding of predicted temperatures for tests that had numerous measurement points throughout a single compartment. This is typical of zone models for which the primary underlying assumption of two relatively uniform control volumes or layers within a compartment leads to relatively uniform predictions of target temperatures in the upper or lower layer. For measurement quite close to the ceiling, this banding is somewhat lessened because of the calculation of a ceiling-jet temperature; radiation from uniform surface temperatures adjacent to a layer also impact the calculation. The more spatially detailed calculations of a CFD model do not show this behavior. This assumption of uniform conditions within a layer also leads to some underprediction of temperature and heat flux for targets near the fire.

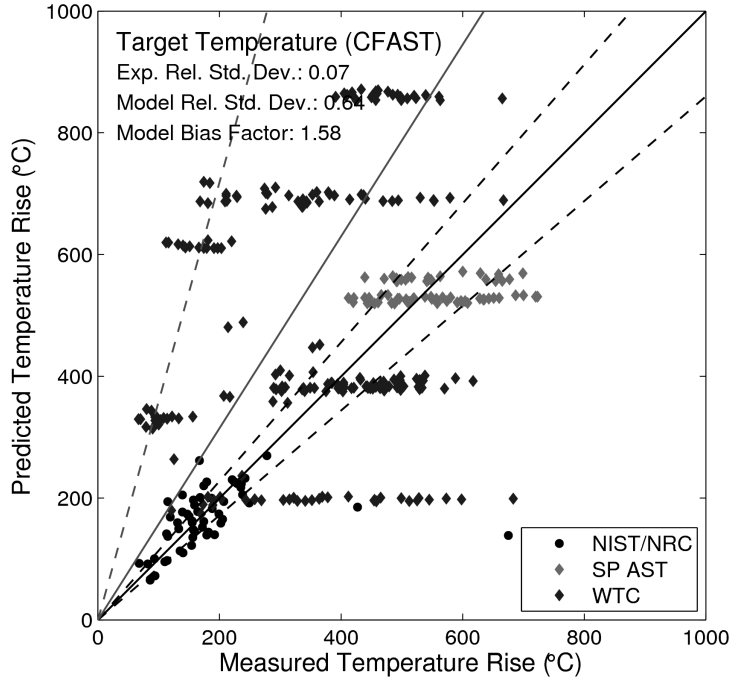

Figure 5-40. Target Temperature (CFAST).

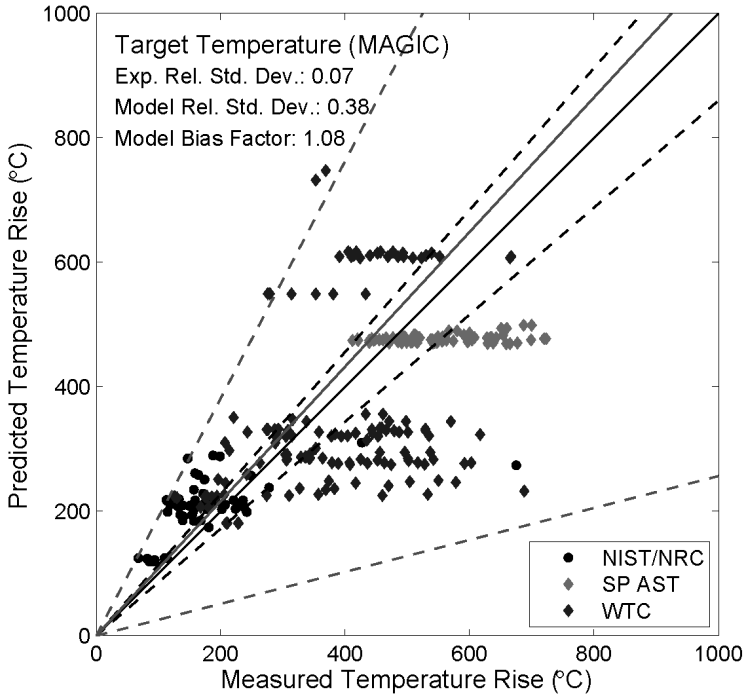

Figure 5-41. Target Temperature (MAGIC).

CFD Model: The FDS results are shown in Figure 5-42. The FDS results show no obvious bias or trend. The targets include various types of electrical cables, steel beams, trusses, and columns. In the WTC experiments, the steel is both protected and unprotected. In cases involving protected steel, FDS calculates the heat penetration through the sprayed-on insulation material.

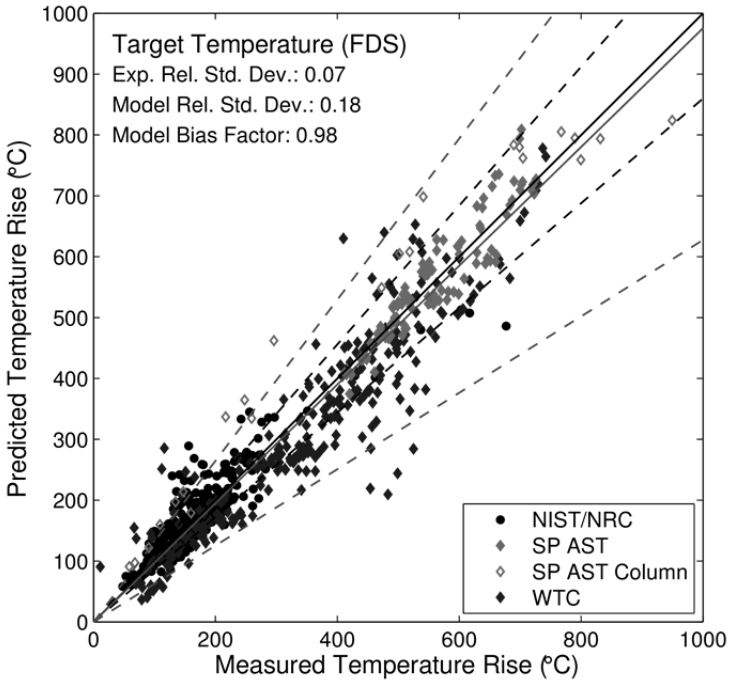

Figure 5-42. Target Temperature (FDS).

5.2.9 Target Heat Flux

Thermal radiation and convection are important modes of heat transfer in fires. The models included in this study address heat flux with various levels of sophistication, from simply estimating flame radiation from a point source to solving the full radiation transport equation. The empirical models include simple estimates of flame radiation from a point or cylindrical source. Zone models include these same estimates and also include radiation exchange between hot and cold layers and surfaces. CFD models solve the radiation transport equation that predicts the gains and losses of thermal radiation from each individual gas and solid phase grid cell.

The measured heat fluxes range from nearly 0 kW/m^2 to nearly 120 kW/m^2. The empirical correlations cannot address all cases, however. For NPP applications, the ability to predict heat-flux values at the lower end of the scale is most important, because damage criteria for common electrical cable types (thermoplastic and thermoset) are 6 kW/m^2 and 11 kW/m^2 (see Table 8-2 in Volume 2 of NUREG/CR-6850 (EPRI 1011989)).

Empirical Correlations:

The results for the point-source radiation and solid-flame correlations are shown in Figure 5-43 and Figure 5-44 respectively. Note that the point-source radiation model has higher uncertainty

for measurements closer to the flame, which is expected because the fire is represented as a point source.

An attempt was made to include all of the experimental data from the WTC Experiments. However, because some of the heat-flux gauges in the WTC Experiments were immersed in the hot gas layer or plume, the radiation correlations significantly underpredicted the target heat flux and the uncertainty was very large. Therefore, only heat flux gauges that were not immersed in the hot gas layer or plume were included.

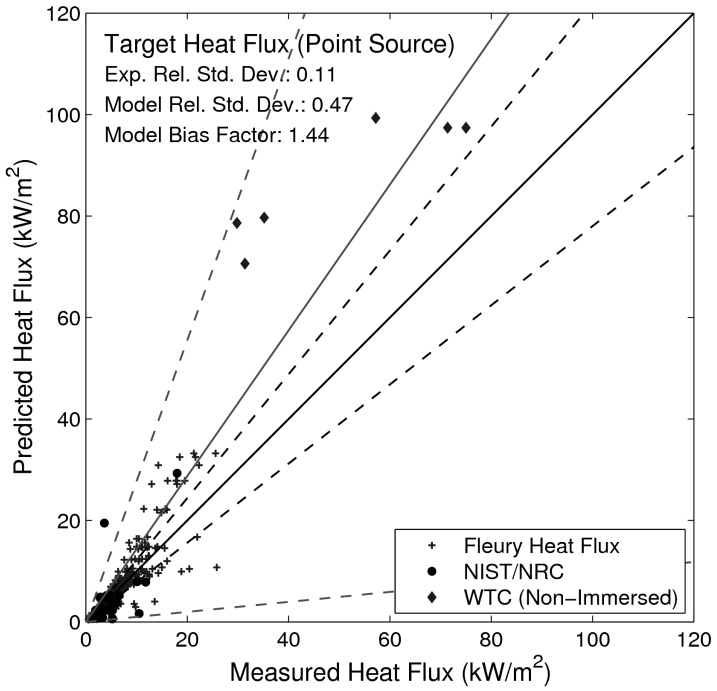

Figure 5-43. Target Heat Flux (Point Source).

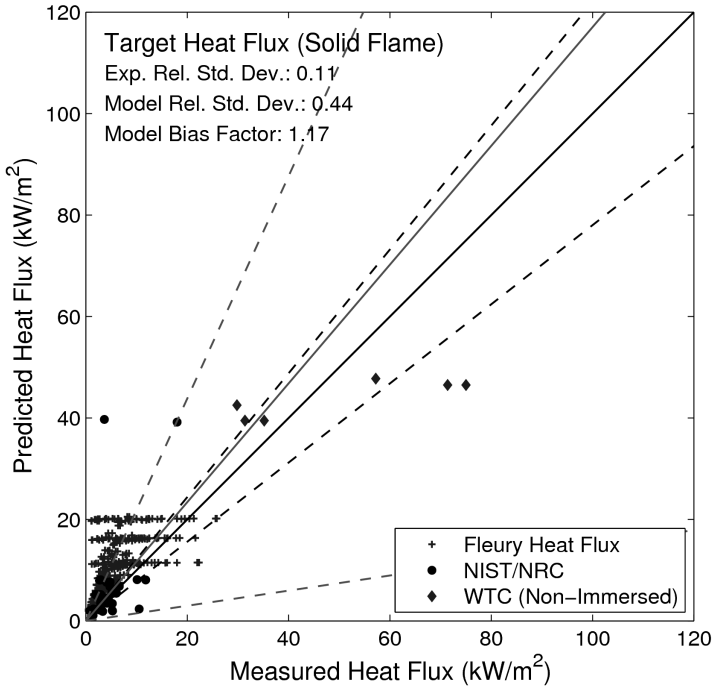

Figure 5-44. Target Heat Flux (Solid Flame).

Zone Models: The results for CFAST and MAGIC are shown in Figure 5-45 and Figure 5-46 respectively. Prediction of heat flux to targets and target surface temperature largely depends on local conditions surrounding the target. Two zone models such as CFAST and MAGIC predict an average representative value of gas temperature in the upper and lower regions of a compartment. Thus, the models can be expected to underpredict values near a fire source and overpredict values for targets remote from a fire. The uncertainty values for both models are driven by a few outliers in the data. Note that the two points that are significantly underpredicted in the NIST/NRC series are from a single experiment in which the fuel pan was moved close to the heat flux gauges. This was done in several of the experiments, but only these two points displayed a noticeable underprediction.

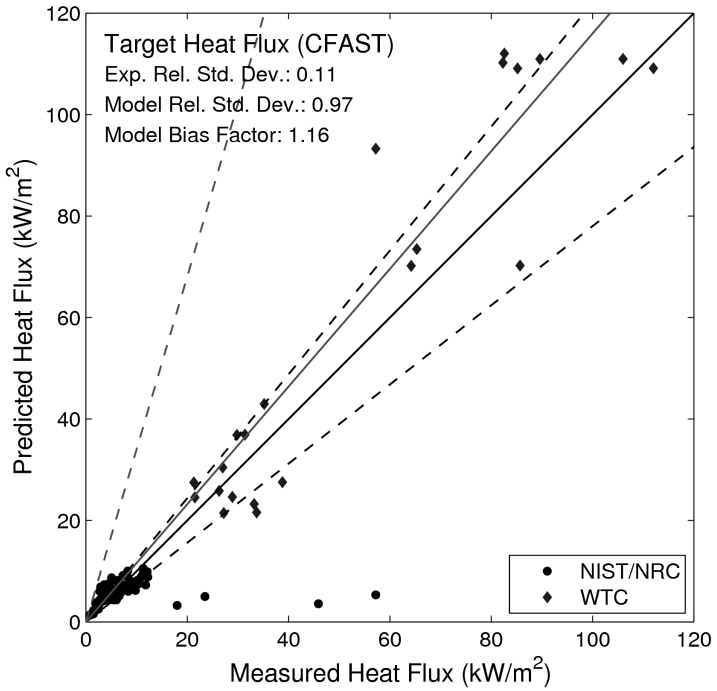

Figure 5-45. Target Heat Flux (CFAST).

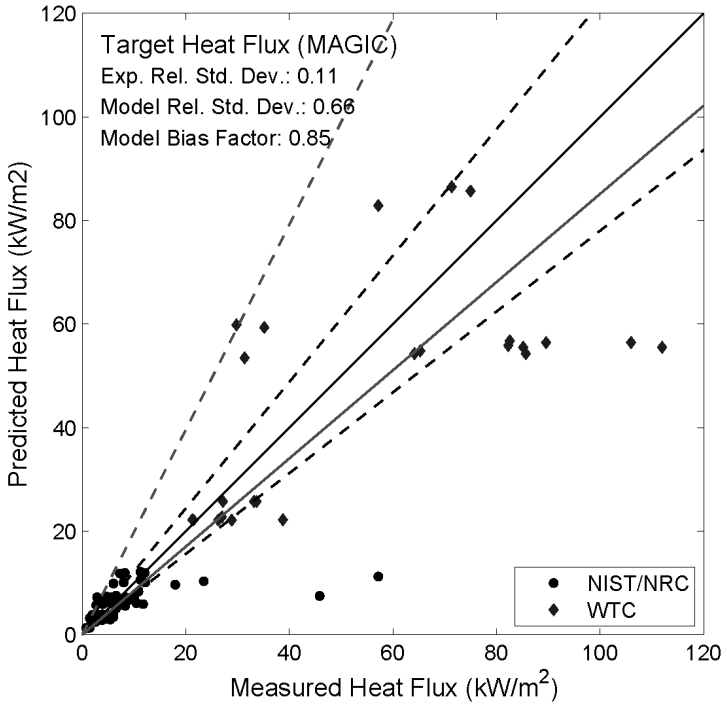

Figure 5-46. Target Heat Flux (MAGIC).

CFD Model: The FDS results are shown in Figure 5-47. A large number of heat flux measurements in the range from 1 kW/m^2 to 10 kW/m^2 dominate the bias and scatter of the FDS predictions. However, the limited measurements at higher heat fluxes do not significantly diverge from the trend indicated by the lower values. Note that the two points that are significantly underpredicted in the NIST/NRC series are from a single experiment in which the fuel pan was moved close to the heat-flux gauges. This was done in several of the experiments, but only these two points displayed a noticeable underprediction.

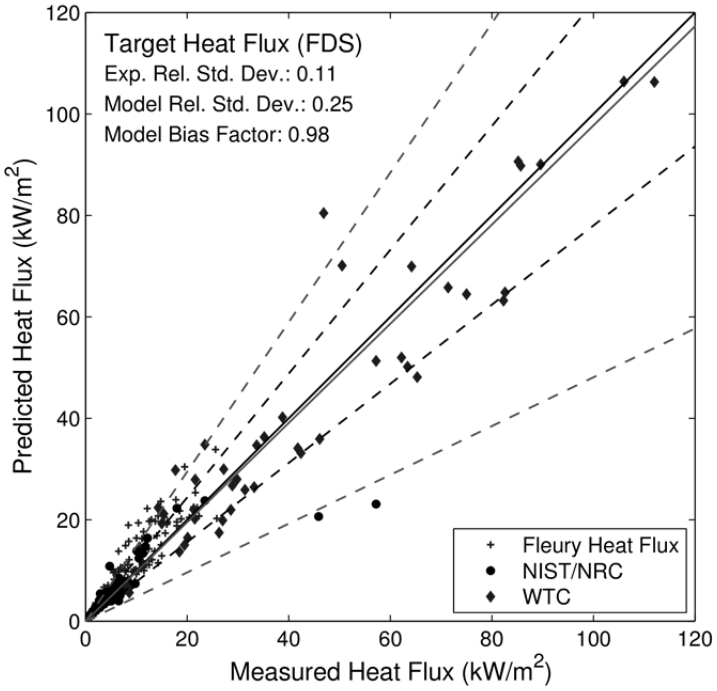

Figure 5-47. Target Heat Flux (FDS).

5.2.10 Surface Temperature

Compartment surfaces include the compartment walls, ceiling, and floor. The empirical correlations do not address the temperatures of the various compartment surfaces.

The range of measured surface temperatures extends to nearly 1000°C (1832°F), typical of targets fully immersed in flames.

Zone Models: Surface temperatures for CFAST and MAGIC are shown in Figure 5-48 and Figure 5-49, respectively. The models are capable of predicting the surface temperature of a wall, assuming that its composition is fairly uniform and its thermal properties are well characterized. Predictions are typically within 10 percent to 30 percent of the measured values. Generally, the models overpredict the far-field fluxes and temperatures and underpredict the near-field measurements. This is consistent with the single representative hot gas layer temperature assumed by zone fire models. Both models show a horizontal banding of predicted temperatures for tests which had numerous measurement points throughout a single compartment. This is typical of zone models for which the primary underlying assumption of two relatively uniform control volumes or layers within a compartment leads to relatively uniform

predictions of target temperatures in the upper or lower layer. For measurement quite close to the ceiling, this banding is somewhat lessened because of the calculation of a ceiling-jet temperature; radiation from uniform surface temperatures adjacent to a layer also impact the calculation. The more spatially detailed calculations of a CFD model do not show this behavior. This assumption of uniform conditions within a layer also leads to some underprediction of temperature and heat flux for targets near the fire.

The uncertainty in the surface temperature predictions is particularly influenced by the underprediction of ceiling surface temperatures. Both CFAST and MAGIC calculate a uniform ceiling temperature enhanced by the presence of a ceiling jet. Still, the underlying weakness of the zone model assumption of relatively uniform layer and surface temperatures becomes especially apparent in the calculated ceiling temperatures for compartments where a fire is located.

The wall temperatures and heat fluxes in MAGIC were calculated by placing individual targets in the walls. The targets are characterized by the thermophysical properties and thickness of the wall. This evaluation does not include either of MAGIC's output options "Wall Temperature" or "Wall Heat Flux," which are available in the Wall output category. Experimental measurements were compared with MAGIC's "Total Absorbed Heat Flux" output option.

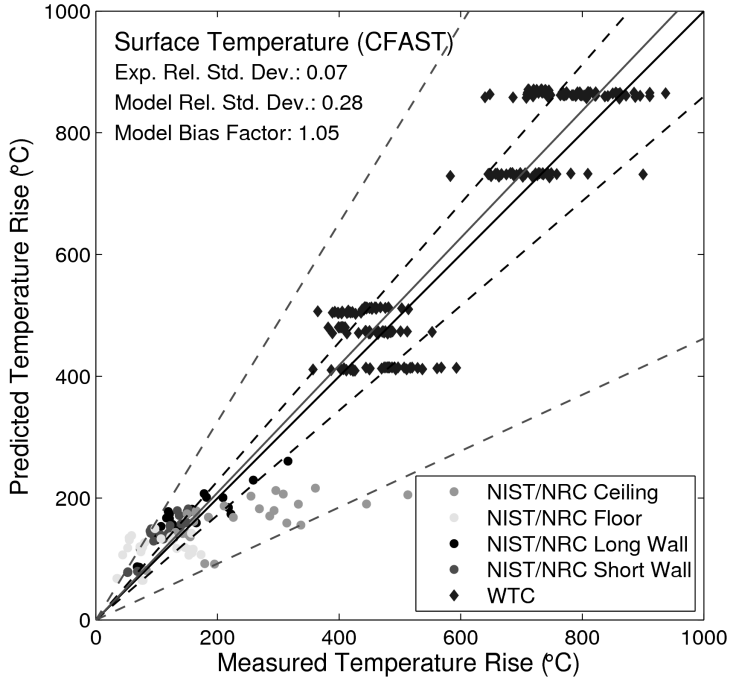

Figure 5-48. Surface Temperature (CFAST).

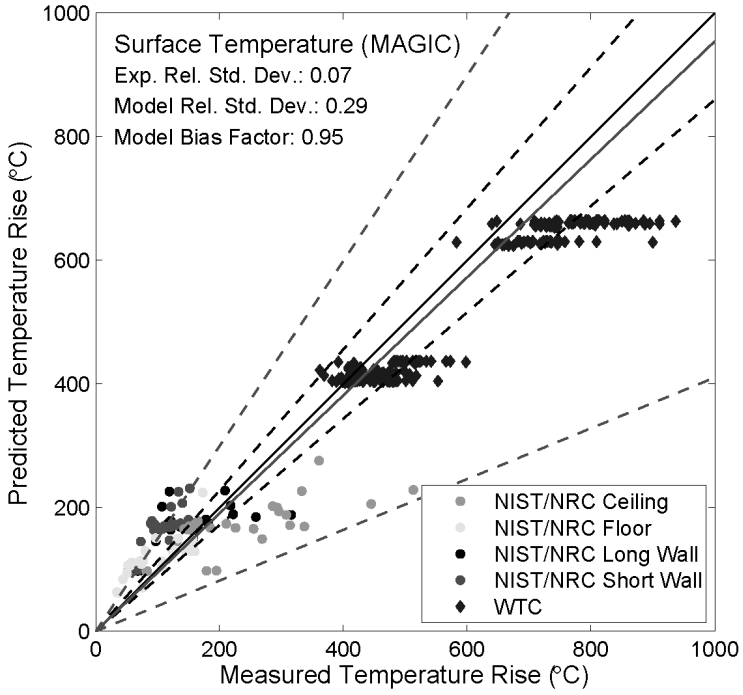

Figure 5-49. Surface Temperature (MAGIC).

CFD Model: The FDS results are shown in Figure 5-50. The FDS results indicate no particular trend or bias. The two sets of experiments considered included a large number of point measurements on all compartment surfaces. FDS treats all of these surfaces in the same way, except for a slightly different convective heat transfer coefficient depending on whether the surface is vertical or horizontal. The results do not indicate a greater or lesser degree of accuracy for either.

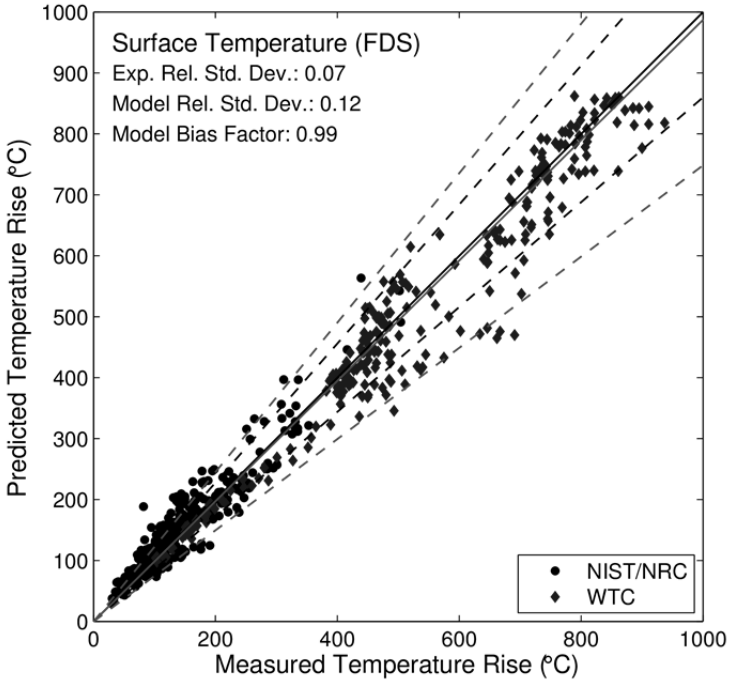

Figure 5-50. Surface Temperature (FDS).

5.2.11 Surface Heat Flux

Surface heat flux is generally treated in the same manner as target heat flux, just as surface temperature is treated in the same manner as target temperature. In a CFD model, there are slight differences in the convective heat transfer coefficient, but in most cases, radiation heat transfer is the dominant model of surface heating.

The measured heat fluxes range from approximately 0 kW/m^2 to 120 kW/m^2. For NPP applications, predicted heat fluxes beyond 11 kW/m^2 suggest target damage; thus, the accuracy of the models is most important at the lower end of the range.

The empirical correlations do not address heat flux to various compartment surfaces.

Zone Models: The results for CFAST and MAGIC are shown in Figure 5-51 and Figure 5-52 respectively. Trends similar to those for surface temperature predictions are seen in the surface heat flux predictions for the two zone models. Generally, the models overpredict far-field fluxes and temperatures and underpredict near-field measurements. This is consistent with the single representative hot gas layer temperature assumed by zone fire models. Both models also tend to somewhat underpredict ceiling temperatures and overpredict floor temperatures, likely because they both use the simple point source radiation algorithm for heat transfer from the fire.

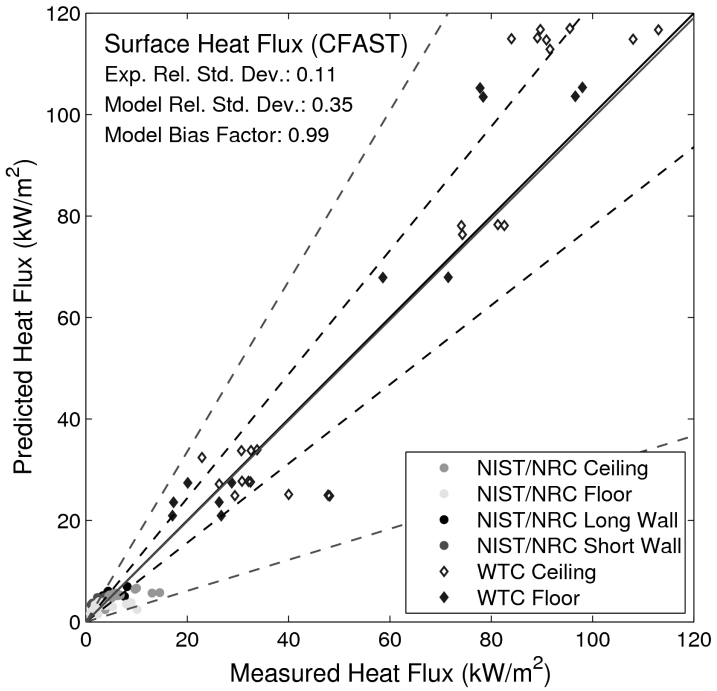

Figure 5-51. Surface Heat Flux (CFAST).

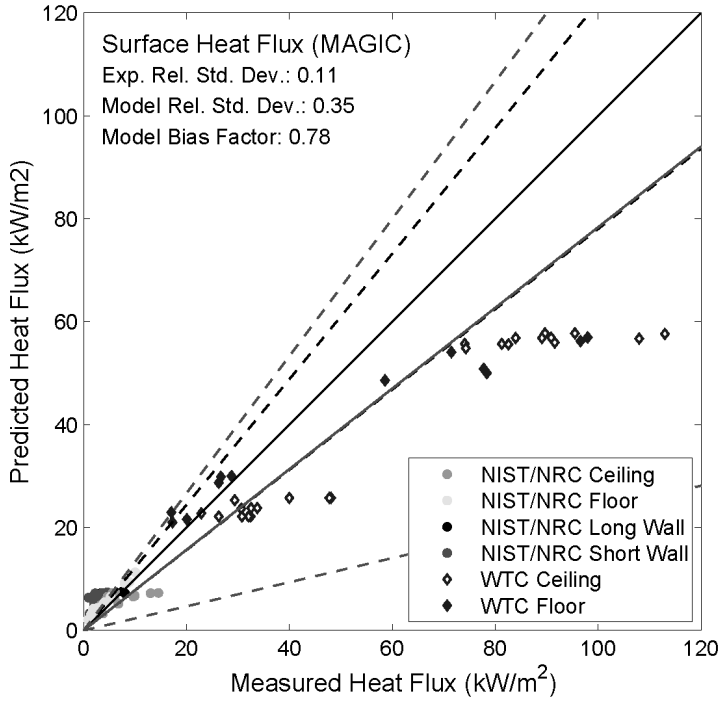

Figure 5-52. Surface Heat Flux (MAGIC).

CFD Model: The FDS results are shown in Figure 5-53. The FDS model uncertainty for the heat flux to walls, floors, and ceilings is based on data from two sets of experiments. In the NIST/NRC tests, most of the heat fluxes are relatively low because gauges were applied to surfaces that were remote from the fire. The purpose of these measurements was to assess the overall loss of energy from the entire compartment. The heat flux measurements in the WTC experiments, however, were made relatively close to the fire because the intent of the experiments was to assess the impact of a relatively large fire on structural elements and wall linings.

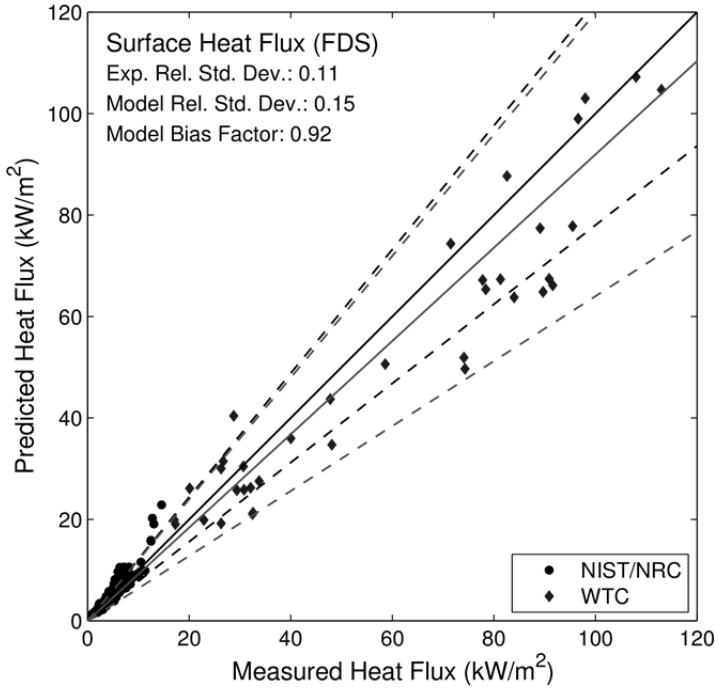

Figure 5-53. Surface Heat Flux (FDS).

5.2.12 Cable-Failure Time

Even though an electrical cable is considered to be a "target," a separate output quantity is included in this study to assess the models' ability to predict the time to cable failure. This is an indirect way of assessing the models' prediction of temperature. The models only predict the interior temperature of the cable, and the failure time is considered to be the time at which the predicted temperature rises above an experimentally determined value.

The THIEF model assumes that an electrical cable is a homogenous cylinder with constant values of specific heat and thermal conductivity and that the density is determined from its mass per unit length (McGrattan, 2008). The THIEF model has been implemented in various ways within the five fire models (FDT^s, FIVE-Rev2, CFAST, MAGIC, and FDS) discussed in this report. Both the FDT^s and FIVE-Rev2 have standalone implementations; the other three models use implementations appropriate to the type of model. The user's guide for each model should be reviewed for details concerning the respective implementation.

The measured failure times range from a few minutes to nearly a half hour. The longer failure times are typical of cables protected by steel conduit.

Standalone THIEF Model: The THIEF model has been implemented in FDT^s and THIEF's predictions of the CAROLFIRE experiments are shown in Figure 5-54.

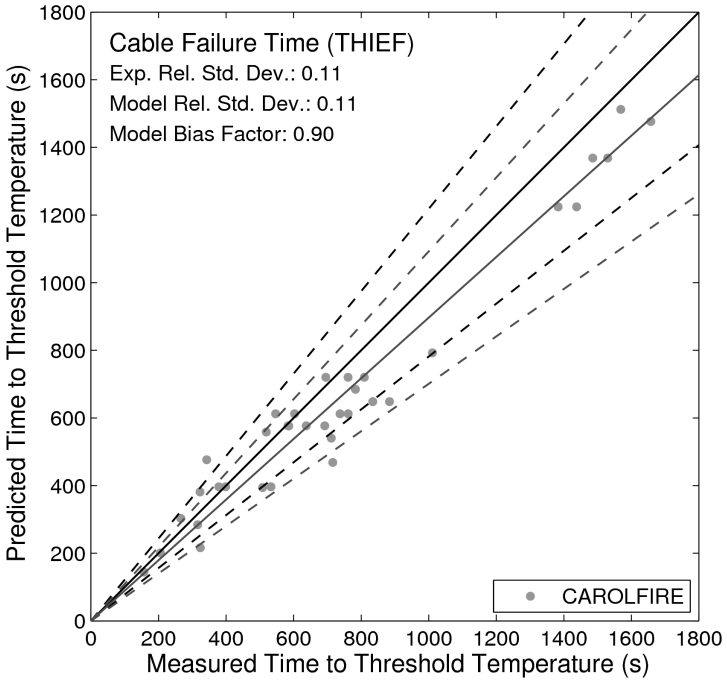

Figure 5-54. Cable-Failure Time (THIEF).

THIEF Model within a CFD Model: The FDS results are shown in Figure 5-55. The THIEF model is implemented in FDS. It differs from the FDT^s version only in that FDS predicts the time-varying gas temperature and heat flux to the cable surface. For example, the CAROLFIRE experimental apparatus was modeled in FDS to better predict the thermal environment surrounding the cable target.

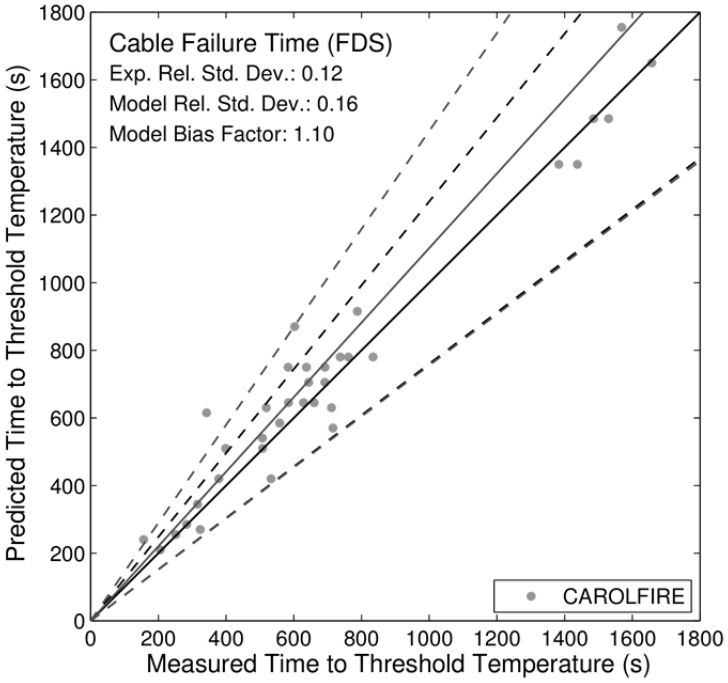

Figure 5-55. Cable Failure Time (FDS).

5.2.13 Sprinkler Activation Time

Much like an electrical cable, a sprinkler is merely a "target" with a particular set of thermal properties, such as the response time index (RTI) that indicates the sensitivity of the sprinkler's fusible link or glass bulb. Activation is assumed to occur when the link or bulb reaches a predetermined threshold temperature.

The experiments range from relatively small residential sprinklers in the Vettori experiments to relatively large industrial sprinklers in the UL/NFPRF experiments. The basic physics of both scenarios are mostly the same. Note that an extra set of experiments, the "Vettori Sloped Ceiling" experiments, was conducted by Vettori at NIST. The results of those experiments were only compared to those of FDS because none of the other models have the ability to model a sloped ceiling.

Empirical Correlation: The results for the Alpert correlation are shown in Figure 5-57. The empirical correlations can only predict ceiling jet flows for the simplest geometries. For this reason, for the Vettori experiments, only a subset of the experimental data (from tests with a smooth, horizontal, and unobstructed ceiling) was included.

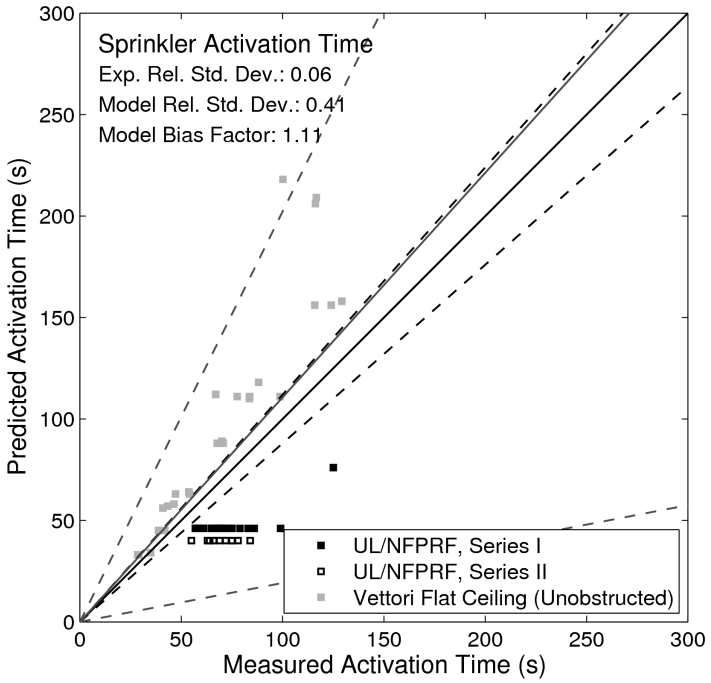

Figure 5-56. Sprinkler Activation Time.

Zone Models: Sprinkler activation times for CFAST and MAGIC are shown in Figure 5-57 and Figure 5-58 respectively. The results from the two models are similar but not identical. In general, CFAST predicts activation times somewhat shorter than those of MAGIC, particularly for the obstructed ceiling cases in the Vettori flat ceiling test series. The difference is likely caused by different assumptions in the two models for the gas temperature surrounding the sprinkler. Although both models use an RTI based calculation of heat transfer to the sprinkler, CFAST uses the ceiling jet gas temperature while MAGIC uses the (typically somewhat cooler) temperature of the hot gas layer, leading to longer activation times for MAGIC.

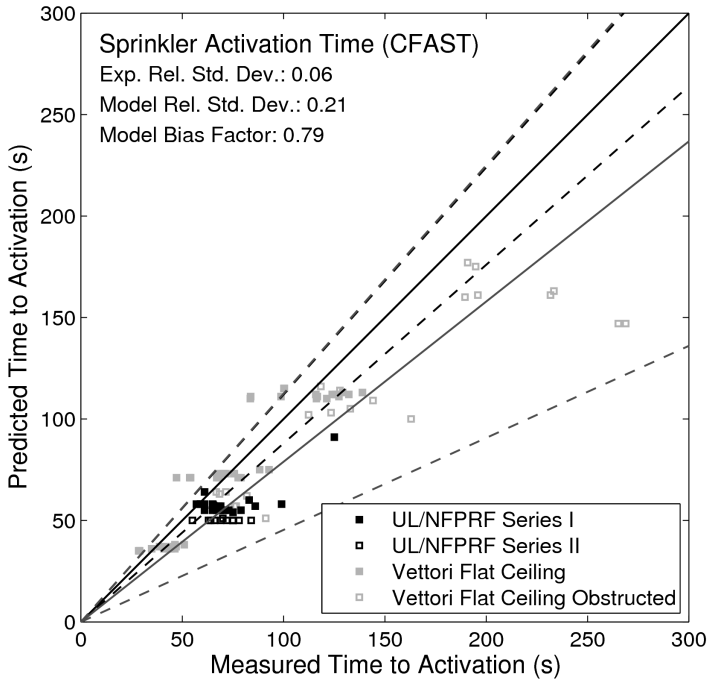

Figure 5-57. Sprinkler Activation Time (CFAST).

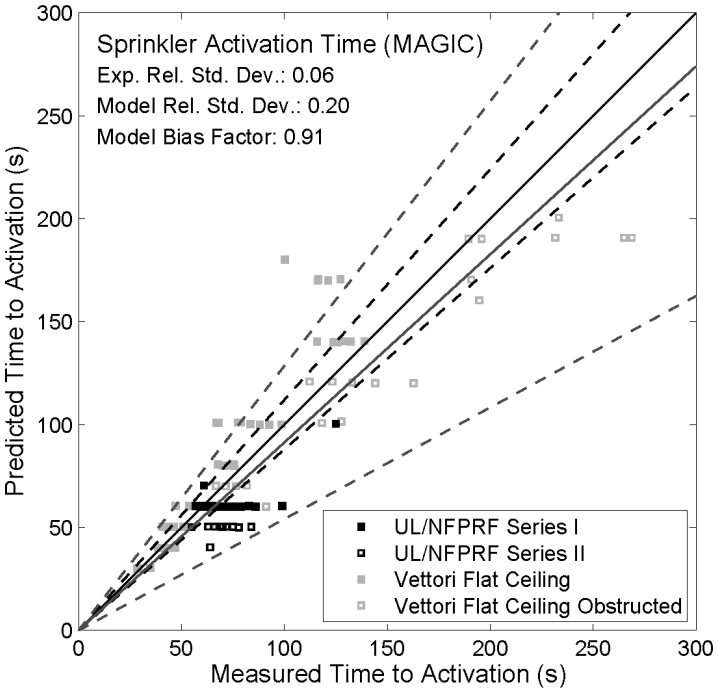

Figure 5-58. Sprinkler Activation Time (MAGIC).

CFD Model: The FDS results are shown in Figure 5-59. FDS underpredicts sprinkler activation time by about 7 percent. Note that data from both Vettori's flat- and sloped ceiling experiments are included. The zone and empirical models do not have the ability to model a sloped ceiling. FDS models a sloped ceiling as a series of stair-stepped obstructions. There appears to be a greater degree of model uncertainty associated with the more challenging sloped ceiling experiments.

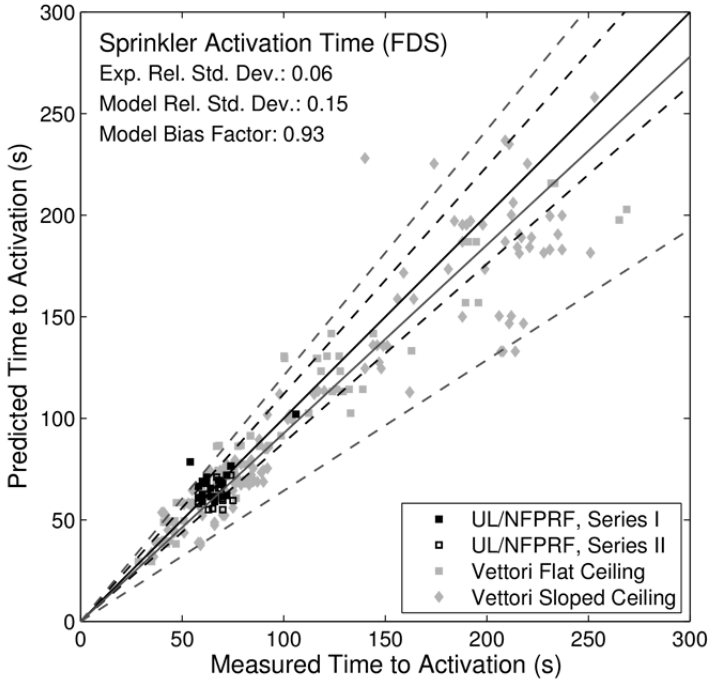

Figure 5-59. Sprinkler Activation Time (FDS).

5.2.14 Smoke Detector Activation Time

Smoke detectors can be modeled in a variety of ways. A popular method is to assume that the detector behaves like a very sensitive sprinkler with a low activation temperature and RTI. CFD models such as FDS have an alternative approach in which the smoke concentration and gas velocity in the vicinity of the detector is predicted and a simple time-lag equation is solved to account for the transport of smoke into the sensing chamber. This latter approach requires a set of empirical parameters that characterize the particular geometry of the device. The former approach typically treats all detectors as the same by using fixed values of activation temperature and RTI. In this validation study, only one set of data is used, from the NIST Home Smoke Alarms experiments. These experiments involved seven different types of detectors, but none of the time-lag parameters required by the alternative approach were provided in the test report. Therefore, all of the models below use the simple temperature rise approach with fixed values of activation temperature and RTI.

Empirical Correlations: The results for smoke detector activation time using the low RTI, low temperature rise assumption are shown in Figure 5-60. The temperature and velocity of the gases near the detector are predicted using the Alpert ceiling jet correlation, and the activation time is predicted under the assumption that the smoke detector responds like a sprinkler with an

RTI of 5 $(m \cdot s)^{0.5}$ and activation temperature of 5 °C above ambient. Note that only the smoke detectors that were located in the fire room of the NIST Smoke Alarms Experiments were included because the Alpert ceiling jet correlation cannot account for multiple rooms.

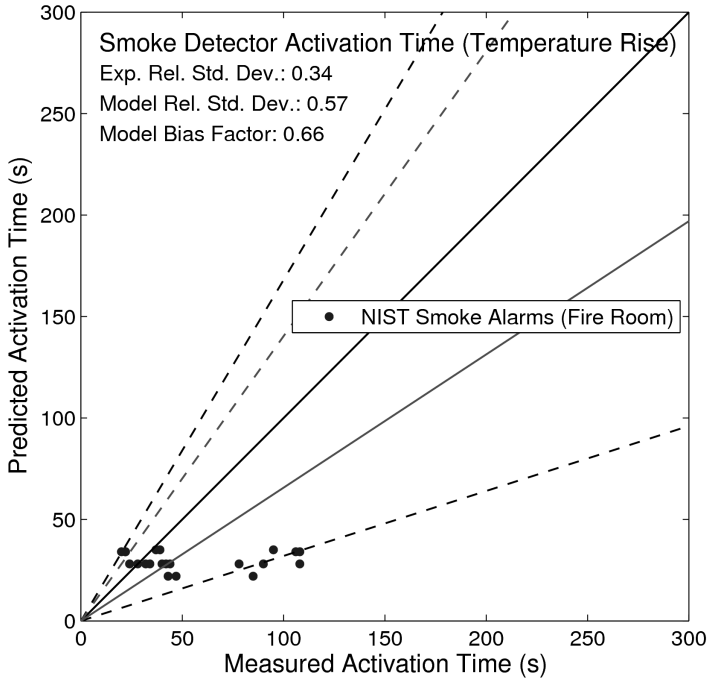

Figure 5-60. Smoke-Detector Activation Time (Temperature Rise).

Zone Models: The results for CFAST and MAGIC are shown in Figure 5-61 and Figure 5-62 respectively. Like its predictions of the sprinkler activation times, CFAST's predictions of smoke alarm activation time tend to be a bit shorter than those of MAGIC. Both models treat smoke alarms in the same manner as heat detectors and sprinklers, with a fixed activation temperature (5 °C above ambient temperature) and RTI (a value of 5 $(m\ s)^{1/2}$). As with sprinkler activation, CFAST uses the ceiling jet gas temperature while MAGIC uses the (typically somewhat cooler) temperature of the hot gas layer, leading to typically longer activation times for MAGIC.

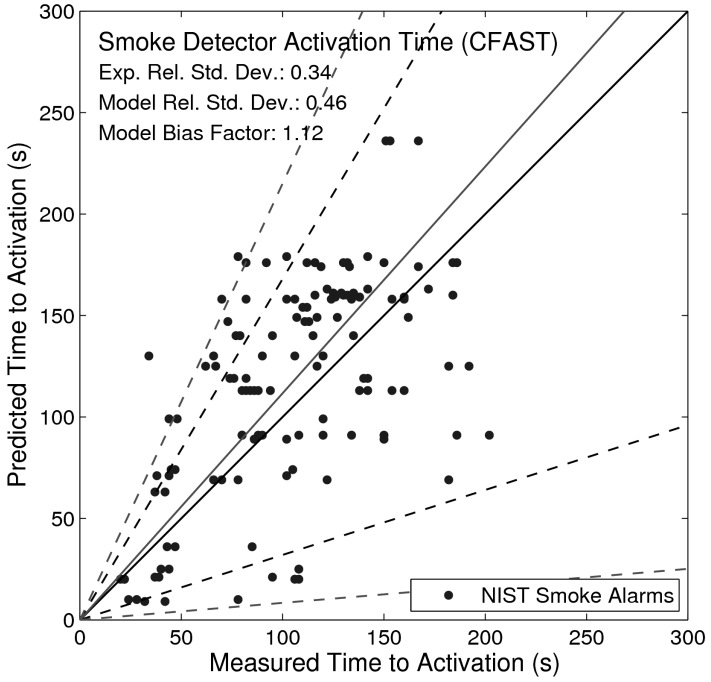

Figure 5-61. Smoke Detector Activation Time (CFAST).

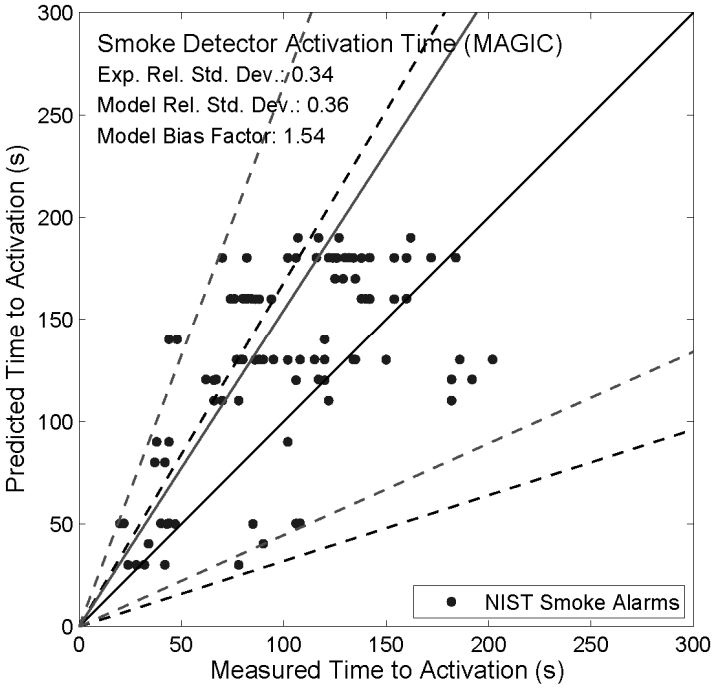

Figure 5-62. Smoke Detector Activation Time (MAGIC).

CFD Model: The FDS results are shown in Figure 5-63. FDS can model smoke detector activation time either by assuming that the detector acts like a sprinkler with a low RTI or by calculating the time for the smoke concentration to reach an alarm threshold within the detector. For the latter method, FDS requires several parameters that characterize the lag time and activation concentration. For the NIST Smoke Alarms experiments, these parameters are not provided; thus, FDS uses the same temperature-rise algorithm as the empirical and zone models. Note that the experimental and model uncertainty values are 0.29 rather than 0.34, as reported in subsection 3.3.3, because the calculation of the model uncertainty does not allow a value less than the experimental uncertainty.

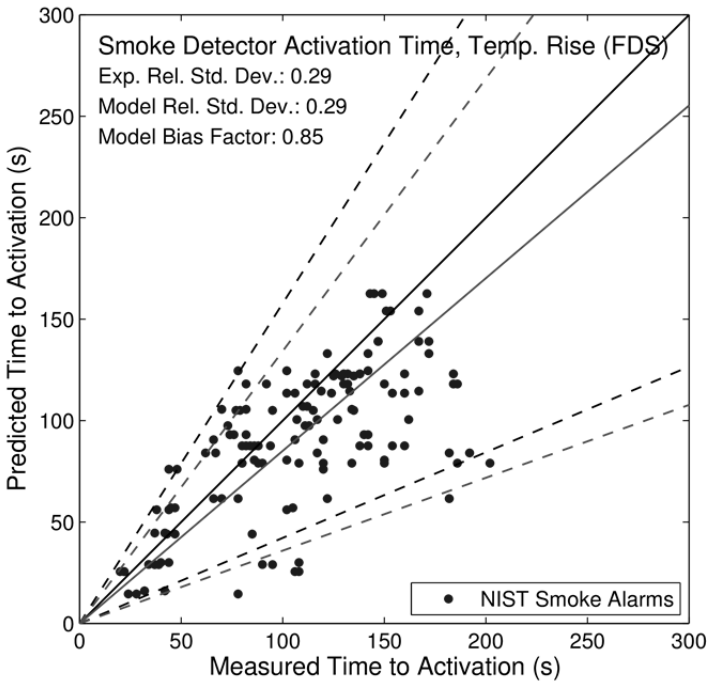

Figure 5-63. Smoke Detector Activation Time (FDS).

5.3 Summary of Validation Results

Table 5-1 summarizes the results of this validation study. As discussed in Section 5.1, the predictive capabilities of the models are assessed based on the quantitative values of relative difference between model prediction and experimental measurements.

Note that the values in Table 5-1 are based on the versions of the models listed in Section 1.3. These values do not apply to earlier versions of the models. In particular, the model-accuracy metrics that were cited in NUREG-1934 (EPRI 1023259) in 2012 are based on earlier versions of the models.

In general, the CFD model, FDS, is the most accurate, followed by the zone models, followed by the empirical correlations. This is to be expected because CFD models are more faithful to the underlying physics, but they also require hours or days to complete calculations that can be done in less than a minute by the other models.

There are some exceptions to the general hierarchy of models. For example, FDS is of comparable accuracy to the zone models in predicting plume temperatures. This is not surprising because the zone models use well established empirical correlations of plume temperatures, whereas FDS predicts these temperatures by solving the governing fluid flow equations. At best, FDS should predict comparable temperatures.

The zone and CFD models all overpredicted smoke concentration by approximately a factor of three, possibly because the models do not account for smoke losses to the walls and ceiling.

The zone models are relatively accurate in predicting the average HGL temperature, but less accurate in predicting localized surface temperatures and heat flux.

Table 5-1. Summary of model-uncertainty metrics.

Output Quantity	Empirical Correlations			CFAST		MAGIC		FDS		Exp
	Corr.	δ	$\tilde{\sigma}_M$	δ	$\tilde{\sigma}_M$	δ	$\tilde{\sigma}_M$	δ	$\tilde{\sigma}_M$	$\tilde{\sigma}_E$
HGL Temp. Rise, Natural Ventilation	MQH	1.17	0.15	1.20	0.36	1.13	0.30	1.02	0.12	0.07
HGL Temp. Rise,Forced Ventilation	FPA	1.29	0.32	1.15	0.19	1.08	0.17	1.21	0.22	0.07
	DB	1.18	0.25							
HGL Temp. Rise, No Ventilation	Beyler	1.04	0.37	1.00	0.08	1.07	0.16	1.20	0.12	0.07
HGL Depth	ASET/YT	-	-	1.05	0.34	1.17	0.31	1.03	0.06	0.05
Ceiling Jet Temp. Rise	Alpert	0.86	0.11	1.16	0.39	1.04	0.45	0.98	0.14	0.07
Plume Temp. Rise	Heskestad	0.84	0.33	1.07	0.20	1.04	0.20	1.20	0.21	0.07
	McCaffrey	0.90	0.31							
Oxygen Concentration	N/A			1.00	0.15	0.93	0.22	1.01	0.11	0.08
Smoke Concentration	N/A			3.69	0.68	3.71	0.66	2.63	0.59	0.19
Pressure Rise	N/A			1.77	0.63	1.49	0.45	0.96	0.27	0.21
Target Temp. Rise	Steel	1.29	0.45	1.58	0.64	1.08	0.38	0.98	0.18	0.07
Target Heat Flux	Point Source	1.44	0.47	0.97	1.16	0.85	0.66	0.98	0.25	0.11
	Solid Flame	1.17	0.44							
Surface Temp. Rise	N/A			1.05	0.28	0.95	0.29	0.99	0.12	0.07
Surface Heat Flux	N/A			0.99	0.35	0.78	0.35	0.92	0.15	0.11
Cable Failure Time	THIEF	0.90	0.11	-	-	-	-	1.10	0.16	0.12
Sprinkler Activation Time	Sprinkler	1.11	0.41	0.79	0.21	0.91	0.20	0.93	0.15	0.06
Smoke Detector Act. Time	Temp. Rise	0.66	0.57	1.12	0.46	1.54	0.36	0.85	0.29	0.34

Notes:

Experiments that had compartments with ceiling vents, high wall vents, multi-story configurations, irregular geometry, or complex wall materials were not included in the evaluation of the empirical correlations for HGL temperature.

There was insufficient data to derive the uncertainty statistics for the ASET/YT correlation.

Refer to subsection 5.2.3 for an explanation of the use of Alpert's correlation in unconfined vs. compartment scenarios.

The evaluation of the empirical correlations for Target Heat Flux only included targets that were not immersed in the hot gas layer or plume.

The evaluation of the empirical correlations for Sprinkler Activation Time only included sprinklers that were located on a smooth, horizontal, and flat ceiling.

The evaluation of the empirical correlation for Smoke Detector Activation Time only included detectors located in the room of origin.

6
CONCLUSION

This study provides further justification for verification and provides validation through comparisons between experimental data and predictions for the most current versions of the five fire-modeling tools used in the nuclear industry.

The most current versions of all five models have been verified by this study as appropriate for fire-protection applications, within the assumptions for each individual model or sub-model. The project team used guidance in ASTM E1355 about the theoretical basis and mathematical and numerical robustness to make this determination.

The validation results are presented in the form of a relative bias factor and standard deviation for each of the predicted quantities that are considered important for nuclear power-plant (NPP) fire-modeling applications. These accuracy metrics are based on the relative differences between model predictions and applicable experimental measurements. The predictive capability considers the uncertainty in the experimental measurements. The following observations are based on review of these results and generally apply to the five fire models considered in this study:

1. The results of this study apply only to the versions of the models listed in Section 1.3. These results cannot be applied to earlier versions of the models. NUREG-1934 (EPRI 1023259) contains results from earlier versions of these models.
2. The experiments considered in this study represent configurations that are typical of NPP applications. Not all possible NPP scenarios have been evaluated in this study. For a variety of reasons, experimental data is limited. Users should evaluate independently whether the results of this study are applicable to their specific scenario. Table 3-3 provides guidance in this matter.
3. For the fire scenarios considered in the current validation study, and for the output quantities of interest, the libraries of empirical correlations (FDT^s, FIVE) have fewer capabilities than the zone models or FDS. The correlations that the libraries contain are typically empirically deduced from a broad database of experiments. The correlations are based on fundamental conservation laws and have gained a considerable degree of acceptance in the fire-protection engineering community. However, because of their empirical nature, these correlations should be used within their limits of applicability.
4. The zone models, CFAST and MAGIC, predict global quantities like HGL temperature, HGL depth, and compartment pressure well, but are less accurate than FDS in predicting localized quantities such as ceiling-jet and surface temperatures and heat flux. This is expected given that zone models are designed to predict average quantities.
5. In general, FDS is more accurate than the empirical and zone models. However, for certain quantities, such as plume temperature rise in the absence of a hot gas layer, empirical and zone models should provide comparable accuracy because they are based on time-averaged experimental measurements whereas FDS must compute the time-dependent fluid dynamics directly.
6. The decision to use any of these models depends on many considerations. Real fire scenarios rarely conform neatly to some of the simplifying assumptions inherent in the models. Although engineering calculations and two-zone models can be applied in instances

in which the physical configuration is complex, their accuracy cannot be ensured. CFD model predictions can be more accurate in more of these complex scenarios. However, the time it takes to get and understand a prediction might also be an important consideration in the decision to use a particular model for a specific scenario. FDS is computationally expensive and, while the zone models produce answers in seconds to minutes, FDS provides comparable answers in hours to days. FDS is better suited to predict fire environments within more complex configurations because it predicts the local effects of a fire.

7. Like all predictive models, the best predictions come with a clear understanding of the limitations of the model and of the inputs provided to do the calculations. The bias factor and standard deviation values listed in Table 5-1 can be applied to the results of a given fire model's prediction as uncertainty bounds. This uncertainty should be combined with uncertainty in the various user-selected input parameters.

7
REFERENCES

NOTE: Reference entries use the names of the organizations that were in effect when the document was published. Keep in mind that the American Society for Testing and Materials is now ASTM International and that the National Bureau of Standards is now the National Institute of Standards and Technology.

Alpert, R.L., "Ceiling Jet Flows," DiNenno, P.J., et al., eds., *SFPE Handbook of Fire Protection Engineering*, 4th Edition, National Fire Protection Association, Quincy, MA, 2008.

American Society for Testing and Materials, "Standard Guide for Evaluating the Predictive Capability of Deterministic Fire Models," ASTM E1355-05a, West Conshohocken, PA, 2005.

Barnett, J.R., and C.L. Beyler, "Development of an Instructional Program for Practicing Engineers HAZARD I Users," NIST GCR 90-580, National Institute of Standards and Technology, Gaithersburg, MD, August 1990.

Benmamoun, A., "Rapport d'analyse et des modifications du code FORTRAN" ["Report of the analysis and modifications of the FORTRAN code"], SYSAM-SE-0310AB, 2004.

Beyer, C.L., "Fire Hazard Calculations for Large Open Hydrocarbon Fires," DiNenno, P.J., et al., eds., *SFPE Handbook of Fire Protection Engineering*, 4th Edition, National Fire Protection Association, Quincy, MA, 2008.

Budnick, E.K., D.D. Evans, and E.K. Nelson, "Simplified Fire Growth Calculations," Cote, A.E., ed., *NFPA Fire Protection Handbook*, 18th Edition, National Fire Protection Association, Quincy, MA, 1997.

Bukowski, R.W., and J.D. Averill. "Methods for Predicting Smoke Detector Activation," *Proceedings of the Fire Suppression and Detection Research Application Symposium, "Research and Practice: Bridging the Gap," February 25–27, 1998, Orlando, FL*, National Fire Protection Research Foundation, Quincy, MA, 1998.

Bukowski, R.W, et al., "Performance of Home Smoke Alarms: Analysis of the Response of Several Available Technologies in Residential Fire Settings," NIST Technical Note 1455-1, February 2008 Revision, National Institute of Standards and Technology, Gaithersburg, MD.

Cobalt Blue, Inc., "FOR_STUDY (FORTRAN Code Analyzer)," Alpharetta, GA, available at http://www.cobalt-blue.com/fy/fymain.htm (accessed on June 30, 2014).

Cooper, L.Y., "Estimating the Environment and the Response of Sprinkler Links in Compartment Fires with Draft Curtains and Fusible Link-Actuated Ceiling Vents - Part I: Theory," NBSIR 88-3734, National Bureau of Standards, Gaithersburg, MD, 1988.

Custer, R.L.P., B.J. Meacham, and R.P. Schifiliti, "Design of Detection Systems," DiNenno, P.J., et al., eds., *SFPE Handbook of Fire Protection Engineering*, 4th Edition, National Fire Protection Association, Quincy, MA, 2008.

DiNenno, P.J., et al., eds., *SFPE Handbook of Fire Protection Engineering*, 4th Edition, National Fire Protection Association, Quincy, MA, 2008.

REFERENCES

Evans, D.D, "Calculating Sprinkler Actuation Time in Compartments," *Fire Safety Journal* 9(2):147–155, July 1985.

Fleury, R, "Evaluation of Thermal Radiation Models for Fire Spread Between Objects," Christchurch, NZ: University of Canterbury, 2010.

Foote, K.L, "1986 LLNL Enclosure Fire Tests Data Report," Technical Report UCID-21236, Lawrence Livermore National Laboratory, August 5, 1987.

Gautier, B., "Plan Qualité du Logiciel MAGIC" ["Quality Plan for the MAGIC Software"], Note EDF/DER HT 31/95/025/B, Electricité de France, Paris, France, November 1996.

Gay, L., and E. Wizenne (2012a), "MAGIC (Version 4.1.3) - User's Guide," H-I81-2008-02077-EN, Electricité de France, Paris, France, March 2012.

Gay, L., and E. Wizenne (2012b), "MAGIC (Version 4.1.3) - Mathematical Model," H-I81-2008-02092-EN, Electricité de France, Paris, France, March 2012.

Gay, L., and E. Wizenne (2012c), "MAGIC (Version 4.1.3) - Validation," H-I81-2008-02085-EN, Electricité de France, Paris, France, April 2012.

Gott, J.E., et al., "Analysis of High Bay Hangar Facilities for Fire Detector Sensitivity and Placement," NIST TN 1423, Gaithersburg, MD, February 1997.

Gottuk, D., C. Mealy, and J. Floyd, "Smoke Transport and FDS Validation," *Fire Safety Science—Proceedings of the Ninth International Symposium*, International Association for Fire Safety Science, London, UK, 2008, pp. 129–140.

Hamins, A., et al., "Federal Building and Fire Safety Investigation of the World Trade Center Disaster: Experiments and Modeling of Structural Steel Elements Exposed to Fire," NIST NCSTAR 1-5B, National Institute of Standards and Technology, Gaithersburg, MD, September 2005.

Heskestad, G. and M.A. Delichatsios, "Environments of Fire Detectors, Phase 1: Effects of Fire Size, Ceiling Height and Material," Volumes 1 and 2, NBS GCR 77-86 and NBS GCR 77-95, National Bureau of Standards, Gaithersburg, MD, May 1977.

Heskestad, G., "Fire Plumes, Flame Height and Air Entrainment," DiNenno, P.J., et al., eds., *SFPE Handbook of Fire Protection Engineering*, 4th Edition, National Fire Protection Association, Quincy, MA, 2008.

Hostikka, S., M. Kokkala, and J. Vaari, "Experimental Study of the Localized Room Fires," VTT Tiedotteita - Meddelanden - Research Notes 2104, VTT Technical Research Centre of Finland, Espoo, Finland, 2001.

Karlsson, B., and J. Quintiere, *Enclosure Fire Dynamics*, Boca Raton, FL: CRC Press, 2000.

Klein-Heβling, W., M. Röwekamp, and O. Riese, "Evaluation of Fire Models for Nuclear Power Plant Applications: Fuel Pool Fire Inside a Compartment," Gesellschaft für Anlagen- und Reaktorsicherheit (GRS) mbH, Köln, Germany, November 2006.

McCaffrey, B.J., "Purely Buoyant Diffusion Flames: Some Experimental Results," NBSIR 79-1910, National Bureau of Standards, Gaithersburg, MD, October 1979.

McCaffrey, B.J., J.G. Quintiere, and M.F. Harkleroad, "Estimating Compartment Temperature and Likelihood of Flashover Using Fire Test Data Correlation," *Fire Technology* 17(2): 98–119, 1981.

McGrattan, K., A. Hamins, and D. Stroup, "Sprinkler, Smoke & Heat Vent, Draft Curtain Interaction—Large Scale Experiments and Model Development," NISTIR 6196-1, National Institute of Standards and Technology, Gaithersburg, MD, September 1998.

McGrattan, K., et al., "Fire Dynamics Simulator Technical Reference," NIST Special Publication 1018, Sixth Edition, National Institute of Standards and Technology, Gaithersburg, MD, November 2013.

McGrattan, K., et al., "Fire Dynamics Simulator User's Guide," NIST Special Publication 1019, Sixth Edition, National Institute of Standards and Technology, Gaithersburg, MD, November 2013.

McGrattan, K. and B. Toman, "Quantifying the predictive uncertainty of complex numerical models," *Metrologia* 48(3):173–180, June 2011.

Milke, J.A., "Smoke Management for Covered Malls and Atria," *Fire Technology* 26(3):223–243, August 1990.

Milke, J.A., "Analytical Methods for Determining Fire Resistance of Steel Members," DiNenno, P.J., et al., eds., *SFPE Handbook of Fire Protection Engineering*, 4th Edition, National Fire Protection Association, Quincy, MA, 2008.

Milke, J.A., "Smoke Management by Mechanical Exhaust or Natural Venting," DiNenno, P.J., et al., eds., *SFPE Handbook of Fire Protection Engineering*, 4th Edition, National Fire Protection Association, Quincy, MA, 2008.

Mowrer, F.W., "Lag Time Associated With Fire Detection and Suppression," *Fire Technology* 26(3):244–265, August 1990.

Mowrer, F.W., "Methods of Quantitative Fire Hazard Analysis," TR-100443, Electric Power Research Institute, Palo Alto, CA, May 1992.

Mulholland, G. W., and C. Croarkin, "Specific Extinction Coefficient of Flame Generated Smoke," *Fire and Materials* 24(5):227–230, September/October 2000.

National Fire Protection Association, "Performance-Based Standard for Fire Protection for Light Water Reactor Electric Generating Plants," NFPA 805, Quincy, MA, 2001.

Opert, K.M., "Assessment of Natural Vertical Ventilation for Smoke and Hot Gas Layer Control in a Residential Scale Structure," College Park, MD: University of Maryland, 2012.

Overholt, K.J., "Verification and Validation of Commonly Used Empirical Correlations for Fire Scenarios," NIST Special Publication 1169, National Institute of Standards and Technology, Gaithersburg, MD, 2014.

Peacock, R.D., S. Davis, and W.T. Lee, "An Experimental Data Set for the Accuracy Assessment of Room Fire Models," NBSIR 88-3752, National Bureau of Standards, Gaithersburg, MD, April 1988.

Peacock, R.D., G.P. Forney, and P.A. Reneke, "CFAST: Consolidated Model of Fire Growth and Smoke Transport (Version 6) - Technical Reference Guide," Special Publication 1026, Version 6, Revision 1, National Institute of Standards and Technology, Gaithersburg, MD, 2013.

Peacock, R.D., P.A. Reneke, and G.P. Forney, "CFAST: An Engineering Tool for Estimating Fire Growth and Smoke Transport, Version 6 - User's Guide," Special Publication 1041, Version 6, Revision 1 National Institute of Standards and Technology, Gaithersburg, MD, 2013.

REFERENCES

Peacock, R.D., and P.A. Reneke, "CFAST: Consolidated Model of Fire Growth and Smoke Transport (Version 6) - Software Development and Model Evaluation Guide," Special Publication 1086, Version 6, Revision 1, National Institute of Standards and Technology, Gaithersburg, MD, 2013.

Polyhedron Software, Ltd., "plusFORT Version 6," Standlake, UK, available at http://www.polyhedron.com/products/fortran-tools/plusfort-with-spag/plusfort-version-6.html, (accessed June 30, 2014).

Riese, O., D. Hosser, and M. Röwekamp, "Evaluation of Fire Models for Nuclear Power Plant Applications: Flame Spread in Cable Tray Fires," *GRS* 214(5), GRS mbH, Köln, Germany, September 2006.

Röwekamp, M., et al., "International Collaborative Fire Modeling Project (ICFMP): Summary of Benchmark Exercises No. 1 to 5," GRS-227, GRS mbH, Köln, Germany, September 2008.

Sheppard, D.T., and D.R. Steppan, "Sprinkler, Heat & Smoke Vent, Draft Curtain Project – Phase 1 Scoping Tests," Underwriters Laboratories, Inc., Northbrook, IL, May 1997.

Sheppard, D.T., and B.W. Klein, "Burn Tests in Two Story Structure with Hallways," ATF Laboratories, Ammendale, MD, 2009.

Sjöström, J., A. Byström, and U. Wickström, "Large scale test on thermal exposure to steel column exposed to pool fires," Technical Report 2012:04, SP Technical Research Institute of Sweden, Boras, Sweden, 2012.

Society of Fire Protection Engineers, "Assessing Flame Radiation to External Targets from Pool Fires," SFPE Engineering Guide, Bethesda, MD, March 1999.

Society of Fire Protection Engineers, "Fire Exposures to Structural Elements," SFPE Engineering Guide, Bethesda, MD, November 2005.

Society of Fire Protection Engineers, "Piloted Ignition of Solid Materials Under Radiant Exposure," SFPE Engineering Guide, Bethesda, MD, January 2002.

Society of Fire Protection Engineers, "Predicting Room of Origin Fire Hazards," SFPE Engineering Guide, Bethesda, MD, November 2007.

Society of Fire Protection Engineers, "Substantiating a Fire Model for a Given Application," SFPE Engineering Guide, Bethesda, MD, June 2010.

Society of Fire Protection Engineers, "SFPE Engineering Standard on Calculating Fire Exposures to Structures," SFPE S.01.2001, Bethesda, MD, 2011.

Steckler, K.D., J.G. Quintiere, and W.J. Rinkinen, "Flow Induced by Fire in a Compartment," NBSIR 82-2520, National Bureau of Standards, Gaithersburg, Maryland, September 1982.

Tanaka, T., and T. Yamana, "Smoke Control in Large Scale Spaces (Part 1: Analytic Theories for Simple Smoke Control Problems)," *Fire Science and Technology* 5(1):31–40, January 1985.

U.S. Nuclear Regulatory Commission, "Voluntary Fire Protection Requirements for Light Water Reactors; Adoption of NFPA 805 as a Risk-Informed, Performance-Based Alternative," *Federal Register*, Vol. 69, No. 115, June 16, 2004, pp. 33536–33551 (69 FR 33536).

U.S. Nuclear Regulatory Commission, "Fire Risk" addendum to "Memorandum of Understanding between U.S. Nuclear Regulatory Commission and Electric Power Research Institute, Inc., on Cooperative Nuclear Safety Research," Revision 1, May 18, 2001.

U.S. Nuclear Regulatory Commission, "Fire Dynamics Tools (FDT^s): Quantitative Fire Hazard Analysis Methods for the U.S. Nuclear Regulatory Commission Fire Protection Inspection Program," NUREG-1805, December 2004.

U.S. Nuclear Regulatory Commission, Supplement 1 to "Fire Dynamics Tools (FDT^s): Quantitative Fire Hazard Analysis Methods for the U.S. Nuclear Regulatory Commission Fire Protection Inspection Program," NUREG-1805, July 2013.

U.S. Nuclear Regulatory Commission, "Verification and Validation of Selected Fire Models for Nuclear Power Plant Applications, Volume 1: Main Report," NUREG-1824 (EPRI 1011999), May 2007.

U.S. Nuclear Regulatory Commission, "Nuclear Power Plant Fire Modeling Analysis Guidelines (NPP FIRE MAG)," NUREG-1934 (EPRI 1023259), November 2012.

U.S. Nuclear Regulatory Commission, "An Experimental Investigation of Internally Ignited Fires in Nuclear Power Plant Control Cabinets - Part I: Cabinet Effects Tests," NUREG/CR-4527 (SAND86-0336), Volume 1, April 1987.

U.S. Nuclear Regulatory Commission, NUREG/CR-4527, "An Experimental Investigation of Internally Ignited Fires in Nuclear Power Plant Control Cabinets - Part II: Room Effects Tests," NUREG/CR-4527 (SAND86-0336), Volume 2, November 1988.

U.S. Nuclear Regulatory Commission, "Enclosure Environment Characterization Testing for the Base Line Validation of Computer Fire Simulation Codes," NUREG/CR-4681 (SAND86-1296), March 1987.

U.S. Nuclear Regulatory Commission, Volume 1, "Summary and Overview," of "EPRI/NRC-RES Fire PRA Methodology for Nuclear Power Facilities," NUREG/CR-6850 (EPRI 1011989), September 2005.

U.S. Nuclear Regulatory Commission, Volume 2, "Detailed Methodology," of "EPRI/NRC-RES Fire PRA Methodology for Nuclear Power Facilities," NUREG/CR-6850 (EPRI 1011989), September 2005.

U.S. Nuclear Regulatory Commission, Supplement 1 to "Fire Probabilistic Risk Assessment Methods Enhancements," NUREG/CR-6850 (EPRI 1019259), September 2010.

U.S. Nuclear Regulatory Commission, "Report of Experimental Results for the International Fire Model Benchmarking and Validation Exercise 3," NUREG/CR-6905 (NIST SP 1013-1), May 2006.

U.S. Nuclear Regulatory Commission, Volume 1, "Test Descriptions and Analysis of Circuit Response Data," of "Cable Response to Live Fire (CAROLFIRE)," NUREG/CR-6931 (SAND2007-600/V1), April 2008.

U.S. Nuclear Regulatory Commission, Volume 2, "Cable Fire Response Data for Fire Model Improvement," of "Cable Response to Live Fire (CAROLFIRE)," NUREG/CR-6931 (SAND2007-600/V2), April 2008.

U.S. Nuclear Regulatory Commission, Volume 3, "Thermally-Induced Electrical Failure (THIEF) Model," of "Cable Response to Live Fire (CAROLFIRE)," NUREG/CR-6931 (NISTIR 7472), April 2008.

Vettori, R., "Effect of an Obstructed Ceiling on the Activation Time of a Residential Sprinkler," NISTIR 6253, National Institute of Standards and Technology, Gaithersburg, MD, November 1998.

REFERENCES

Vettori, R., "Effect of Beamed, Sloped, and Sloped Beamed Ceilings on the Activation Time of a Residential Sprinkler," NISTIR 7079, National Institute of Standards and Technology, Gaithersburg, MD, December 2003.

Walton, W.D., "ASET-B, a Room Fire Program for Personal Computers," NBSIR 85-3144, National Bureau of Standards, Gaithersburg, MD, December 1985.

Walton, W.D., and P.H. Thomas, "Estimating Temperatures in Compartment Fires," DiNenno, P.J., et al., eds., *SFPE Handbook of Fire Protection Engineering*, 4th Edition, National Fire Protection Association, Quincy, MA, 2008.

Wickström, W., R. Jansson, and H. Tuovinen, "Verification Fire Tests on Using the Adiabatic Surface Temperature for Predicting Heat Transfer," SP Report 2009:19, SP Technical Research Institute of Sweden, Boras, Sweden, 2009.

NRC FORM 335
(12-2010)
NRCMD 3.7

U.S. NUCLEAR REGULATORY COMMISSION

BIBLIOGRAPHIC DATA SHEET

(See instructions on the reverse)

1. REPORT NUMBER
(Assigned by NRC, Add Vol., Supp., Rev., and Addendum Numbers, if any.)
NUREG-1824
Supplement 1
DRAFT

2. TITLE AND SUBTITLE

Verification and Validation of Selected Fire Models for Nuclear Power Plant Applications
Supplement 1
Draft Report for Comment

3. DATE REPORT PUBLISHED

MONTH	YEAR
November	2014

4. FIN OR GRANT NUMBER

5. AUTHOR(S)

D. Stroup (NRC), A. Lindeman (EPRI), K. McGrattan (NIST), R. Peacock (NIST),
K. Overholt (NIST), F. Joglar (Kleinsorg), S. LeStrange (Kleinsorg), S. Montanez (Kleinsorg)

6. TYPE OF REPORT
Technical

7. PERIOD COVERED (Inclusive Dates)

8. PERFORMING ORGANIZATION - NAME AND ADDRESS (If NRC, provide Division, Office or Region, U. S. Nuclear Regulatory Commission, and mailing address; if contractor, provide name and mailing address.)

U.S. Nuclear Regulatory Commission, Office of Nuclear Regulatory Research, Washington, DC 20555-0001
Electric Power Research Institute, 3420 Hillview Avenue, Palo Alto, CA 94304
National Institute of Standards and Technology, 100 Bureau Drive, Gaithersburg, MD 20899
Kleinsorg Group Risk Services, a Division of Hughes Associates, 3610 Commerce Drive, Baltimore, MD 21227

9. SPONSORING ORGANIZATION - NAME AND ADDRESS (If NRC, type "Same as above", if contractor, provide NRC Division, Office or Region, U. S. Nuclear Regulatory Commission, and mailing address.)

Division of Risk Analysis
Office of Nuclear Regulatory Research
U.S. Nuclear regulatory Commission
Washington, DC 20555-0001

Electric Power Research Institute
3420 Hillview Avenue
Palo Alto, CA 94304

10. SUPPLEMENTARY NOTES
M.H. Salley, NRC Project Manager

11. ABSTRACT (200 words or less)

There is a movement to introduce risk informed and performance based (RI/PB) analyses into fire protection engineering practice, both domestically and worldwide. This movement exists in both the general fire protection and the nuclear power plant (NPP) fire protection communities. The U.S. Nuclear Regulatory Commission (NRC) has used risk informed insights as part of its regulatory decision-making since the 1990s. In 2001, the National Fire Protection Association (NFPA) issued the 2001 Edition of NFPA 805, "Performance Based Standard for Fire Protection for Light Water Reactor Electric Generating Plants." In July 2004, the NRC amended its fire protection requirements in Section 50.48, "Fire Protection," of Title 10, "Energy," of the Code of Federal Regulations to permit existing reactor licensees to voluntarily adopt fire protection requirements contained in NFPA 805 as an alternative to the existing deterministic fire protection requirements. One key tool needed to further the use of RI/PB fire protection is the availability of verified and validated (V&V) fire models that can reliably predict the consequences of fires. In 2007, the NRC, together with the Electric Power Research Institute (EPRI) and the National Institute of Standards and Technology (NIST), conducted a research project to verify and validate five fire models that have been used for NPP applications. The results of this effort were documented in a seven volume report, NUREG 1824 (EPRI 1011999), "Verification and Validation of Selected Fire Models for Nuclear Power Plant Applications." This supplement expands on the previous V&V effort and evaluates the latest versions of the five fire models including additional test data for validation of the models.

12. KEY WORDS/DESCRIPTORS (List words or phrases that will assist researchers in locating the report.)
Fire Hazard Analysis (FHA), Fire Modeling, Fire Probabilistic Risk Assessment (PRA), Fire Probabilistic Safety Assessment (PSA), Fire Protection, Fire Safety, Nuclear Power Plant, Risk-informed Performance-based (RI/PB) Regulation, Verification and Validation (V&V)

13. AVAILABILITY STATEMENT
unlimited

14. SECURITY CLASSIFICATION
(This Page)
unclassified
(This Report)
unclassified

15. NUMBER OF PAGES

16. PRICE

Federal Recycling Program

UNITED STATES
NUCLEAR REGULATORY COMMISSION
WASHINGTON, DC 20555-0001

OFFICIAL BUSINESS

NUREG-1824
Supplement 1, Draft

Verification and Validation of Selected Fire Models for Nuclear Power Plant Applications

November 2014